Doctoraatsproefschrift nr. 949 aan de faculteit Bio-Ingenieurswetenschappen aan de K.U.Leuven

STRUCTURAL ANALYSIS OF THE ANGIOGENESIS IN THE CHICKEN CHORIOALLANTOIC MEMBRANE

Eva VERHOELST

Promotoren:

Prof. J. De Baerdemaeker, K.U.Leuven

Prof. E. Decuypere, K.U.Leuven

Leden van de examencommissie:

Prof. B. Goddeeris, K.U.Leuven, voorzitter

Prof. B. Nicolaï, K.U.Leuven

Prof. J. Buyse, K.U.Leuven

Dr. Ir. B. De Ketelaere, K.U.Leuven

Dr. Ir. W. Saeys, K.U.Leuven

Dr. Ir. H. van den Brand, Wageningen Universiteit

Proefschrift voorgedragen tot het behalen van de graad van Doctor in de Bio-Ingenieurswetenschappen

Maart 2011

ISBN 978-90-8826-181-7
D/2011/11.109/3

TABLE OF CONTENTS

SAMENVATTING

Gedurende de laatste decennia wordt in de pluimveesector meer en meer onderzoek verricht naar technieken om de ontwikkeling van het kuiken te kunnen opvolgen qua groei, gezondheid en kwaliteit. Op basis van deze kennis kunnen dan de incubatiecondities gecontroleerd en geoptimaliseerd worden, en in het bijzonder de gassamenstelling. Een belangrijke parameter van de ontwikkeling van het kuiken die waarschijnlijk verandert onder invloed van verschillende gasconcentraties is de angiogenese in het chorioallantois-membraan (CAM), het gasuitwisselingsorgaan van het kippenembryo. Om grote incubatie-experimenten met telkens verschillende gassamenstellingen van de lucht uit te kunnen voeren, en de verschillen in angiogenese in het CAM te kunnen kwantificeren, is er nood aan een objectieve en snelle methode. Dit is bij voorkeur een niet-destructieve methode zodat de opvolging van langdurige effecten mogelijk wordt.

In dit onderzoek werd eerst een destructieve methodologie ontwikkeld om snel, objectief en kwantitatief veranderingen in de angiogenese in het CAM van kippenembryo's te meten. De monsters werden genomen met minimale verstoring van het CAM door het ei leeg te laten lopen terwijl het CAM aan de eischaal bleef vasthangen, die dan in stukken verdeeld werd. Er werd een beeldvormingopstelling opgebouwd die bestond uit een commerciële digitale camera en een macro lens met 5x vergroting om foto's te nemen met voldoende resolutie (2.64 µm/pixel). Om het contrast tussen bloedvaten en achtergrond te vergroten, werd groene diffuse belichting gebruikt. Via specifiek ontwikkelde algoritmen werden de beelden automatisch binair gemaakt om vervolgens twee structurele parameters van het bloedvatennetwerk te kunnen bepalen, namelijk de vasculaire fractie (VF) en de fraktale dimensie (FD). De verhouding van de herhaalbaarheids- en reproduceerbaarheidsvariatie tot de variatie in de monsters was 0.32 voor VF en 0.21 voor FD. In een validatie-experiment werd één groep eieren geïncubeerd onder hypoxische, *i.e.* lage O_2, condities en een andere onder normoxische condities als controle. Vroege hypoxie stimuleerde de angiogenese, maar chronische hypoxie verhinderde de groei met significante verschillen tussen beide groepen. Deze resultaten waren in overeenstemming met de gegevens uit de literatuur.

Vervolgens werd deze nieuw ontwikkelde methodologie gebruikt om de angiogenese te kwantificeren in het CAM onder normale en onder hypercapnische, *i.e.* hoge CO_2, condities gedurende de eerste tien dagen van incubatie. Twee experimenten werden uitgevoerd waarin hetzelfde CO_2-profiel werd toegepast. De groei van het vasculair netwerk werd opgemeten na de afwijkende condities qua gassamenstelling, namelijk van embryonale dag (ED) 10 tot en met ED 14 of 16. In één experiment werd ook het embryogewicht vergeleken tussen beide groepen. Zowel VF als FD, en het embryogewicht waren hoger in de hypercapnie groep in vergelijking met de controle groep. Er werd gesuggereerd dat hypercapnie de angiogenese deed toenemen via een pH-afhankelijke verhoging van VEGF en bFGF, twee belangrijke angiogenetische factoren. Bovendien bleek hypercapnie persistente effecten te hebben vermits de relatief sterkere toename van de structurele parameters tussen ED 13 en 14 in de controle groep, verschoven was naar een relatief sterkere toename tussen ED 12 en 13 in de hypercapnie groep in vergelijking met de toename tussen de andere ED.

Tenslotte werden in dit onderzoek de eerste stappen ondernomen tot de ontwikkeling van een niet-destructieve techniek. Dergelijke technieken zijn noodzakelijk om éénzelfde individu op te volgen gedurende zijn hele leven en zo langetermijneffecten op te kunnen meten, alsook de inter-individuele variabiliteit te elimineren. *Spatially resolved* spectroscopie (SRS) werd gekozen omdat hierbij het opgemeten signaal informatie geeft zowel over de bloedconcentraties in het weefsel als over de structuur van het weefsel. De metingen werden rechtstreeks op het CAM uitgevoerd omdat de eischaal tot enkele praktische problemen leidde die opgelost moeten worden in verder onderzoek om tot een werkelijke niet-destructieve techniek te komen. Tussen de drie onderzochte ED (ED 10, 13 en 16) werden significante verschillen aangetoond in de bloedwaarde berekend op basis van het signaal van de detector het dichtste bij de bron. De afname van de bloedwaarde met ED in dit onderzoek toonde een hogere lichtabsorptie door bloed aan en bevestigde bijgevolg de toename van de bloedconcentratie met ED. Het reflectantieprofiel in functie van de bron-detector afstand werd gefit met een eenvoudig exponentieel model. De macht van de exponentiële functie nam significant af met ED. Via de diffusietheorie werden de absorptie- en gereduceerde lichtverstrooiingscoëfficiënten van het CAM-weefsel geschat. De

absorptiecoëfficiënt nam toe met ED en de gereduceerde lichtverstrooiingscoëfficiënt nam af.

Samengevat levert dit werk een nieuwe snelle en objectieve destructieve methodologie om veranderingen in de angiogenese in het CAM onder verschillende incubatiecondities te kwantificeren. Er werd aangetoond dat vroeg prenatale hypercapnie, één van de potentieel bevorderlijke condities tijdens de incubatie, de groei van het vasculaire netwerk in het CAM stimuleerde. Voor het eerst werd *spatially resolved* spectroscopie gebruikt als aanloop naar niet-destructieve technieken om het CAM-weefsel te analyseren. Deze metingen toonden significante verschillen in de lichtpropagatie in het CAM-weefsel van verschillende ED aan.

ABSTRACT

During the last decades, the poultry sector is in search of ways to monitor chicken embryonic growth, health and quality, as to control and optimize the incubation conditions, especially the gas concentrations. One of the parameters of chicken development which may change under different gas concentrations is the angiogenesis in the chorioallantoic membrane (CAM), the organ for gas exchange of the chicken embryo. To be able to perform large incubation experiments under different gaseous conditions, and quantify the changes in the angiogenesis in the whole CAM, an objective and fast method is necessary, preferably non-destructive to allow the detection of long-term effects.

In this research, first, a fast, objective, and quantitative destructive methodology was developed to assess changes in the overall vascular development in the CAM of chicken embryos. Samples were taken with minimal disturbance of the CAM by emptying the egg so that the CAM stayed attached to the shell, which was then cut into pieces. An imaging set-up was made with a commercial digital camera and a macro lens set at 5x magnification to take pictures with sufficient resolution (2.64 µm/pixel). Green diffuse illumination was used to enhance the contrast between the blood vessels and the background which improved the image processing. The latter was done with specific computer algorithms to calculate automatically the vascular fraction (VF) and the fractal dimension (FD), two structural parameters of the vascular network, on binary images. The ratio of the repeatability and reproducibility variation compared to the parts variation was 0.32 for VF and 0.21 for FD. In a validation experiment, one group was incubated under hypoxic, *i.e.* low O_2, conditions and the other under normoxic conditions. It was shown that early hypoxia stimulated the angiogenesis while chronic hypoxia impeded growth with significant differences between both groups, which was in accordance with literature data.

Secondly, this newly developed methodology was used to quantify the angiogenesis in the CAM under normal and early hypercapnic, *i.e.* high CO_2, conditions during the first ten days of incubation. Two experiments were conducted in which the same CO_2 profile was applied. The development of the vascular network was monitored after the deviating gaseous conditions, from embryonic day (ED) 10 until ED 14 or 16. In one experiment, also embryo

weights were compared between both groups. Both VF and FD, and the embryo weight were shown to be higher in the hypercapnia group compared to the control group. It was suggested that hypercapnia induced an increase in angiogenesis via a pH-dependent increase of VEGF and bFGF, two important angiogenic factors. Moreover, hypercapnia had persistent effects since the relatively higher increase of the structural parameters between ED 13 and 14 in the control group, was shifted to a relatively higher increase between ED 12 and 13 in the hypercapnia group compared to the increase between the other ED.

Finally, the first steps towards a non-destructive technique are taken in this research. Only by the use of non-destructive techniques it is possible to follow-up one individual throughout its life and measure long-term effects, and also eliminate inter-individual variability. Spatially resolved spectroscopy (SRS) was chosen because the signal contains both information on the concentrations of blood in the tissue and on the structure of the tissue. Measurements were performed directly on the CAM tissue as the eggshell poses some practical problems which should be addressed in further research to come to a really non-destructive technique. Significant differences between the three measured ED (ED 10, 13, and 16) were observed in the blood value calculated based on the signal detected by the fiber shortest to the source. The decrease of the blood value in this research with ED demonstrated the higher light absorption by blood, and consequently confirmed the increase in blood content with ED. The reflectance profile versus source-detector distance was fitted to a simple exponential model. The power of the exponential function decreased significantly with ED. Using the diffusion theory, estimates of the absorption and reduced scattering coefficient were calculated. The absorption coefficient increased with ED and the reduced scattering coefficient decreased.

In conclusion, this work provides a new, fast and objective destructive methodology to quantify changes in the angiogenesis of the CAM under different incubation conditions. Early prenatal hypercapnia, one of the potentially beneficial conditions during incubation, was shown to stimulate the growth of the vascular network in the CAM. Spatially resolved spectroscopy was used, for the first time, to analyze the CAM tissue as initial phase to a non-destructive technique. Based on these measurements, significant differences in the light propagation in the CAM tissue of different ED were detected.

LIST OF ABBREVIATIONS

bFGF	basic fibroblast growth factor
CAM	chorioallantoic membrane
ED	embryonic day
EBC	extrapolated boundary condition
FD	fractal dimension
Hb	hemoglobin
HbO_2	oxygenated hemoglobin
NIR	near infrared light
NIRS	near infrared spectroscopy
R&R	Repeatability and reproducibility
RH	relative humidity
SRS	spatially resolved spectroscopy
VDI	vascular density index
VEGF	vascular endothelial growth factor
VF	vascular fraction
VIS	visual light
ZBC	zero boundary condition

LIST OF SYMBOLS

γ	gamma parameter
δ	penetration depth of light
θ	scattering angle
λ	wavelength
μ_a	absorption coefficient
μ_{eff}	effective attenuation coefficient
μ_s	scattering coefficient
μ'_s	reduced/ transport scattering coefficient
μ_t	total attenuation coefficient
μ'_t	reduced/transport total attenuation coefficient
ρ	source-detector distance
Φ	fluence rate
A	internal reflection parameter
B	dark current
BV	blood value measured in reflectance mode
CO_2	carbon dioxide
D	diffusion coefficient
f	collection fiber
g	anisotropy factor
g_1	first moment of the phase function (= g)
g_2	second moment of the phase function
$I_{Integrating\ sphere}$	intensity measured in the integrating sphere
I_{Tissue}	intensity measured on the tissue
mfp	mean free path
mfp'	effective/transport mean free path
n	refractive index

n_{rel}	relative refractive index
n_t	refractive index of the tissue
n_v	refractive index of the air
N	ratio scattering to absorption coefficient
N'	ratio transport scattering to absorption coefficient
O_2	oxygen
pCO_2	carbon dioxide pressure
pO_2	oxygen pressure
$p(\hat{s}',\hat{s})$	phase function
r_d	internal reflection of uniformly diffuse radiation
R	reflectance
$R_{Measured}$	measured reflectance
$R_{Theoretical}$	theoretically modeled reflectance
s	scaling factor
s^2_{gauge}	gauge R&R variance
s^2_O	variance component due to the operator
s^2_{OP}	variance component due to the interaction between the operator and the parts
s^2_P	variance component due to the parts
s^2_R	residual variance component
$s^2_{reproducibility}$	variance component due to the reproducibility
$s^2_{repeatability}$	variance component due to the repeatability
s^2_{total}	total variance
sphere	integrating sphere
T	integration time
z_0	depth of isotropic point source in the tissue
$<z>$	average photon depth reaching a detector

Chapter 1

General Introduction

1.1 The importance of the chicken incubation period

The poultry sector becomes more and more aware of the importance of optimizing the conditions during incubation, besides optimizing the management conditions post hatch, to obtain well developed and healthy chicken (Collin *et al.*, 2007; De Oliveira *et al.*, 2008). Not only high levels of hatchability are important, but also a good quality of the chick resulting in a good health and posthatch performance (Willemsen *et al.*, 2008). The selection in broilers provides a high potential for good quality chicken. However, this is only achieved with optimal management, not only post hatch but also during the incubation, since they become more vulnerable to non-optimal management conditions (Collin *et al.*, 2007; De Oliveira *et al.*, 2008; Decuypere *et al.*, 2000; Hulet, 2007; Yahav, 2000). Moreover, due to the selection for rapid growth and the associated reduction in slaughter age in broiler chicken, the embryonic period becomes a relative greater proportion of the chicken life (De Oliveira *et al.*, 2008; Hulet, 2007). Furthermore, recent research shows that the conditions imposed during the embryonic life may have important consequences on health and disease in adult life. These findings led to the developmental origins of health and disease paradigm (Barker, 1995; Barker *et al.*, 1990; Gluckman and Hanson, 2004; Gluckman *et al.*, 2005). For example, ascites, a syndrome which is related to cardiovascular and pulmonary ailments, is one of the most important causes of non-infectious mortality in the broiler sector, and therefore has a major impact on production and animal welfare. It is associated with a discrepancy between O_2 need and O_2 supply (Summers, 1993). This condition normally occurs at high altitude because of the lower O_2 pressure in the air. However, nowadays the problem arises also at sea level because of the increased O_2 demand in chicken selected for rapid growth. One of the hypotheses postulates that the onset of the disease might already be set at embryonic stage due to stress such as hypoxic, *i.e.* low O_2, conditions that occur in the second half of the incubation. The embryo continues to grow, however the O_2 consumption is limited due to the gas exchange possibilities. This period of critical hypoxia may trigger structural changes in the lungs and/or the heart from which a predisposition to ascites arises (Decuypere *et al.*, 2000). Consequently, the incubation period has an important potential of improving the birds growth, metabolism and health. The latter have consequences for animal welfare as well as for economical profit.

1.2 Parameters of the incubation period

To be able to optimize the incubation period, parameters to evaluate the development, metabolism and health of the embryo should be determined and monitored during embryonic growth under different conditions. Plausible parameters are the embryonic weight, organ weight and morphology, gas analysis of the blood and air cell, heat production measurements, hormone levels and angiogenesis, *i.e.* blood vessel development, in the chorioallantoic membrane (CAM). The important variables during incubation which must be controlled to ensure good post hatch chick quality are the temperature, humidity, turning of the eggs and gas concentrations. The latter provide a yet rather unused potential for optimizing the growth and health of the chicken.

1.3 The parameters addressed in this research

In nature, the hen, by sitting on the eggs, increases the local temperature around the egg, the humidity and the CO_2 concentration whereas the O_2 concentration is decreased. Walsberg (1980) report an increase of the CO_2 concentration from 0.05 % in the beginning to 0.9 % in the end of incubation in a 13-egg clutch, and a decrease in O_2 concentration from 20.9 % to 20.0 %. Several recent studies have investigated the effect of hypercapnia, *i.e.* high CO_2 concentrations, on growth performance (Bruggeman *et al.*, 2007; Buys *et al.*, 1998; De Smit *et al.*, 2006; Everaert *et al.*, 2008). It is already shown that early hypercapnic incubations, in correspondence with the natural situation, may have beneficial effects. An increase in CO_2 during early incubation is reported to improve hatchability, accelerate pre- and postnatal growth, and hatching time (De Smit *et al.*, 2006; Tona *et al.*, 2007). Although these results are promising, there is a need for optimization of the dose and administration time window (De Smit *et al.*, 2006), and in consequence a need for knowledge about the physiological changes induced by different hypercapnia levels.

One of the parameters of chicken embryonic development which changes under different gas concentrations is the angiogenesis in the CAM. This is the organ for gas exchange during most of the embryonic development of the chicken, and is similar to the placenta in mammals. It is formed when the chorion and allantois fuse around 100 hours of incubation.

At embryonic day (ED) 5 it comes in contact with the inner shell membrane. By ED 10-11, the CAM extends to line the entire surface of the inner shell membrane. Gas exchange between the embryo and the environment is a passive diffusion process before lung ventilation starts at internal pipping. Both the eggshell and the CAM contribute to the resistance to this diffusion process. From literature data it is shown that the vasculature in the CAM, and correlated diffusing capacity of the CAM follows a pattern parallel to the O_2 uptake of the embryo, with a steady increase from around ED 6 to 14-15, after which a plateau phase is reached (Kurz *et al.*, 1995; Rahn *et al.*, 1979; Tazawa and Whittow, 2000). Finally, the CAM degenerates when lung ventilation is initiated during internal pipping (Ackerman and Rahn, 1981; Tazawa and Whittow, 2000).

It is demonstrated that early prenatal hypoxia increases angiogenesis in the CAM (Dusseau and Hutchins, 1989). The effects of hypercapnia on the angiogenesis in the CAM are not yet investigated. Hypercapnia may have a direct effect on the angiogenesis (Holmes *et al.*, 1994; Irie *et al.*, 2005). Systemic acidosis, resulting from hypercapnia or induced by other methods increases angiogenesis too (Holmes *et al.*, 1994; 1998). Up to date, no research is performed on the effect of hypercapnic conditions during incubation on the angiogenesis in the CAM. There is a need for a technique to monitor these changes. As the CAM is the organ for gas exchange, differences in angiogenesis in this membrane may have a major impact on the metabolism of the embryo and subsequently on the growth and health of the embryo. A better gas exchange is expected to result in a higher growth rate, a higher embryo weight and a better health. However, the relation between the O_2 exchange rate, and the embryo weight and/or health is not unambiguous. For example, in eggs with a lower eggshell conductance, and therefore a lower O_2 exchange rate, the embryonic mortality during the plateau phase of maximal O_2 uptake is lower (Bamelis, 2003). Following up the angiogenesis in the CAM as one of the parameters which influences the O_2 and CO_2 concentrations in the embryo, may elucidate aspects of these relations.

1.4 Research questions

Due to the high rate of angiogenesis that accompanies its development, the CAM is probably the most widely used *in vivo* assay for studying angiogenesis (Staton *et al.*, 2004). That is why different methods have already been developed to quantify angiogenesis in the CAM, although in another research domain than in the incubation research. In the studies for (anti-)angiogenic factors using the CAM, *i.e.* the CAM assays, test substances (stimulators or inhibitors) are added to a support, such as a graft or sponge, and placed on the CAM, either *in ovo*, by the use of a window in the eggshell, or *ex ovo* when the whole contents of the egg is placed in a petri dish (Ribatti *et al.*, 1996; Richardson and Singh, 2003). The first quantifications are based on visual examination of the CAM through the microscope and manual counting of the vessel density, which is subjective and time-consuming (Dusseau and Hutchins, 1989). To overcome these problems, digital cameras mounted on microscopes are used and the vessel density is calculated with the help of computer programs (Kirchner *et al.*, 1996; Parsons-Wingerter *et al.*, 1998). These methods however are not suitable to monitor the changes in angiogenesis in the CAM quantitatively under different gaseous incubation conditions during normal development. First, all of them make use of a microscope which enlarges the place on the CAM where (anti-)angiogenic factors are applied. However, for the analysis of CAM development under different environmental conditions, spot measurements are not sufficient because they will not be representative for the whole CAM as there may be local differences. Second, the egg should not be disturbed before the actual measurement because every disturbance, for example making an opening in the eggshell, can affect the normal angiogenesis in the CAM. Romanoff (1960) describes that after removal of the eggshell, the CAM may become both hypertrophic or atrophic within a short period (at least 2 hours). Third, the differences due to various environmental stress factors are possibly smaller than in the case of application of (anti-) angiogenic factors, and therefore require a highly sensitive method. Besides a high resolution, it is also a requisite to be able to analyze many samples. Only by analyzing large numbers of samples, the small differences between the groups can be detected over the random variability always present in a group of eggs. For that reason, the sample preparation and measuring technique must be easy and fast.

Finally, non-destructive techniques are necessary to follow up the chicken development throughout the incubation, and post hatch until slaughter age, as to eliminate inter-individual variability and reveal long-term effects of several changes. The embryo weight can be followed non-destructively by spectral transmission measurements until ED 10. Later on, the absorption in the egg is too high to be able to measure transmission (Kemps *et al.*, 2010). The angiogenesis in the CAM has the potential of being measured non-destructively later during incubation since it lies just underneath the eggshell. Moreover, blood has a very specific absorption spectrum of light. Therefore, it seems to be an excellent parameter to follow up non-destructively via spectroscopic measurements.

1.5 Objectives and outline of the dissertation

The aim of this study is the development of a technique to monitor the changes in angiogenesis in the CAM quantitatively, under different gaseous incubation conditions. Research of this kind asks for a multidisciplinary approach since it involves physiological and technical knowledge. Figure 1.1 gives a schematic overview of the structure of this dissertation. In the second chapter (2), an overview of the literature associated with different aspects of the research will be presented. First, literature data on the effects of different gas concentrations during incubation of the chicken embryo will be shortly reported. Secondly, the important aspects of angiogenesis and its regulation in general, and specific in the chicken embryo will be described. Thirdly, the existing methods to characterize the vasculature will be demonstrated, both in humans and in the chicken CAM. The main objective is then divided into three sub-objectives resulting in three experimental parts. The following three chapters (3, 4, and 5) will elucidate these experimental parts. From the study of the existing methods to analyze the vasculature, these appear to be inappropriate for this kind of research. Therefore, first, an objective, quantitative, destructive methodology to assess endogenous overall vascular development in the CAM of chicken embryos under different incubation conditions is developed. It is not meant to replace the existing CAM assays. But it provides a method for measuring the normal angiogenesis in the CAM of chicken embryo's. Moreover, some aspects may also be used to improve the existing CAM assays. This new methodology is evaluated for its reproducibility

and repeatability, and is validated in one experiment where eggs are incubated under hypoxic conditions from which it is known that they stimulate angiogenesis when induced from incubation day 7 until incubation day 14 (Dusseau and Hutchins, 1989). The results are published in Verhoelst *et al.* (in press-a), and will be presented in chapter 3. Secondly, this fast and objective destructive methodology is used to quantify the changes in the vascular network of the CAM under hypercapnic conditions, built up gradually during the first ten days of incubation. The results are published in Verhoelst *et al.* (in press-b), and will be presented in chapter 4. Thirdly, a spectroscopic technique is investigated for its use in measuring changes in angiogenesis in the CAM during chicken embryonic development as a first step towards a potential non-destructive and non-invasive monitoring technique. These results will be shown in chapter 5. In a final chapter (6), the general conclusions and perspectives for further research will be summarized.

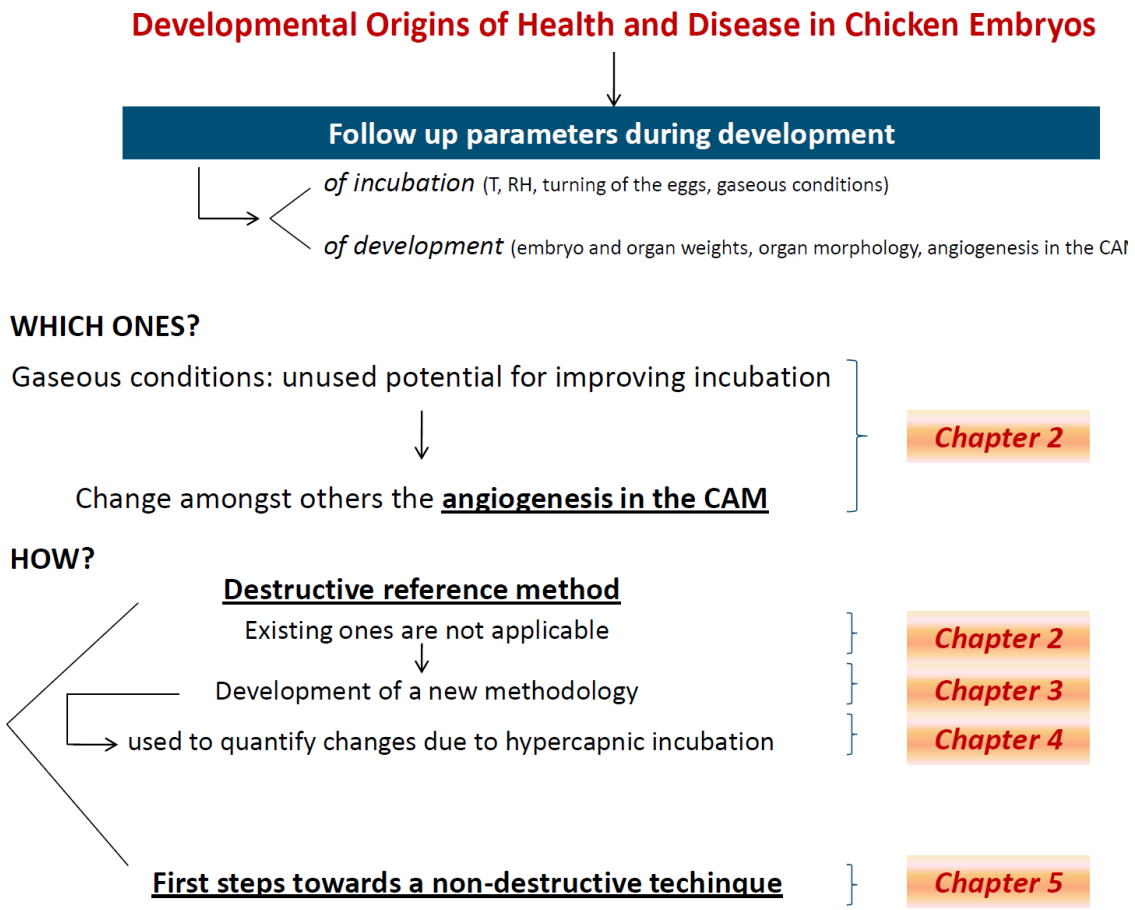

Figure 1.1 Overview of the structure of this dissertation

Chapter 2

Angiogenesis in the CAM:

A Multidisciplinary Approach

- Literature Study -

2.1 Introduction

The structural analysis of the angiogenesis in the chorioallantoic membrane of the chicken embryo, and the detection and interpretation of changes due to incubation under different gas concentrations, requires knowledge of different disciplines. In this second chapter, an overview is given of the important aspects which form the background for the research presented in this dissertation. The focus is put on the influence of different gas concentrations on the incubation of chicken embryos (section 2.2), angiogenesis and its regulation in general (section 2.3), and specific for the chicken embryo (section 2.4). Furthermore, the existing methods, destructive as well as non-destructive, for the structural analysis of the blood vessel development in general (section 2.5), and also specifically for the chicken embryo (section 2.6) are reviewed.

2.2 Gas concentrations during incubation of the chicken embryo

In this section, only the important aspects of the gas concentration during incubation of the chicken embryo for this research are mentioned. It is not intended to give a full review. This can be found elsewhere in more detail (Mortola, 2009; Onagbesan *et al.*, 2007).

In the beginning of their development, chicken embryos exchange O_2 and CO_2 with the environment by simple diffusion through the pores of the eggshell. The primary organ for gas exchange is the area vasculosa, a well vascularized region of the yolk sac. However, already early in development, this area vasculosa becomes insufficient to accommodate the rise in embryonic metabolism and the associated need for O_2. Hence, around 100 hours of incubation, the allantois fuses with the chorion to form the chorioallantoic membrane (CAM). This is a well vascularized membrane, analogous to the placenta of mammals, which lines the inside of the eggshell completely at embryonic day (ED) 10-11 (Ackerman and Rahn, 1981; Mortola, 2009; Romanoff, 1960; Tazawa and Whittow, 2000). The diffusing capacity of the CAM increases with the growth of the embryo but reaches a plateau around ED 15-16. This diffusing capacity is a function of the capillary blood flow, the contact time of the red blood cells with O_2, the mean oxygenation velocity during the contact time, and the hematocrit value (Tazawa and Mochizuki, 1976). The O_2 diffusing capacity increases mainly

by the increased surface area and increased blood volume associated with an increased vascular density (Defouw *et al.*, 1989). Due to its dense vascular network, the CAM creates an ideal setting for gas exchange with the environment. From the moment of internal pipping in the air cell, the lungs start to function and gradually replace the CAM as respiratory organ (Ackerman and Rahn, 1981; Mortola, 2009; Romanoff, 1960; Tazawa and Whittow, 2000). The formation of blood vessels in the CAM and associated gas exchange will be reviewed in paragraph 2.4.3.

Nowadays, chicken embryos develop in incubators in which the gaseous environment is controlled by ventilation to achieve optimal hatchability and chick quality. O_2 concentrations are around 21 %, and CO_2 concentrations are allowed to rise up to 0.5% at varying periods during incubation (Onagbesan *et al.*, 2007).

O_2 concentrations in the nest during incubation under natural conditions may decrease until 20.0 % (Walsberg, 1980). At high altitude however, lower partial pressures of O_2 may be experienced by the embryo due to the lower atmospheric pressure (Hassanzadeh *et al.*, 2002). The effect of hypoxia, *i.e.* reduced O_2 availability for the embryo, on incubation results depends on the duration (chronic or acute), timing during incubation, and intensity (Onagbesan *et al.*, 2007). Hypoxia reduces the weight of the embryo, but seems to spare essential organs such as the brains (Giussani *et al.*, 2007; Miller *et al.*, 2002). The tolerance of the embryo to hypoxia increases with age (Onagbesan *et al.*, 2007). However, hypoxia in the last stages of development may predispose the chicken embryo to cardiovascular diseases in adult life, such as seen in ascites chicken, by structural changes in the cardiovascular and pulmonary system (Decuypere *et al.*, 2005). Hypoxia may also alter the vascular endothelial function. These changes in function may be persistent, which may finally lead to cardiovascular disease in adult life (Ruijtenbeek *et al.*, 2000). In general, hypoxia may compromise survivability and health in adult life. However, different researchers report adaptations to incubations under hypoxia, namely an increased vascular network of the CAM under early hypoxia (Dusseau and Hutchins, 1989; Strick *et al.*, 1991), and a higher affinity of the red blood cells for O_2 (Dragon and Baumann, 2003). Molenaar *et al.* (2010) describe a more efficient nutrient utilization in embryos incubated at low O_2 from day 7 until day 19 when 21 % O_2 is reestablished at day 19. Hassanzadeh *et al.* (2004) report

an influence of high altitude conditions on the endocrine function of the embryo. This affects hatching parameters, thereby lowering the incidence of ascites mortality in broilers incubated at high altitude and growing at high altitude compared with those incubated at low altitude but growing at high altitude. Moreover, there seem to be adaptations to hypoxia induced by the hens laying conditions. Giussani *et al.* (2007) compared in their research 5 different groups for their growth and hatchability. The 5 groups comprised eggs laid at high altitude and incubated at high altitude (HAHA), eggs laid at sea level and incubated at sea level (SLSL), eggs laid at sea level but incubated at high altitude (SLHA), eggs laid at high altitude and incubated at sea level (HASL), and eggs laid at sea level and incubated at high altitude but with exogenous O_2 delivery (SLHA+O_2). At high altitude incubation (HAHA, SLHA), there was an increase in embryonic mortality and a decrease in weight with sparing of the vital organs such as the brains. However, in HAHA these effects were dampened, and with O_2 supply (SLHA+O_2) the effects were suppressed. In conclusion, eggs laid at high altitude seem to have an advantage over eggs laid at sea level but incubated at high altitude.

Under natural conditions the CO_2 concentration in the nest builds up from 0.05% to 0.9% by the end of incubation due to the metabolism of the embryo (Walsberg, 1980). During early incubation, the CO_2 concentrations around the eggs increase as well due to the CO_2 removed from the venous blood in the brood patch of the hen (Decuypere, 2010). Since hypercapnic incubation might have some advantages on the development of the chicken embryo, it is applied in incubation practice. However, there is still a need for knowledge about the different mechanisms by which hypercapnia interacts with the development. De Smit *et al.* (2006) compared the natural evolution of CO_2 in the incubator between a closed incubation for the first ten days and a normal ventilated incubation keeping the CO_2 concentration at 0.1%, and studied the effect on embryo growth and hatchability. In the closed incubation, CO_2 levels could rise up to 1.5 %. The embryos of the closed incubation had significantly higher weights and hatched earlier with a narrower spread of hatch. Post hatch this higher weight was maintained. Buys *et al.* (1998) investigated the effect of hypercapnia (0.4 %) during the third week of incubation and reported an earlier hatch and a lowered ascites incidence during the growing period compared to embryos incubated under normal CO_2 concentrations. As well as for hypoxia, the effect of hypercapnia will depend on the

duration, timing, intensity, and also on the starting conditions such as line, storage of the eggs, and flock-age (Witters, 2009).

Both hypoxia and hypercapnia may also interact with the temperature. Temperature is a very crucial parameter for development of the chicken embryo since it influences the metabolic rate (Lourens, 2008; Romanoff, 1960). The eggshell temperature as a measure for the embryonic temperature is determined by the balance between heat production and heat transfer from the egg. Lourens *et al.* (2005) report that a constant eggshell temperature of 37.8 °C throughout incubation results in the highest hatchability and highest embryonic development in terms of embryo length and weight. So, the embryonic temperature, the gas exchange possibilities, or a combination of both may limit the embryonic development. Before the plateau phase of O_2 consumption is reached, eggshell temperature has a significant effect on the heat production measured by the O_2 uptake and CO_2 consumption of the embryo. Later in incubation, during the plateau phase, O_2 availability becomes more important in determining embryonic heat production (Lourens *et al.*, 2007). The combination of high embryonic temperature and low O_2 levels from day 7 until 19 is negative for the embryonic development as this significantly increases embryonic mortality during the third week of incubation (Molenaar *et al.*, 2010).

2.3 Angiogenesis and its regulation in mammals

Gas exchange, metabolism, growth, and angiogenesis during development are tightly linked. To monitor and control embryonic growth under different gaseous environments, one of the important parameters to measure is the blood vessel development in the chorioallantoic membrane since this may be altered. In what follows, first, a short description of the structure and function of blood vessels and their formation will be given. Subsequently, the most important, known mechanisms of the regulation of angiogenesis in mammals will be reviewed in more detail. After all, all these processes are very similar and just as complex in mammals as in birds (Burt, 2007; Ruijtenbeek *et al.*, 2002). In this way, the research is placed in a more general framework which forms a background for interpretation of the results in the study. Thereupon, in the next section, the already revealed specific processes in avian angiogenesis will be reviewed.

2.3.1 Structure and function of blood vessels

Blood vessels consist of endothelial cells, which line the lumen, and for larger vessels also mural cells, namely pericytes in medium-sized, and smooth muscle cells in large vessels. Arteries and arterioles (smaller) carry the blood that comes from the heart to the organs, which is O_2 rich except in the arteries going to the lungs. The veins and venules (smaller) carry the blood that comes from the organs to the heart, which is oxygen poor except in the veins coming from the lungs.

The function of the blood vessels is the transport of blood with molecules to exchange with tissues and organs as to keep homeostasis in the healthy organism. Malformation and dysfunction of blood vessels contribute to many diseases (Adams and Alitalo, 2007).

2.3.2 Formation of blood vessels

Vasculogenesis is the *de novo* formation of blood vessels by the differentiation of endothelial cells from mesodermal precursors, namely angioblasts. It occurs in early embryogenesis to form the primary capillary plexus. Research points out the possible role of circulating endothelial precursors in forming blood vessels in adult life too (Carmeliet, 2003).

Angiogenesis is the process of generating new blood vessels derived as extensions from the existing vasculature (figure 2.1).

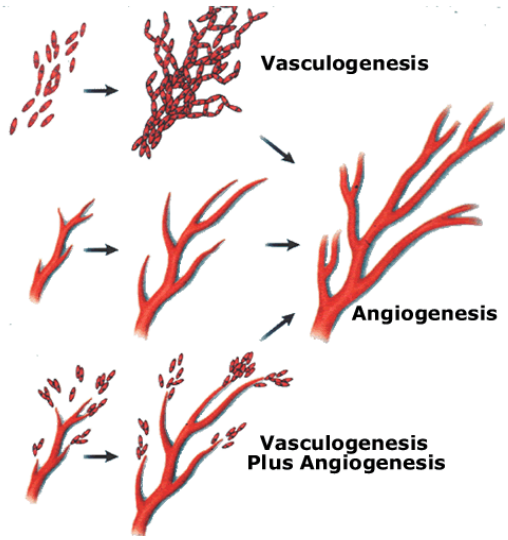

Figure 2.1 Vasculogenesis and Angiogenesis (Harvey and Rosenthal, 1999)

There are different mechanisms of angiogenesis, namely sprouting, intussusception, elongation and incorporation of circulating endothelial progenitor cells into growing vessels (Gargett and Rogers, 2001). Intussusception is the formation of transcapillary pillars of interstitial tissue in the vascular lumen (figure 2.2) (Djonov *et al.*, 2000; Kurz *et al.*, 2003; Patan *et al.*, 1997). Arteriogenesis is the maturation of the endothelium-lined channels formed by angiogenesis via recruitment of smooth muscle cells (Carmeliet, 2000).

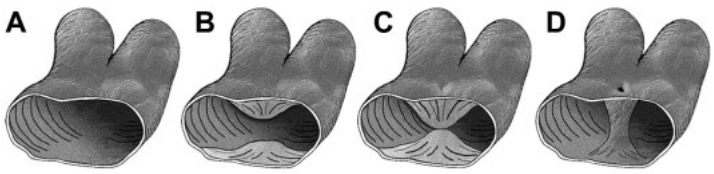

Figure 2.2 Basic steps of intussusception: protrusion of opposing capillary walls into the lumen (A and B) and creation of a contact zone between the endothelial cells (C). The fused endothelial cells form a transcapillary pillar, invaded later by myofibroblasts or pericytes (D) (Kurz *et al.*, 2003).

2.3.3 Regulation of angiogenesis

In early development the primary network is formed by vasculogenesis and consists of the aorta, the major veins and a honeycomb-like plexus connecting these major vessels. This

network is modified by angiogenic remodeling to form the branching pattern of the mature vasculature. The vessel walls mature, as endothelial cells integrate with supporting cells (smooth muscle cells and pericytes) and the surrounding matrix, and the blood vessels stabilize. All these processes must be tightly regulated (Yancopoulos *et al.*, 2000).

Blood vessel formation is regulated through a balance between angiogenic stimuli and angiogenic inhibitors. Endothelial cells are most of the time in quiescent state. Whenever positive regulators predominate, the endothelial cells become activated and angiogenesis will occur. The regulators can be physical factors such as hypoxia and pH, and can be molecules such as cytokines (Adams and Alitalo, 2007). The cytokines act directly on the endothelial cells via binding to a receptor or indirectly via inducing the production of direct-acting regulators by non-endothelial cells. Moreover, the extracellular matrix and its interactions with the growth factors play a role in the regulation of angiogenesis (Adams and Alitalo, 2007).

There are three families of vascular endothelium-specific growth factors: (1) the *VEGF family* (VEGF-A or VEGF, VEGF-B, VEGF-C, VEGF-D, VEGF-E, and placental growth factor PlGF), (2) the *angiopoietin family* (Ang1, Ang2, Ang3, and Ang4), and (3) the *ephrin family* (Ephrin-B1, Ephrin-B2, and Ephrin-A1). The latter are important in the differentiation in arteries or veins. Ephrin-B2 ligand is a marker for arterial endothelium and EphB4 receptor marks venous endothelium (Yancopoulos *et al.*, 2000).

Beside the differences in growth factors themselves, there are also differences in the receptors with which the growth factors can interact, and so induce different processes. VEGF is a very critical vascular regulator and its dosage must be regulated in spatial, temporal and quantitative manner. By binding to a specific receptor on the endothelial cell membrane, the cell becomes activated and a cascade of reactions is initiated. The main receptors for the VEGF family are tyrosine kinases, namely vascular endothelial growth factor receptor VEGFR-1, VEGFR-2, and VEGFR-3 (figure 2.3). Those transmembrane receptors are expressed selectively on vascular endothelial cells (Otrock *et al.*, 2007). VEGFR-2 mediates the growth and permeability actions of VEGF while VEGFR-1 has a negative role, by acting as a decoy receptor, since it has a weak tyrosine phosphorylation in response to VEGF (Ferrara, 2004; Genetech, 2009; Meyer *et al.*, 2006). VEGFR-3 is crucial for lymphatic

vessel formation but may also play a role in blood vessel formation. The angiopoietins bind to the Ties, also a family of receptor tyrosine kinases mainly expressed in the vascular endothelium (figure 2.3). The angiopoietins, particularly Ang1, bind primarily to Tie2, which stabilizes the mature blood vessels. The antagonist of Ang1, Ang2 is induced by endothelium to be remodeled and destabilizes the blood vessels (Yancopoulos *et al.*, 2000). PIGF, or placental growth factor, strongly expressed in the placenta of mammals, may also be important in adult vascular remodeling. It binds to VEGFR-1 and has therefore a weak stimulatory effect on angiogenesis. It is more likely to form long, poorly branched vessels (Ancar and Chardonnens, 2003). VEGF-B seems to have a role in coronary vascularization and growth. VEGF-C binds to the VEGFR-3 receptor and plays a role in lymphatic vessel formation. VEGF-D and VEGF-E have a still unknown physiological role (Yancopoulos *et al.*, 2000). In addition, non-vascular endothelium-specific growth factors are also required for blood vessel formation, like the fibroblast growth factor family (FGF), the transforming growth factor family (TGF) and the platelet derived growth factor (PDGF), which all have supporting roles for the angiogenic process (Donati and Gozdzikiewicz, 2008; Yancopoulos *et al.*, 2000).

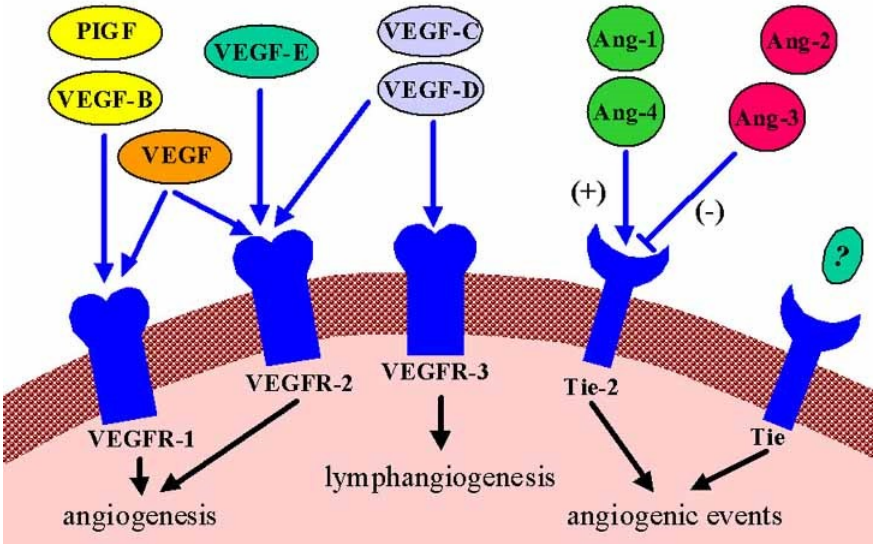

Figure 2.3 The VEGF family of endothelial-specific growth factors includes VEGF (VEGF-A), placental growth factor (PlGF), VEGF-B, VEGF-C, VEGF-D, and VEGF-E. These bind differentially (indicated by arrows) to receptors VEFGR-1, -2, and -3, promoting either angiogenesis (VEGFR-1 and 2) or lymphangiogenesis (VEGFR-3). The angiopoietins (Ang-1, -2, -3, and -4) interact with the Tie-2 receptor. Whereas Ang-1 and Ang-4 are agonists, with binding causing angiogenic events, Ang-2 and

Ang-3 are antagonists, and cause inhibitory effects at this receptor, leading to vascular regression. The role of Tie-1 is less well defined. (Brat *et al.*, 2003)

Also physical factors influence angiogenesis, directly or indirectly via interactions with the molecular regulators. (1) *Hypoxia* affects angiogenesis through different molecular factors. The most important one is the hypoxia-inducible factor-1 (HIF-1), a heterodimer and key regulator, via binding to DNA, in many processes among which angiogenesis. HIF-1α upregulates the transcription of hypoxia-inducible genes and so the formation of VEGF, PDGF-β, TGF-α and erythropoietin (EPO) (George and Kaelin, 2003). In normoxic conditions the von Hippel-Lindau tumor suppressor protein (VHL) binds to HIF-1α, which is then destroyed by proteolysis, so preventing transcriptional activation of its target genes. In hypoxic conditions, HIF-1α is not degraded and can activate its target genes. This factor plays a crucial role in tumor malignancy via the angiogenic switch (Bradbury, 2001). Hypoxia plays also an important role in placental and embryonic vascularization (Ancar and Chardonnens, 2003). Recent research demonstrates that blood vessel formation induced by VEGF leads to leaky and immature vessels, but blood vessel formation induced by HIF-1α leads to stable blood vessels (Yancopoulos *et al.*, 2000). (2) A second physical factor is the *pH*. The microenvironment of the majority of tumors is acidic due to the anaerobic glycolysis. Although microvascular growth in acidic conditions in the absence of growth factors is retarded compared to normal conditions, the stimulatory effect of VEGF and bFGF on angiogenesis is enhanced by low pH (Burbridge *et al.*, 1999). Goerges and Nugent (2003), who find an increased binding activity of VEGF to endothelial cells and to the extracellular matrix (ECM) under acidic conditions, suggest that VEGF is stored in the ECM, and released when the pH returns to neutral values. Moreover, the transcription of VEGF is shown to be increased by acidic pH (D'arcangelo *et al.*, 2000; Fukumura *et al.*, 2001; Xu *et al.*, 2002). (3) Another physical factor is the *shear-stress* induced by the blood flow as soon as the heart begins beating (Kurz, 2000; Le Noble *et al.*, 2004).

In contrast with the vast research on the influence of hypoxia on angiogenesis, less is known about the influence of hypercapnia on angiogenesis, although both conditions may coincide. Howell *et al.* (2004) and Ooi *et al.* (2000) conducted different studies to assess the role of hypercapnia alone, and hypercapnia in combination with hypoxia, in vascular remodeling

causing pulmonary hypertension. They found that hypercapnia stimulated angiogenesis, although the changes were less pronounced than caused by hypoxia alone. In combination with hypoxia however, hypercapnia reduced the effect of hypoxia, and there were no significant differences in angiogenesis compared to the control group. Holmes *et al.* (1994; 1998) investigated the influence of hypercapnia on neovascularization in the case of retinopathy in prematurity. Hypercapnia resulted in retinal neovascularization of premature rats. Moreover, they found that general systemic acidosis, resulting from CO_2 inhalation or induced via other methods, caused neovascularization. A critical decrease in blood pH was necessary (pH decrease to 7.1). A short period of 24 hours was enough to induce the effect, but the minimum duration of acidosis required was not determined. A period of recovery was not necessary, although neovascularization was maximal after 2 to 5 days of recovery. So, the effect of acidosis on angiogenesis was maximal a certain time after the initial trigger. The vascular changes induced by acidosis were sustained. Leske *et al.* (2006) found that VEGF as well as insulin-like growth factor-1 (IGF-1) could play an important role in the process. Irie *et al.* (2005) found that CO_2-rich water bathing as treatment of peripheral vascular disorder had, beside its nitric oxide (NO)-mediated vasodilatation effect, also an effect on new vessel formation mediated by VEGF and NO.

From the literature data described above, it can be concluded that angiogenesis is regulated by a whole range of different kinds of factors. All of them have to act in harmony to form functional vessels (Yancopoulos *et al.*, 2000).

2.4 Angiogenesis during development of the chicken embryo

To understand the angiogenesis during chicken development, first a short overview of avian embryogenesis will be given (paragraph 2.4.1). In the following paragraph (2.4.2), the avian embryonic and extraembryonic angiogenesis is described with, in the third paragraph (2.4.3), emphasis on the angiogenesis in the CAM.

2.4.1 Avian embryogenesis

After mating, the male sperm cell unites with the female ovum to form a single cell. Cell divisions start about 5 hours after fertilization and continue until the egg is laid. The cluster

of cells is called the blastoderm, which is a layer of cells that develops on the surface of the yolk and which gives rise to the embryo. Initially, the dividing cells form one layer, but as cell division continues the blastoderm is divided in an epiblast and a hypoblast. Later on it divides into the three germ layers, the ectoderm, mesoderm and endoderm, from which the embryo develops (Romanoff, 1960).

The germinal disk can be distinguished in an area pellucida, the central transparent area of the blastoderm and an area opaca, the opaque peripheral area of the blastoderm, continuous with the yolk. The latter consists of the area vasculosa, the vascularized zone and the area vitellina, the outer nonvascular zone of the area opaca which consists of ectoderm and endoderm (figure 2.4). The sinus terminalis is a circular blood sinus bordering the area vasculosa, and forming the advancing edge of the area vasculosa (Romanoff, 1960).

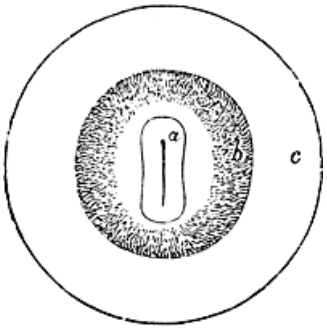

Figure 2.4 Germinal disk in the avian egg: a=area pellucida, b=area vasculosa, c=area vitellina (Baker and Harris, 1892; Clipart, 2009)

The mesoderm cleaves into an upper, or somatic, and a lower or splanchnic layer (figure 2.5). Spaces between these layers are enclosed and form the coelom. The ectoderm and the somatic mesoderm constitute the somatopleure. The endoderm and splanchnic mesoderm make up the splanchnopleure. The medial portions of the somatopleure, splanchnopleure, and coelom become incorporated in the body. The extraembryonic portions give rise to the membranes, namely the yolk sac, the amnion, the allantois, and the chorion. These membranes are semiautonomous from the embryo. Their functions are nourishment, protection, respiration and segregation of waste products. The amnion and the chorion are derived from the extraembryonic somatopleure, and the yolk sac develops from the extraembryonic splanchnopleure. The allantois arises from tissue that is transferred from the

yolk sac to the hind-gut and so also arises from the splanchnopleure. It grows out into the extraembryonic coelom as a diverticulum of the intestine. The body of the embryo becomes detached from the extraembryonic tissues, except for the umbilicus. The endodermal and ectodermal tissue gives functioning epithelial cells in the membranes, and the mesodermal tissue supplies the blood to and from this epithelium (Romanoff, 1960).

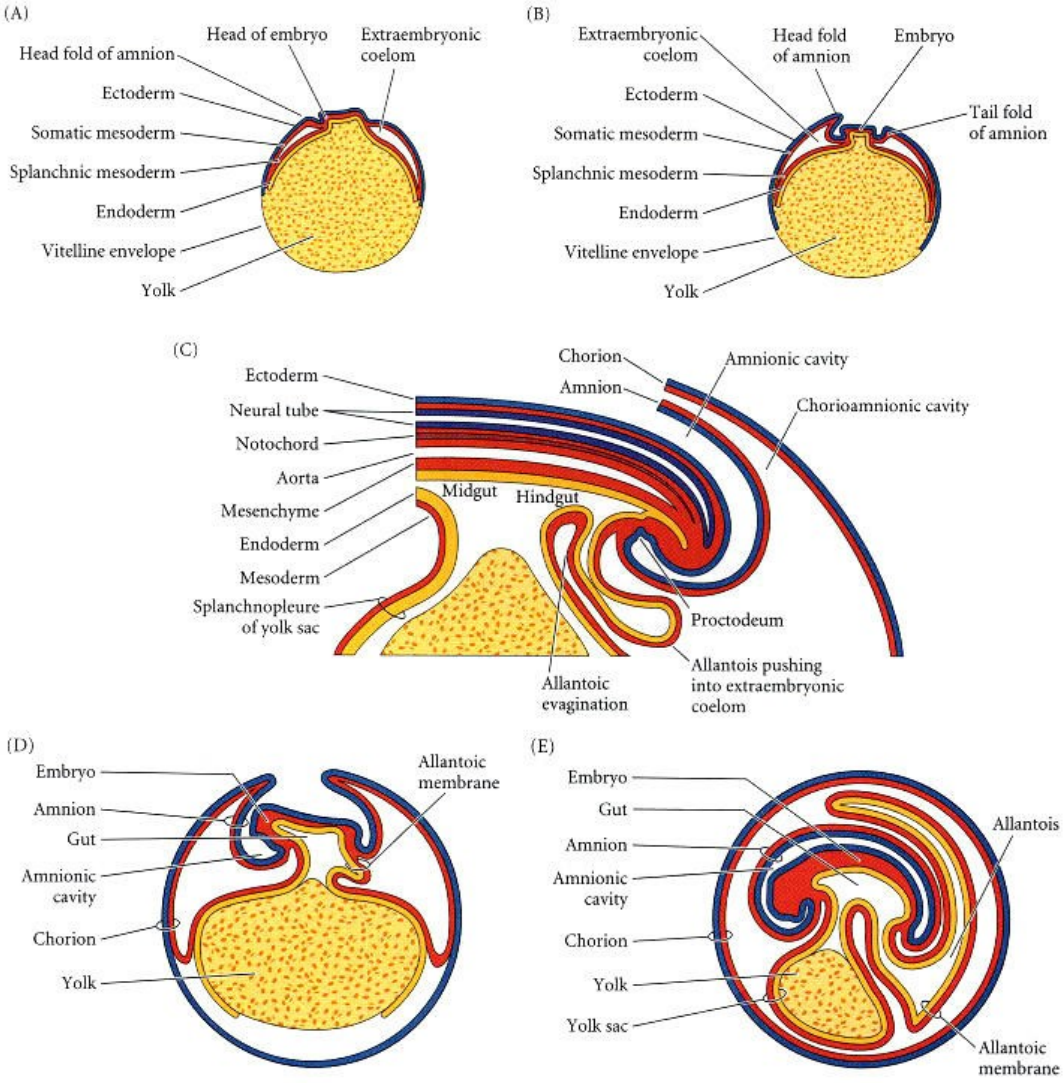

Figure 2.5 Schematic drawings of the extraembryonic membranes of the chick. The embryo is cut longitudinally, and the albumen and shell coatings are not shown. (A) A 2-day embryo. (B) A 3-day embryo. (C) Detailed schematic diagram of the caudal (hind) region of the chicken embryo, showing the formation of the allantois. (D) A 5-day embryo. (E) A 9-day embryo (Scott, 2003).

2.4.2 Avian embryonic and extraembryonic angiogenesis

Because of the limited diffusion distance of molecules (about 100-200 µm for O_2 in embryonic tissue (Eichmann *et al.*, 2005)), the vascular system has to be established early in development. Therefore, it is the first system formed during early embryonic development (Eichmann *et al.*, 2005). The extraembryonic circulation consists of the vitelline and allantoic circulation, while the intraembryonic circulation consists of vessels of head, aortic arch, pulmonary arteries, carotid arteries, dorsal aorta and other vessels (Romanoff, 1960).

Hematic and vascular tissues differentiate simultaneously from the mesoderm. The yolk sac is the major source of blood cells for the first half of the incubation period and continues to produce them almost until the hatching time. Clumps of hemangioblasts are formed in the area opaca which is the initial differentiation of the area vasculosa of the extraembryonic region. The extraembryonic hemangioblasts unite into a plexus of cellular cords/aggregates that become blood vessels. The peripheral cells of the hemangioblastic aggregates will differentiate into vascular endothelium. Many other hemangioblasts are enclosed within these newly formed blood vessels. So clumps of them can be seen adhering to the endothelium and these are called the true blood islands (figure 2.6). These blood islands will differentiate into the first blood cells. The first vascular spaces appear at the 5- to 7-somite stage (around 35 hours of incubation). These vascular spaces coalesce and form a continuous network of vessels, the primary plexus (Romanoff, 1960).

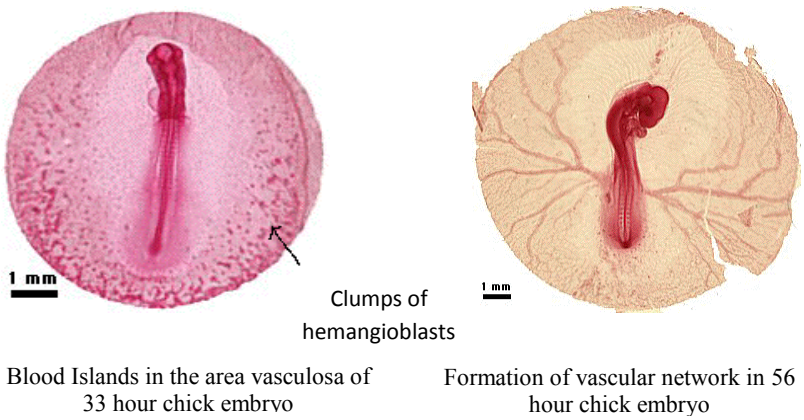

Figure 2.6 The area vasculosa of a 33 hour chicken embryo with blood islands (left image) and a 56 hour chicken embryo with a vascular network (right image) (Brownuniversity, 2009)

In the embryo too, a primary plexus is formed by vasculogenesis. At the 16- or 17-somite stage (end of ED 1), a sufficient number of primitive vessels are present to allow the blood to make a complete circuit through the embryonic body and the area vasculosa. The peripheral vascular spaces coalesce to form the marginal vein, the sinus terminalis, which lines the area vasculosa. In the beginning the blood takes the course of the least resistance. It goes centripetally to the sinus terminalis and from there returns to the embryo. From the 44th hour of incubation the heart begins beating, and the mechanical forces of the blood stream influence the formation of the network and the differentiation of the vitelline vessels into arteries and veins (figure 2.6) (Le Noble *et al.*, 2004). After removal of the heart, the vitelline arteries do not develop, while the area vasculosa continues to grow. This clearly shows the importance of the circulation in the formation of the network. At the 40-somite stage (around 60 hours of incubation), the sinus terminalis begins to break down into capillaries. The development of the vitelline vessels continues until the end of incubation (Romanoff, 1960).

In general, vasculogenesis in the embryo starts when VEGF binds to VEGF-R2 receptor which causes the differentiation of mesodermal cells into endothelial cells as well as their proliferation. When VEGF then binds to VEGF-R1, the formation of the capillary tube occurs, and it acts as a decoy receptor for VEGF-R2 so proliferation decreases. Finally Ang1 binds to the Tie2 receptor tyrosine kinase which leads to interactions between the blood vessel and peri-endothelial cells surrounding the vessel. These cells become pericytes and smooth muscle tissue around the blood vessel as to stabilize it. Further angiogenesis and remodeling requires a combination of Ang2 and VEGF. Ang2 blocks the Tie2 signal so that vessels become unstable by loosening of the support cells. If there is also VEGF, angiogenesis occurs. If not, the endothelium of the blood vessel separates from the peri-endothelial cells, the endothelial cells loose contact with each other, and the blood vessel regresses (Fan, 2009).

2.4.3 Blood vessels in the chorioallantoic membrane

From all extraembryonic membranes, the allantois appears last. The first signs are seen at the 20- to 28-somite stage (70 hours of incubation). It grows as an appendage of the hind-gut, into the extraembryonic coelom (figure 2.5) and spreads toward either pole of the egg (figure 2.7). Around 100 hours of incubation, the mesoderm of the allantois fuses with the

mesoderm of the chorion, and subsequently forms the chorioallantoic membrane (CAM), which then consists of three germ layers, endoderm, mesoderm and ectoderm. It is the embryonic respiratory organ and a deposit for waste products of the kidneys. Moreover it takes care of the calcium uptake out of the shell (Romanoff, 1960).

Around ED 7-8 the CAM has extended throughout the blunt half of the egg and has reached the equator. Eventually, it encloses the entire contents of the egg at ED 10-11. The inner allantoic wall covers the amnion and the yolk sac, and fuses with the amnion at day 7 (Romanoff, 1960).

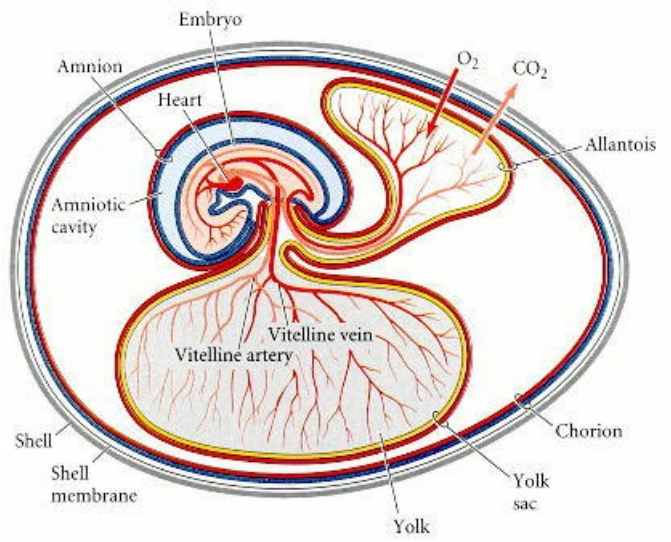

Figure 2.7 Schematic drawing of the embryo, amnion, yolk sac, allantois and chorion with the blood vessels in the yolk sac, the allantois, and the embryo (7 days old) (Scott, 2003)

The CAM is a highly vascularized membrane. The blood vessels from the embryo are connected with the ones from the CAM via the allantoic stalk. The mayor blood vessels are the (left) allantoic or umbilical vein, and the right and left allantoic or umbilical arteries. On ED 13, the terminal capillaries have grown towards the eggshell by penetrating the ectodermal layer. The capillary network is so fine and so dense, it becomes an ideal respiratory organ. Due to the small diameter of the vessels, blood cells are forced to pass one by one. This causes a high reduction of speed which creates essential circumstances for gaseous exchange. When they converge again in larger vessels, the speed increases and the blood passes into the vein rapidly and smoothly. In the chorioallantois, the veins contain

bright red blood, so higher in O_2 contents. After pulmonary respiration begins, the CAM circulation becomes less active and many vessels empty (Romanoff, 1960).

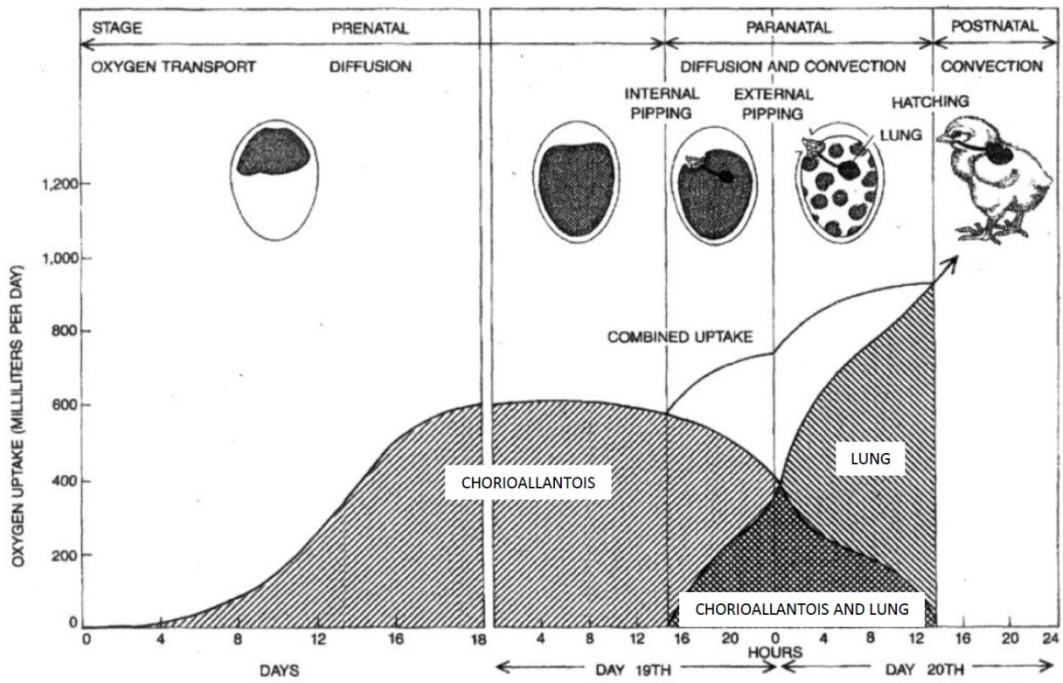

Figure 2.8 O_2 consumption of the chicken embryo. There is a sigmoid increase, and near the end of incubation, a gradual switch from diffusive gas exchange through the CAM to active breathing through the lungs (Rahn *et al.*, 1979)

The growth of the vascular network in the CAM results in an increase of the O_2 diffusing capacity of the CAM in a sigmoid fashion, parallel to the change in O_2 uptake of the embryo. The O_2 consumption of the embryo increases slowly during the first week and a half of incubation (figure 2.8). A sharp increase in O_2 consumption is observed from ED 9 to 14 and it reaches a plateau at ED 15-16 of around 600 mL per day. The latter is the maximum value which can be obtained by passive diffusion through the pores in the eggshell (Tazawa and Whittow, 2000). This maximum value is affected by the eggshell conductance (Bamelis, 2003), which on its turn is affected by, amongst others, breed and breeder flock age (Peebles and Brake, 1987). Kirchner *et al.* (1996) observe a steady increase in density and fractal dimension, a measure for the branching degree and complexity of the vascular network, from days 6 to 14, and afterwards they decrease from day 15 onwards. The increase in density of the larger pre-and postcapillary vessels until day 14 is confirmed by Kurz *et al.*

(1995). Data from Wagner-Amos and Seymour (2003) show an increase in density of the vascular network until day 15. The increase is not linear with time as shown by the study of Nikiforidis *et al.* (1999).

In literature, the development of the pre- and postcapillary network is distinguished from the development of the capillary plexus. While the density of the pre- and postcapillary blood vessels continues to increase until day 14 (Kurz *et al.*, 1995), the capillary plexus is formed and grows rapidly from ED 4-5 via vasculogenesis and sprouting angiogenesis (Melkonian *et al.*, 2002), but the proliferation decreases after ED 11 (Ausprunk *et al.*, 1974; Burton and Palmer, 1992). Schlatter *et al.* (1997) and Melkonian *et al.* (2002) divide the formation of the capillary plexus in three phases. From ED 4 to 5-6, the capillary network forms and expands. The mesodermal blood vessels migrate closer to the ectoderm and differentiate into a plexus by vasculogenesis, followed by sprouting angiogenesis. From ED 7 to 11, the main process is intussusceptive microvascular growth, with associated lower endothelial cell proliferation compared to sprouting (Djonov *et al.*, 2000). From ED 12 to 13, there is expansion of the network with only a small increase in complexity. Meanwhile, from ED 7 onwards until ED 13 the capillaries migrate to the eggshell and invaginate the chorionic ectoderm to minimize the diffusion distance for the exchange of respiratory gases (Wagner-Amos and Seymour, 2003).

The processes involved in the capillary plexus formation are at first sprouting, but very soon intussusceptive microvascular growth is the main process which leads to increased density and complexity, as described above. The pre- and postcapillary vascular network also grows by different angiogenic processes, namely sprouting, elongation, fusion and intussusceptive growth (figure 2.2) (Kurz, 2000). The latter is also called intussusceptive arborization (Djonov *et al.*, 2000).

Up to this date, the vascular growth in the CAM of the chicken embryo seems regulated mainly by VEGF and FGF. Both work as an autocrine or paracrine stimulator of angiogenesis (Ribatti and Presta, 2002). Flamme *et al.* (1991) conclude from their experiments, that basic and probably acidic FGF in the chorioallantoic fluid play an important role in the regulation of the chorioallantoic vascular growth by their angiogenic and mitogenic activity. In this regard the chorioallantoic fluid would be more than a waste reservoir. However, Ribatti *et*

al. (1995) conclude from their results that bFGF located in the CAM, rather than that present in the chorioallantoic fluid, regulates the angiogenesis. The levels of active bFGF reach maximal concentrations between days 10 and 14 of incubation (Ribatti *et al.*, 1995). Ten Busch *et al.* (1997) state that the allantois, aside from being a waste collector, may also be a molecular or metabolic storage area.

In conclusion, angiogenesis in both mammals and birds is a very similar and tightly regulated process. A number of regulating factors and their functions are already revealed. However, still unknown factors and their interactions with the described ones, may also play important roles.

2.5 Structural analysis of blood vessel development

The aim of this research was the development of, on the one hand, a destructive method for quantification of changes in the endogenous angiogenesis in the CAM, which can serve as a reference for, on the other hand, a non-destructive method.

In different medical conditions, the understanding, monitoring and control of the angiogenesis process is very crucial, for example in tumor growth. Therefore, ideas for measuring the angiogenesis in the CAM of the chicken embryo may be found in human medicine and the associated research. Different parameters can be determined to evaluate the angiogenesis, such as the blood volume, vascular density, fractal dimension, diameter of the blood vessels, and length of the blood vessels. Destructive as well as non-destructive techniques exist to measure these parameters. In what follows, first, the destructive methods will be reviewed (paragraph 2.5.1), and second, the non-destructive methods already used in clinical research (paragraph 2.5.2). In section 2.6, the existing techniques for measuring the angiogenesis specifically in the CAM will be described.

2.5.1 Destructive methods

The *different mechanisms of angiogenesis* are investigated destructively by different models, which can be divided in *in vitro* and *in vivo* models. The first ones use endothelial cells, isolated form capillaries or vessels, or vascularized tissue such as rings of the rat aorta. The

cells or tissue are embedded in gels such as a matrigel and the differentiation is evaluated qualitatively or quantitatively. However, since the response *in vitro* may differ from the one in the organism, *in vivo* models are developed. The most widely used *in vivo* model is the chick chorioallantoic membrane (CAM) assay in which different substances are tested for their angiogenic or anti-angiogenic properties by evaluating the vasculature in the CAM under influence of the substance. The CAM assay can be divided in an *in ovo* or *ex ovo* method. The latter one is sometimes classified as an *in vitro* method (Ribatti *et al.*, 2000). In the original form of the CAM assay, a window is made in the eggshell at day 6-9, followed by placing tissue or organ grafts directly on the CAM, after which the window is sealed and the egg is reincubated (figure 2.9). For the *ex ovo* method, the entire egg content is transferred to a culture dish after 72 hours of incubation (figure 2.9). Grafts are placed on the CAM after 3-6 additional days of incubation (Auerbach *et al.*, 2000; Ribatti *et al.*, 2000). The *ex ovo* model allows for multiple applications of substances or simultaneous application of a control and an experimental graft, but the embryo viability is lower (Auerbach *et al.*, 2000; West *et al.*, 2001). The angiogenesis process in these assays can be evaluated qualitatively or quantitatively. The first and most simple evaluation is a qualitative ranking of the response to the test substance on a scale from 0 to 4. The quantitative evaluation of the angiogenic response will be explained in more detail in paragraph 2.6.1. The advantages of the CAM assay are the low cost, the relative ease of preparation, and the lower ethical concerns compared to other animal *in vivo* models (Richardson and Singh, 2003; West *et al.*, 2001). The major drawbacks of the CAM assay can be, depending on the specifications of the assay chosen, the difficulty to acquire good quality images, the difficult and time-consuming quantification, and the low reproducibility. Furthermore, a lot of different methodologies are used to assess the angiogenesis in the CAM making a comparison between results from different laboratories difficult (Hazel, 2003; Richardson and Singh, 2003). Other possible *in vivo* models are the rabbit cornea assay, or the implantation of subcutaneous sponges.

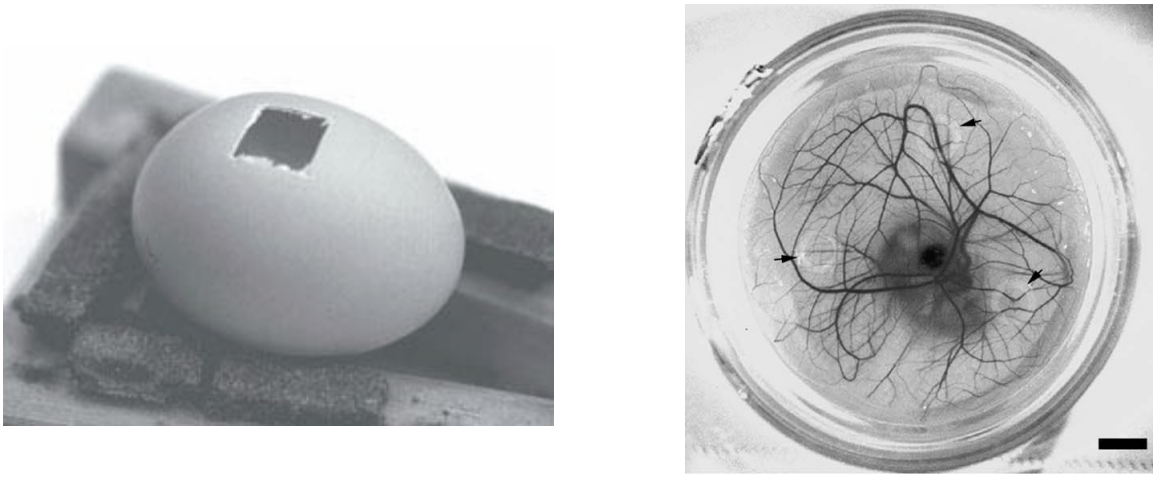

Figure 2.9 Left: Windowed egg with exposed CAM (West *et al.*, 2001); Right: An *ex ovo* CAM at day 10 of incubation on which three rings have been positioned (arrowheads). *En face* images can be generated from any area of the CAM (scale bar = 1 cm) (Seidlitz *et al.*, 2004).

Beside the models used to investigate angiogenesis mechanisms, vascularized tissue in humans and animals can be analyzed, in research settings, with regard to *the morphology and distribution of blood vessels* in the tissue. For this purpose, sections of the tissue are taken, and investigated under the microscope. The most powerful method for examining the three-dimensional microvascular network are vascular casts (Mcdonald and Choyke, 2003). Immediately after surgery the arteries are cannulated to drain the blood. After the blood has washed out, a contrast agent is injected together with a fixative (Konerding *et al.*, 2001). The vasculature can be made visible for light microscopic or scanning electron microscopic examination (Mcdonald and Choyke, 2003).

2.5.2 Non-destructive methods

Although the above described microscopic methods used in the vascular casting or to quantify the angiogenic response in the described models have high resolutions, they cannot be used in clinical studies because of their destructive character. As diagnostic tool, to follow up alterations in angiogenesis during disease, non-destructive methods are developed. These can be divided in optical, magnetic, acoustic, X-ray, and gamma-ray techniques. Some of them are able to measure structural changes in the vascular network, most commonly the diameter of the blood vessels, and others measure functional parameters such as blood

flow, blood vessel permeability, and blood oxygenation level. For the purpose of this research the focus will be laid on the ones that can measure the structure of the blood vessels.

To visualize the structure of the vascular network, different forms of angiography are used. In general, a radio-opaque contrast agent is injected into the blood vessels after which X-ray images are taken. Depending on the type of angiogram, a distinction can be made between conventional angiography, computed tomography (CT) angiography, and magnetic resonance (MR) angiography (Padhani and Neeman, 2001).

Computed tomography (CT) generates a three dimensional image of the inside of a subject based on computer processing of a series of two dimensional sections. This process is called tomographic reconstruction. A contrast agent is injected into a small peripheral vein. Due to the different attenuation coefficients of the tissues and the contrast agent for the X-rays, a grayscale image is obtained (Padhani and Neeman, 2001). It is used for example to detect aneurysms (*i.e.* vessel wall dilatations, at risk of rupture) in the aorta or atherosclerosis in the arteries to the legs (figure 2.10).

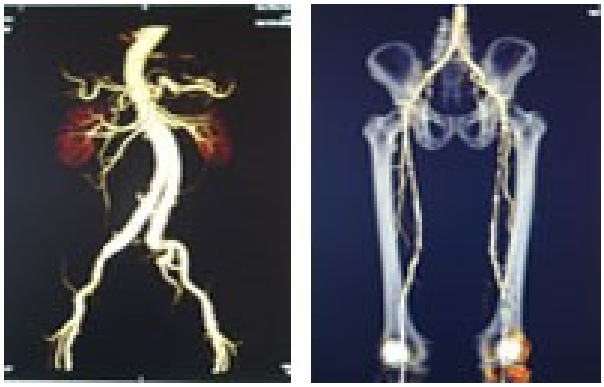

Figure 2.10 A CT angiography of the abdominal aorta (left image) and of the arteries in both legs (right image) (Keywestdiagnostics, 2007).

For magnetic resonance (MR) imaging, the sample is placed in a strong electromagnetic field. The hydrogen atoms align parallel with this field. At the level (slice) where it is desired to 'take a picture', a short, powerful radio signal is sent through the sample perpendicular to the main magnetic field. The hydrogen atoms, which have the same frequency as the radio wave will be excited and start to resonate with the exciting wave. When the radio signal is

turned off, the hydrogen atoms will, after a period of time, return to their original energy state. The absorbed excitation energy will then be released in the form of radio waves, which are detected. The relaxation time depends on the number of atoms and characteristics of the tissue and is measured to construct the image (Padhani and Neeman, 2001). Magnetic contrast agents can be applied to increase the resolution. As for CT angiography, the goal of this imaging technique is to diagnose stenosis (*i.e.* abnormal narrowing), occlusion or aneurysms. MR angiography is used for example to evaluate the arteries of the neck (figure 2.11).

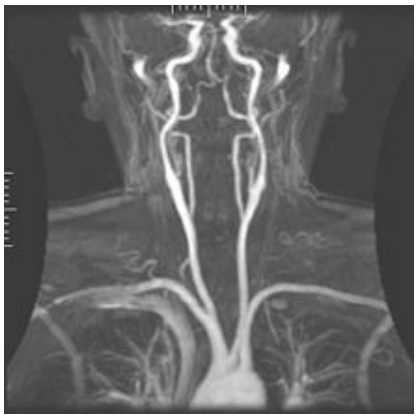

Figure 2.11 A MR angiography of the neck arteries (Glazer, 2006).

Another technique is Positron Emission Tomography (PET), in which gamma rays are used. A radiotracer is introduced and the concentration is measured after an appropriate uptake period. During its decay process, the radionuclide emits a positron which interacts with an electron in the environment. Both combine resulting in the emission of two gamma rays in opposite directions. These emissions are detected by two detectors on opposite sites of the sample (Padhani and Neeman, 2001). PET does not really visualize the vascular structure, however the blood volume can be measured from the signal (Mcdonald and Choyke, 2003) (figure 2.12).

Instead of electromagnetic radiation with small wavelengths, also sound waves are used, namely in ultrasound imaging to produce an echogram. Different tissues have different acoustic impedances. After the sound wave passes through the sample, it is detected using an array of ultrasound detectors (Foster, 2002; Li, 2002). The use of an intravascular agent may enhance the contrast (Li, 2002). The vascular ultrasound technique images the

macroscopic blood vessels in the body. A specific, often used form of vascular ultrasound is Color Flow Doppler ultrasound. This technique uses the Doppler effect to visualize blood flow, for example the one in the carotid bifurcation (figure 2.13). The carotid artery supplies the head and neck with blood, and divides in the neck in an external and internal carotid artery. Atherosclerotic narrowing of this carotid bifurcation is the most important risk factor for stroke (Dinkel *et al.*, 2001).

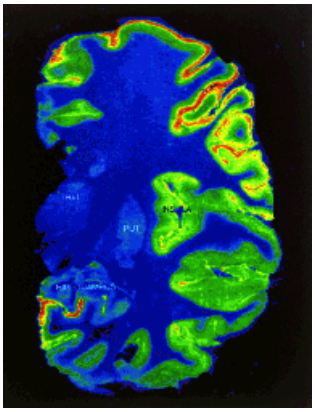

Figure 2.12 A PET scan of the blood volume in the brain (Kahn, 1994).

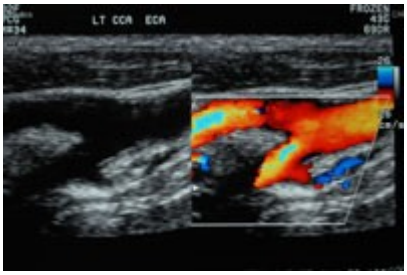

Figure 2.13 Vascular ultrasound image of the carotid bifurcation (Keywestdiagnostics, 2007).

All these current angiographic methods in the clinical setting are excellent for evaluating larger arteries and veins. However, they do not reach sufficient spatial resolution to image the microvasculature. The eye is the only exception, since blood vessels as small as 25 µm can be visualized in fluorescence retinal angiography by injecting sodium fluorescein or indocyanine green (Bennet, 2001; Jensen, 2004; Mcdonald and Choyke, 2003) (figure 2.14). Moreover, for all techniques mentioned, motion can cause accuracy problems (Padhani and Neeman, 2001).

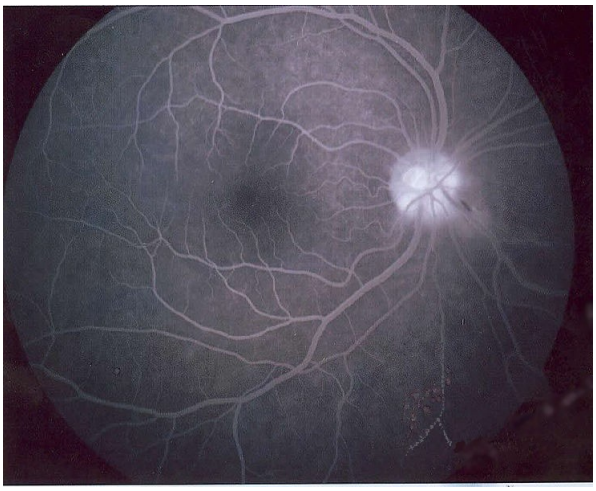

Figure 2.14 Fluorescein angiography of the retina (Bacud, 2007)

In research settings higher resolutions can be achieved, however, at the cost of large radiation and contrast agent exposure (Mcdonald and Choyke, 2003). MRI and CT can reach a resolution of several µm to nm (MRI: 90 nm (Mamin *et al.*, 2007), CT: 150 nm (Numata *et al.*, 2007)), and PET and ultrasonography can reach several mm to µm (PET: 980 µm (Park *et al.*, 2007), ultrasound: 30 µm (Ni *et al.*, 2008)). Overall, there remains a need for non-destructive and non-invasive *in vivo* imaging methods that are suited for visualizing and measuring microvasculature, especially for use in clinical settings.

2.6 Structural analysis of blood vessel development in the CAM of the chicken embryo

As described above, the CAM assay is probably the most widely used assay for angiogenic research (Staton *et al.*, 2004). Hence, many different imaging and evaluating techniques exist to determine the endogenous angiogenesis in the CAM and/or the changes in angiogenesis due to different (anti-) angiogenic factors applied on the CAM. These techniques will be discussed more in detail below. The few existing non-destructive techniques already used to analyze the CAM vasculature in research settings are also mentioned.

2.6.1 Destructively

In studying the angiogenesis in the CAM, a distinction has to be made between the capillary plexus and the pre- and postcapillary vessels, since both require different techniques. The capillary plexus is studied after dissection, fixation and staining, followed by viewing of the cross sections through a microscope at high magnification (figure 2.15) (Ausprunk *et al.*, 1974; Burton and Palmer, 1992; Defouw *et al.*, 1989; Kurz *et al.*, 1995; Melkonian *et al.*, 2002; Patan *et al.*, 1993; 1996; 1997; Schlatter *et al.*, 1997; Seidlitz *et al.*, 2004; Wagner-Amos and Seymour, 2003; Wilting and Christ, 1996; Wilting *et al.*, 1993). The pre- and postcapillary vessels are imaged, *en face*, dissected or not dissected, through a microscope at lower magnification (figure 2.16) (Dusseau and Hutchins, 1989; Kirchner *et al.*, 1996; Mckay *et al.*, 2008; Parsons-Wingerter *et al.*, 2006; Parsons-Wingerter *et al.*, 2000; Parsons-Wingerter *et al.*, 1998; Strick *et al.*, 1991). Once imaged, the density of the network can be determined. Some researchers measure also the area of the CAM (Ackerman and Rahn, 1981; Nikiforidis *et al.*, 1999; Richardson and Singh, 2003) or the total blood volume (Wagner-Amos and Seymour, 2003). Others measure the O_2 diffusing capacity of the CAM to evaluate the functionality of the blood vessel network (Tazawa and Whittow, 2000). For the purpose of this research, the different techniques for evaluating the growth of the pre- and postcapillary vessels will be reviewed.

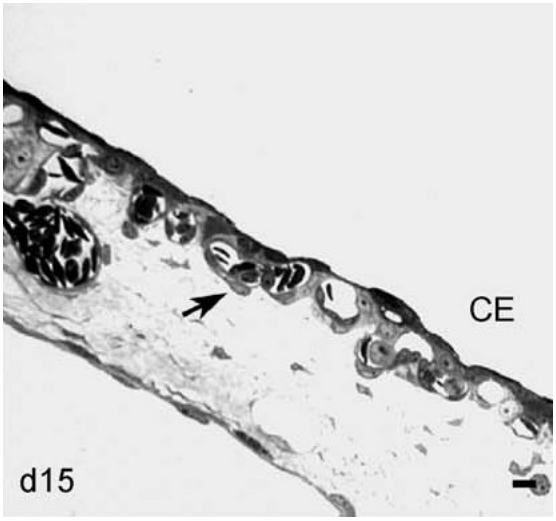

Figure 2.15 Cross section of CAM at day 15 shows the capillary plexus (arrowhead) at the chorionic epithelial surface (CE) (scale bar = 10 µm) (Seidlitz *et al.*, 2004).

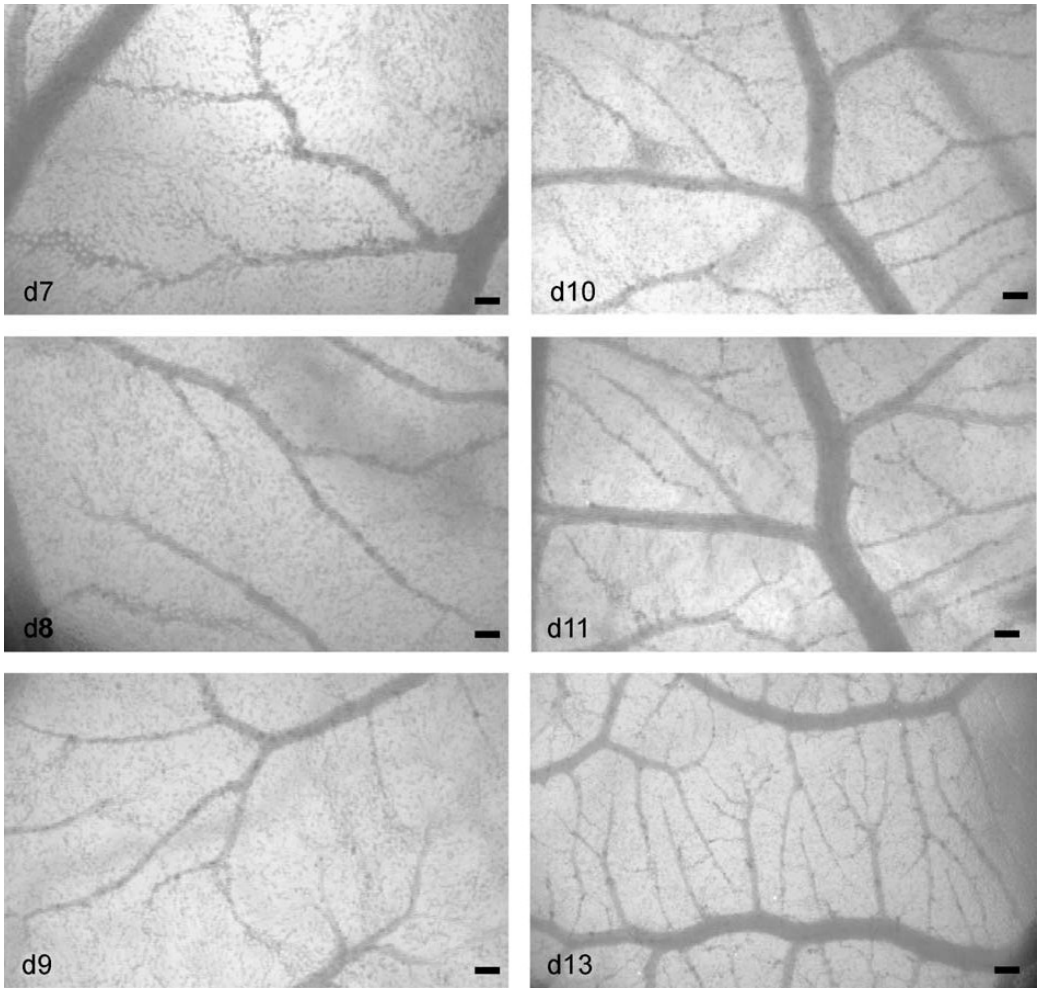

Figure 2.16 *En face* images of the CAM from days 7 to 13 to illustrate the increase in the number of branches in the pre- and postcapillary vessels (scale bar = 100 µm) (Seidlitz *et al.*, 2004)

The vasculature of the CAM is examined through a microscope by the eye or by a camera. The most simple evaluation is the observation of the presence or absence of increased or decreased vascular growth. Another possibility is a morphometric analysis of the blood vessel network. The parameters which are evaluated include vessel density, new vessel formation, vessel tortuosity, vessel branch points, and the development of a spoke wheel, *i.e.* a circular zone in which a large number of vessels are seen converging on the site of the application of the stimulus. For anti-angiogenesis the development of a zone of inhibition or avascular zone is assessed (Richardson and Singh, 2003). This zone of inhibition is scored on a scale from 0-4 or is quantified by determining the area (Ribatti *et al.*, 2000; Richardson and Singh, 2003). The spoke wheel is also evaluated using a score system or quantified by counting the intersections of the vessels with a series of concentric circles. The size of the series of circles varies between different researchers. Maas *et al.* (1999), for example, used a series of concentric circles 0.25 mm apart to evaluate the number of intersections with blood vessels of 10-15 µm diameter. This type of morphometric evaluation is based on stereology (Weibel, 1979). Other parameters, such as the vessel number, length, and area can also be determined using stereological principles. In this context, the vessel length density (mm/mm²) (Gu *et al.*, 2001; Kurz *et al.*, 1995; Strick *et al.*, 1991) or vascular density index (intersections/mm) (Dusseau *et al.*, 1986; Kirchner *et al.*, 1996; Maas *et al.*, 1999; Parsons-Wingerter *et al.*, 1998; Strick *et al.*, 1991) are determined by the grid-intersection method. The intersections of the blood vessels with a grid, overlaid on the image, are counted (Kirchner *et al.*, 1996; Parsons-Wingerter *et al.*, 1998) (figure 2.17).

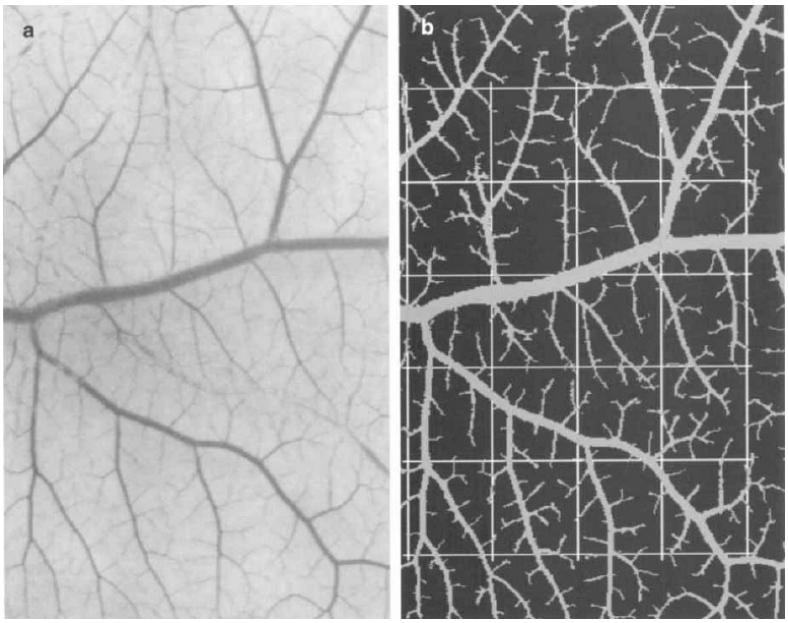

Figure 2.17 a: The vascular network of the CAM at incubation day 12. b: the binary image with a calibrated grid for the intersection count superimposed (edge of one square: 1 mm) (Kurz *et al.*, 1995)

The branching pattern is evaluated by the fractal dimension. Fractals, a concept from mathematics, describe structures which are self-similar. An example is the Koch curve which is constructed starting from a line segment divided into three segments, and replacing the middle segment with the upper two edges of an equilateral triangle (figure 2.18). This process is repeated for every newly formed line segment until infinity. In nature, 'fractal-like' structures can be found which show self-similarity within certain scale ranges. Examples include coastlines, snow flakes, broccoli, bronchial trees and blood vessel networks. The dimension of a line is one, the dimension of a plane is 2, however the dimension of a fractal structure, such as the Koch curve, lies somewhere between 1 and 2, and is called the fractal dimension. It measures the degree of complexity of the structure by evaluating how fast the measured parameter, such as the length of the curve, increases as the scale of measurement increases and finer details are incorporated in the measurement (Green, 1998; Mancardi *et al.*, 2008; Sandau and Kurz, 1997).

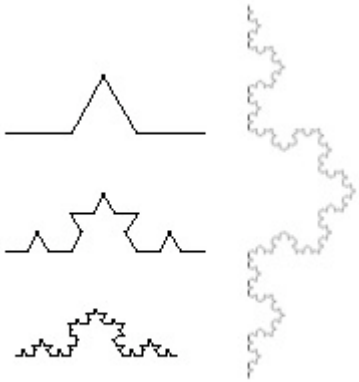

Figure 2.18 Koch curve (Chu-Charroll, 2007)

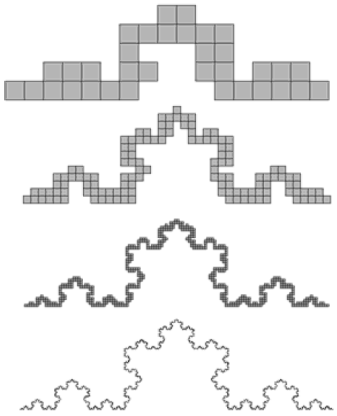

Figure 2.19 Number of boxes covering the Koch curve presented in figure 2.18 on the right side: when the box size decreases (from top to bottom), more boxes are necessary to cover the whole structure (Elert, 2007).

The fractal dimension is calculated via the box-counting method (figure 2.19), which is only possible via automatic counting on binary image. This method is based on the relation between the length of the boxes used and the number of boxes which are necessary to cover the fractal (Frame *et al.*, 2010):

$$N(p) = (1/p)^{FD}$$

with *N(p)*, the number of boxes of size p^2 which cover the fractal structure, *p*, the length of the boxes used, and FD, the fractal dimension. The fractal dimension of the Koch curve is 1.26.

To calculate the fractal dimension of a vascular network, a series of grids with decreasing box size is overlaid on the image (p^2=512²,256²,128²,… with p the length of the boxes in pixels). The fractal dimension is the slope of the least squares regression line of ln(*N(p)*) in function of ln(*1/p*) with *N(p)*, the number of boxes containing at least one blood vessel (Kirchner *et al.*, 1996; Parsons-Wingerter *et al.*, 1998). In this way, the fractal dimension is a measure for the branching degree of the vascular network.

Counting the intersections of the blood vessels with the grid in the grid-intersection method for determining the vessel density was primarily done manually, which was time- and labor-consuming. Dusseau *et al.* (1986) for example, counted the 10-12 µm diameter blood vessels intersecting concentric circles of 4-, 5-, 6-, and 8- mm diameters under the microscope with a 20x objective. In the course of time, manual counting was replaced by semi-automatic techniques. The first step in improvement of the counting technique was image processing of the captured digital microscopic images, as to enhance the contrast of the vasculature. Defining the network or the counting itself was still done manually (Strick *et al.*, 1991). Kirchner *et al.* (1996) made tracings of the blood vessel network with a marker pen. The counts could then be performed on these tracings. Some researchers used available commercial image processing software such as Image-Pro Plus (MediaCybernetics, Bethesda, USA) which automated different steps in the image processing and vessel counting, although at some steps, user input was required (Blatt *et al.*, 2004; Defouw and Defouw, 2000). Gu *et al.* (2001), for example, used Optimas Software (a.e.s., Perth, Australia) for image processing and vessel length count, but the threshold for binarization of the image was user determined. Others developed their own image processing and vessel quantification algorithms (Parsons-Wingerter *et al.*, 2000; Rieder *et al.*, 1995; Sandau and Kurz, 1997). One of the developed counting programs is commercialized under the name of VESGEN 2D. VESGEN 2D, or VESsel GENeration Analysis is an automated, user-interactive software for the quantification of angiogenic and lymphangiogenic trees and networks, developed by Parsons-Wingerter *et al.* (2000) at the Glenn Research Center of the NASA. The input for this software tool is a binary image of the vasculature. On this binary image different parameters of the vasculature can be determined, such as fractal dimension, vessel diameter, avascular spaces, vessel density, and branch point density (Vickerman *et al.*, 2009). However, the most crucial step in all applications is thresholding the image to obtain a binary image in which

background and object, namely the blood vessels, are well separated. The method developed by Rieder *et al.* (1995), to count blood vessels in rat muscle tissue on images of a video fluorescent microscope system, was the first fully automated method. However, for counting blood vessels in the CAM tissue, up to date, only two, recently developed, fully automated methods exists. Blacher *et al.* (2005) introduced an algorithm in Matlab software (The Mathworks Inc., Natick, USA) in which the binary image of the large vessels and the small vessels are obtained in different ways, after which both binary images are combined to form the complete vascular network. They used the *ex ovo* model, and took pictures of the vascular network through a fluorescence microscope at x24 magnification after injection of fluorescent dextran. Doukas *et al.* (2008) proposed a tool that provided vessel length, density and branching points measurements of the vasculature in sections of the CAM, based on conversion to gray scale and adaptive thresholding via the mean of a user-defined neighborhood. No injection of a fluorophore was used contrary to the automatic method of Rieder *et al.* (1995) and Blacher *et al.* (Blacher *et al.*, 2005). They used a camera mounted on a microscope set at x32 magnification to take pictures of the CAM through a window in the eggshell.

From the list above, it is clear that many methods exist to quantify the angiogenesis in the CAM. It is an often used assay, which proved its usefulness by all the different studies performed in the angiogenesis research domain. Nevertheless, Richardson and Singh (2003) report that “the approaches to the use of the CAM remain empirical, uncritical, and inconsistent, precluding meaningful comparison of data generated in different laboratories”. Hazel (2003) describes the major drawbacks as “the assay can be (1) difficult and time-consuming to quantify, (2) not amenable to acquiring good quality in situ images of the results, and (3) poorly reproducible”. So, depending on the used CAM assay, there are differences in the accuracy and precision of the results. Since, very often, no complete evaluation of the used method is given, it is difficult to compare the different results. An overview of the most important studies in which the angiogenesis in the CAM is quanitified, is presented in the appendix at the end of this dissertation. Furthermore, the CAM assay as such, is not appropriate for monitoring the normal development of the angiogenesis in the CAM. Yet, it may provide the starting ideas for a method which is more appropriate for this kind of research.

2.6.2 Non-destructively

To the author's knowledge, there are only a few attempts to test non-invasive techniques for imaging blood vessels in the CAM. None of these are developed specifically for studying angiogenesis in the CAM. Rather, they are part of the search for non-invasive characterization techniques of subsurface chromophores and their spatial distribution in biological tissues, specifically, blood vessels in the upper dermis of the skin. This information is necessary for optimization of the laser treatment of hypervascular lesions such as port wine stain birthmarks (Smithies *et al.*, 1997; Vangemert *et al.*, 1995). These techniques are sometimes tested on the CAM. However, in all studies, a window is made in the eggshell, making it a destructive method for the chicken embryo. Telenkov *et al.* (2002) investigated the use of non-invasive thermal wave imaging of blood vessels in tissue to determine physical dimensions of these blood vessels. This technique was tested on the CAM. The temperature oscillation after intensity modulated laser lighting was measured by an infrared camera, without contact or blood perfusion. Subsequently, the amplitude and phase of the thermal wave at each pixel were determined. The achieved spatial resolution in measuring the CAM blood vessels through a window in the eggshell was 150-200 µm (Telenkov *et al.*, 2002). Kolkman *et al.* (2004) and Zeng *et al.* (2007) tested photoacoustic imaging of blood vessels in the CAM. For photoacoustic imaging, the sample is lighted with nanosecond pulses of laser light in the visible or near-infrared region. Due to the absorption of the light the sample expands as it heats. With this expansion there will be a pressure increase and subsequent decrease as the light is switched off. This creates a photoacoustic signal which is detected by sensitive microphones and spatially resolved to reconstruct an image. The spatial resolution of the imaging system for blood vessel detection in the CAM through a window is 204 µm (figure 2.20).

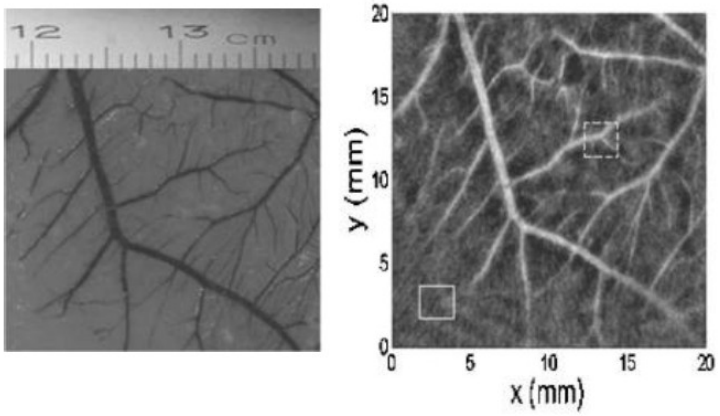

Figure 2.20 Photoacoustic imaging of windowed CAM: photograph of the sample (left image) and the photoacoustic image (right image). The area marked with a broken line shows a blood vessel and with a full line shows background (Zeng *et al.*, 2007)

Beside these tests of non-invasive techniques for imaging the vasculature in the CAM, non-invasive measurements of blood inside an egg are used for detection of blood spots in consumption eggs (Gielen *et al.*, 1979), and for the detection of development in incubated eggs (Bamelis *et al.*, 2002). For both applications, the same technique is used, namely transmission spectroscopy. Blood has a very specific absorption spectrum with absorption peaks of oxygenated hemoglobin at 415 nm, 542 nm, and 577 nm, and absorption peaks of deoxygenated hemoglobin at 431 nm, 555 nm, and 759 nm (Johnson *et al.*, 2007). The presence of blood in the egg is detected by the blood value, which is the ratio of the transmittance at 577 nm, an absorption peak of hemoglobin, and 610 nm, a neutral reference wavelength (Bamelis *et al.*, 2002; Gielen *et al.*, 1979).

2.7 Summary

From this literature overview, it becomes clear that early hypercapnic, *i.e.* high CO_2, conditions may be beneficial to the chicken embryonic development (De Smit *et al.*, 2006). One of the parameters which is most probably influenced by hypercapnia, is the angiogenesis in the chorioallantoic membrane (CAM), the principal organ for gas exchange of the chicken embryo. It is a well vascularized membrane which lies underneath the eggshell to exchange gases with the environment. It is formed around 100 hours of incubation. At embryonic day (ED) 10 this CAM encloses almost the entire contents of the egg, and becomes attached to the shell membranes. It degenerates after internal pipping when lung respiration begins (Romanoff, 1960). Different techniques exist to quantify the angiogenesis in the CAM since it is the most widely used angiogenesis assay. An (anti-) angiogenic factor is applied on top of the CAM and the changes in angiogenesis are measured through microscopic inspection of the area. However, to quantify the overall endogenous angiogenesis in the CAM under different gaseous conditions, these techniques are not appropriate. In addition, they are labor-intensive, time-consuming, and subjective (Doukas *et al.*, 2008; Richardson and Singh, 2003). Moreover, these techniques are destructive. The non-destructive techniques for imaging changes in the structure of the vascular network do not have the necessary resolution to visualize the small pre- and postcapillary blood vessels in the CAM (Mcdonald and Choyke, 2003). Nevertheless, spectroscopic measurements seem to have the potential to measure differences in the blood concentration in the CAM since blood has a very specific light absorption spectrum (Gielen *et al.*, 1979).

Chapter 3

Destructive Methodology to Monitor Angiogenesis in the CAM

(Adapted from Verhoelst *et al.* (in press-a))

3.1 Introduction

The standard methods for quantifying the angiogenesis in the CAM, used in the studies on (anti-)angiogenic factors, described in the previous chapter, are not appropriate for monitoring overall endogenous changes for three reasons. First, spot measurements through a microscope will not be representative for the whole CAM as there may be local differences. Second, the egg should not be disturbed until the actual measurements, as these disturbances may alter the angiogenesis. Romanoff (1960) reports both hypertrophic and atrophic responses of the CAM to removal of the eggshell. Auerbach *et al.* (2000), who describe the problems of different angiogenesis assays, warn for the fact that any irritant, including shell dust from making a window in the shell, or parts of shell membrane which protrude or touch the CAM, may cause an angiogenic reaction. Furthermore, removal of the eggshell alters the O_2 partial pressure differences, and may so alter the angiogenesis (Auerbach *et al.*, 2000). Third, the methodology must be highly sensitive to measure possibly smaller differences compared to the ones due to an (anti-)angiogenic factor. Therefore, a high resolution is obligatory. In addition, the method must be easy and fast to allow for the measurement of large numbers of samples. The latter will allow detection of the small differences over the random variation present in a group of eggs. So, altough there exist methods to quantify the vasculature in the CAM, namely in the angiogenesis research domain, for this research on chicken incubation conditions, a new method should be developed with specific requirements.

In this chapter an objective, quantitative methodology which fulfills these requirements is presented. The proposed methodology is evaluated for its reproducibility and repeatability. Additionally, it is validated in an experiment in which the angiogenesis in the CAM of embryos incubated under hypoxic conditions is compared with the one of embryos incubated under normoxic conditions. Hypoxic conditions during early development are known to stimulate angiogenesis in the CAM (Dusseau and Hutchins, 1989).

3.2 Materials and Methods

3.2.1 Sample preparation

To keep the sample preparation fast, simple and with minimal disturbance of the CAM, sampling is started at embryonic day (ED) 11, when the CAM is completely attached to the eggshell (Romanoff, 1960). The eggs are opened at the sharp end with dissection scissors so that yolk, albumen and embryo can be poured out carefully (Gu *et al.*, 2001). Subsequently, the egg is filled with formalin for retention of the erythrocytes in the blood vessels. After an overnight fixation, the eggs are emptied and divided in 3 bands (A, B, C) which are then each divided in 8 pieces with a diamond blade mounted on a dremel drill (Dremel Multipro, Dremel Europe, Breda, The Netherlands). Pictures can then be taken from every piece of shell with attached CAM (figure 3.1).

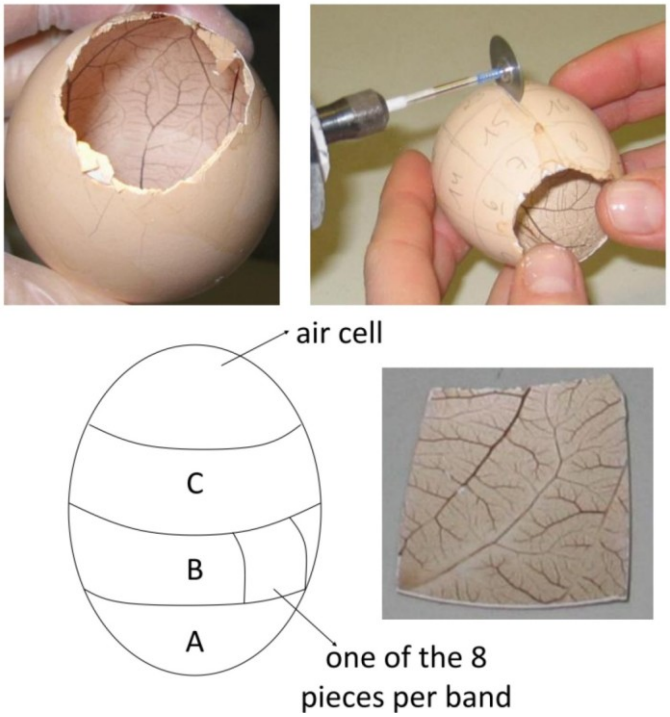

Figure 3.1 Top left side image: the emptied eggshell with attached and fixated CAM. Bottom left side image: division of the eggshell with attached CAM in three bands: A, B and C with C the closest one to the air cell, to allow analysis of local differences in angiogenesis across the egg. Top and bottom right side image: division, by a diamond blade mounted on a dremel drill, of every band in 8 pieces of 1.5 to 1.5 cm which can be photographed.

3.2.2 Measuring Configuration

3.2.2.1 Camera

The camera used to image the angiogenesis in the chicken CAM should meet different requirements. First of all the resolution, expressed as the real pixel size, should be large enough. The smallest pre- and postcapillary vessels in the CAM are around 10 µm (Romanoff, 1960). As a consequence 5 µm per pixel should not be exceeded. Additionally, the dynamic range and the signal to noise ratio (SNR) should be high. The larger the photodiode size on the sensor, the higher the dynamic range and the lower the SNR will be. Moreover, the photosensitive elements on the sensor should not be in close contact with each other as interferences may contribute to a lower SNR. All these aspects lead to the requirements of a large sensor in combination with a high resolution, and low noise levels.

A CANON EOS-1Ds Mark II commercial digital camera with extension tube EF12 II and macro lens MP-E 65mm f/2.8 1-5x (Canon Inc., Tokyo, Japan), set at magnification 5x, is used to take pictures of the vascular network of the shell pieces with attached CAM (figure 3.2). The resolution of this combination is 2.64 µm per pixel, so vessels of 10 µm are represented by almost 4 pixels. The framed part of the sample is 4.4 mm to 6.6 mm. The aperture priority setting is chosen and the diaphragm is set at f/16, the smallest possible opening to have the highest possible depth of field. The camera determines automatically the shutter time, which is 8 seconds. Since the set-up is fixed, a relative high shutter time poses no problem. The ISO value is set to 100 since higher ISO values result in more noise. A piece of eggshell with CAM, from which the blood has run out the vessels, is chosen as white reference. This correction of the white balance increases the contrast between vessels and background.

3.2.2.2 Light source

Hyperspectral measurements are performed on the samples to determine which wavelength results in the highest discriminating power between vessels and background. The hyperspectral imaging system has four components, namely a transportation plate, two 150 W halogen lamps, an ImSpec V10 spectrograph (Spectral Imaging Ltd, Oulu, Finland) coupled with a standard C-mount zoom lens (Cosmicar H6Z810), and a Hitachi KP-F120 monochrome

camera (Hitachi Kokusai Electric Inc., Tokyo, Japan). With this system, spatial as well as spectral information is obtained from the sample. The images of several samples at different wavelengths are compared concerning the discriminant power between blood vessels and background. The intensities at each wavelength measured with the hyperspectral set-up of twenty pixels of blood vessels and twenty pixels of background are tested for significant differences with a t-test. Based on these results, a light source is chosen to enhance the contrast. The samples are illuminated with two Farnell Luxeon Star W/Optic LED's of 530 nm (Farnell, Grace-Hollogne, Belgium) which are placed at 45 degrees at each side of the sample. This light is made diffuse, which results in a uniform illumination of the sample (figure 3.2).

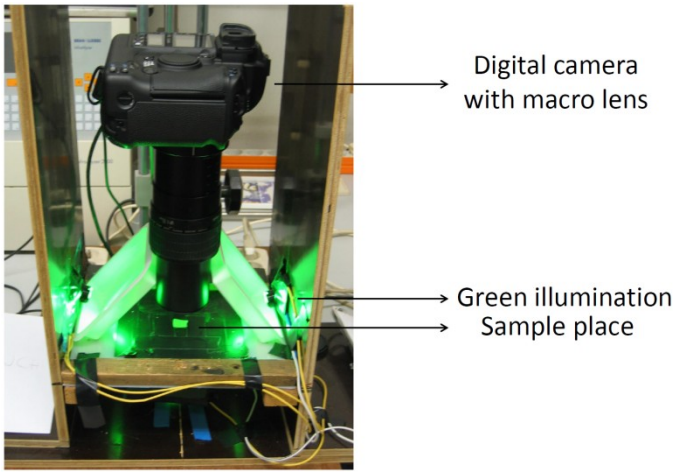

Figure 3.2 The measuring configuration to take pictures of the CAM is constructed with a high resolution commercial digital camera, an extension tube, a macro lens set at magnification 5x, and green illumination from both sides of the sample at 45 degrees.

3.2.3 Image processing

The images are registered as RGB, white balance corrected. To be able to calculate structural parameters of the network automatically, the images are processed to binary images by implementing algorithms in Matlab 7.5 software (The Mathworks Inc., Natick, USA). The different tasks aimed at separating the vascular network from the background (figure 3.3) are illustrated in figure 3.4. As proposed by Blacher (2007) a distinction is made between the small and the large vessels, and binary images of both are obtained in a different way, and then combined (figure 3.3 and figure 3.4).

Figure 3.3 An original picture of a sample of embryonic day (ED) 15 (top image) and the corresponding binary image of the skeleton of the vascular network (bottom image) obtained after the different image processing steps explained in figure 3.4. On this skeleton the two structural parameters can be calculated.

First the green plane is selected. A binary image of the small vessels is obtained via adaptive local thresholding using the mean of each neighborhood of 70x70 pixels as threshold. After taking the inverse of this binary image, so that the pixels belonging to a blood vessel become white, it is further enhanced using an opening operation (structuring element: square, 3 by 3 pixels) to eliminate falsely segmented background pixels.

Larger vessels are not well binarized due to the small size of the neighborhood. The binary image of the large blood vessels is obtained by first taking the inverse of the green plane of the image and performing an opening with a large structuring element (disk, radius 20 pixels) so that all small blood vessels are removed. This image is globally thresholded via Otsu's method (Otsu, 1979), and cleaned up with an opening algorithm (structuring element: disk, radius 24 pixels). Due to the latter, the continuity of the large blood vessels is lost. Therefore a morphological reconstruction is carried out with the image after opening as marker image and the image before opening as mask image.

Both binary images, the one of the small blood vessels and the one of the large blood vessels are then summed and a last opening operation, this time based on the area of the objects (connected components, *i.e.* objects with fewer than 200 pixels are removed), is carried out to eliminate small groups of falsely classified pixels. To ensure continuity of the vessels, a closing operation (structuring element: disk, radius 8 pixels) is implemented. Finally, the clean binary image of the combination of small and large vessels is skeletonized via a thinning procedure until all vessels are only 1 pixel in width, to eliminate the effect of the diameter of the vessel on the calculation of the structural parameters of the network, as only the number of vessels is taken into account in analogy with the manual counting methods. Moreover, to investigate the branching degree, the effect of the diameter must be removed.

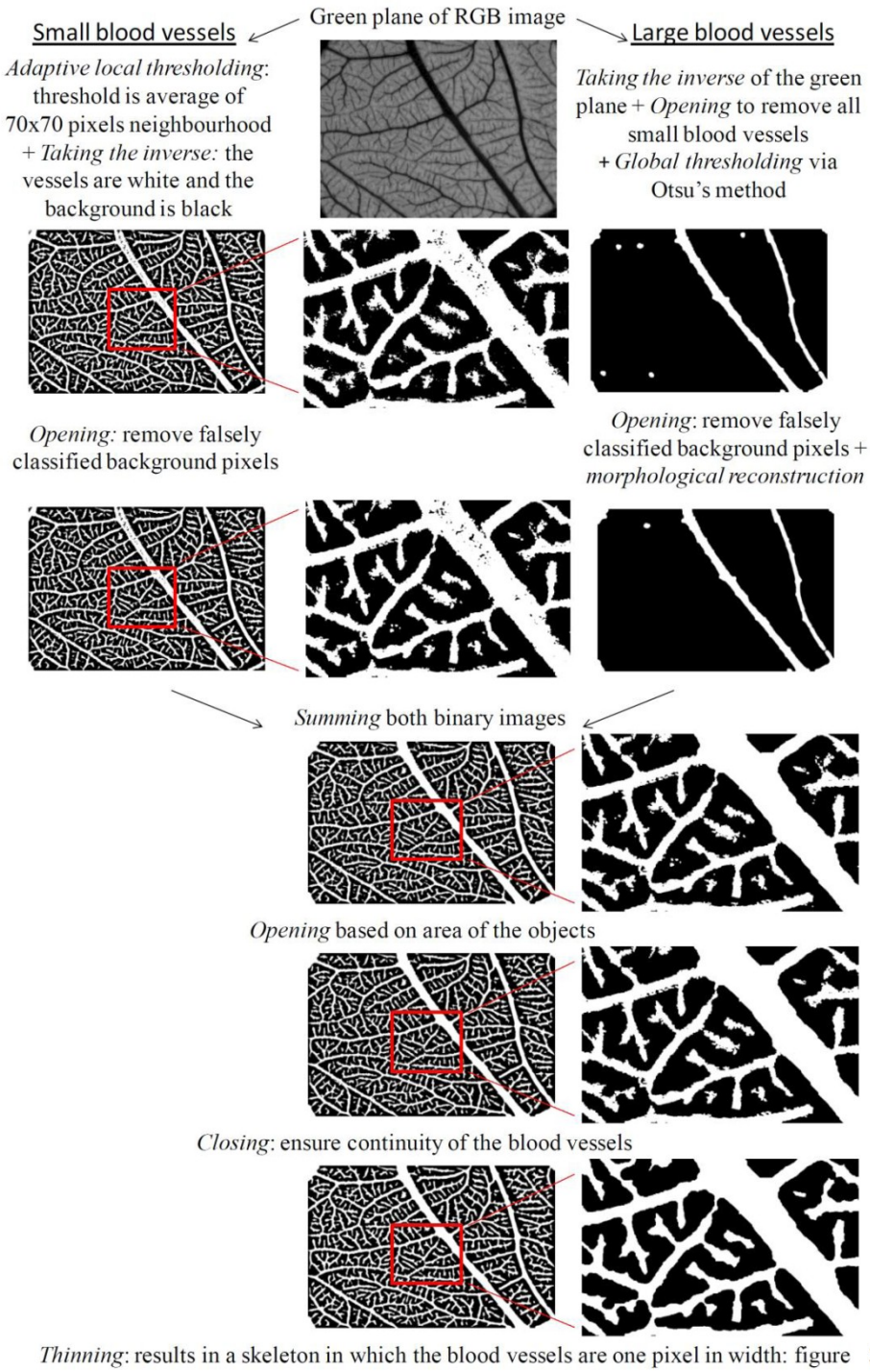

Figure 3.4 Image processing steps to convert the pictures of the samples of CAM into binary images of the vascular network. The mentioned algorithms are implemented in Matlab 7.5 software (The Mathworks Inc., Natick, USA). The presented images are of a sample of embryonic day (ED) 15. To elucidate the effect of the different algorithm steps, a part of certain images is enlarged. The original picture and the final result, namely the skeleton of the vascular network are shown in figure 3.3.

For each image, two structural parameters are obtained, namely the vascular fraction (VF) and the fractal dimension (FD). The first parameter, VF, is a measure of the density of the vascular network, and is calculated using the grid-intersection method. The second parameter, FD, is a measure of the branching degree of the vascular network, and is calculated using the box-counting method (Kirchner *et al.*, 1996; Parsons-Wingerter *et al.*, 1998; Russ, 2001; Sandau and Kurz, 1997).

With the grid-intersection method, the ratio is calculated between the amount of intersections of the vessels with the grid (16x16 pixels box size) placed over the image, and the total amount of possible intersections (figure 3.5). The latter are in fact intersections with the whole membrane and therefore a measure of the total area of the CAM in the image. This makes the vascular fraction independent of the box size. When the grid is chosen too coarse, the estimate of the vascular fraction is not accurate. For box sizes smaller than or equal to 16x16 pixels, the VF remains stable (figure 3.6).

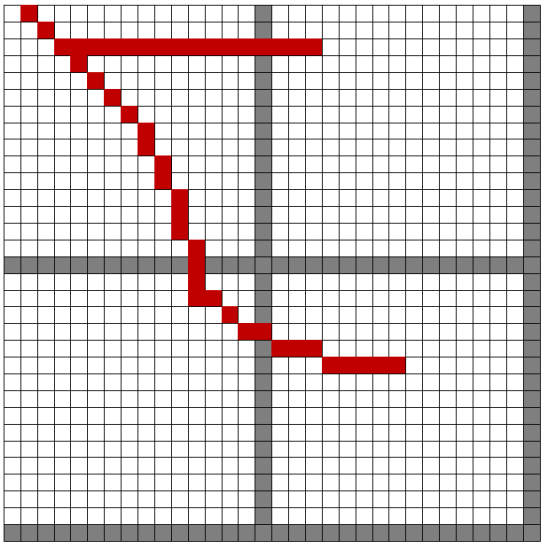

Figure 3.5 An example of the grid-intersection method. The blocks represent pixels of the image; the grid pixels, colored in gray, form a grid with box size 16 x 16 pixels; the blood vessels are one pixel in width in the binary skeleton. Total amount of possible intersections = 124 (32+32+32+32-4) pixels, and real amount of intersections = 3 pixels leading to the value of VF = 0.024.

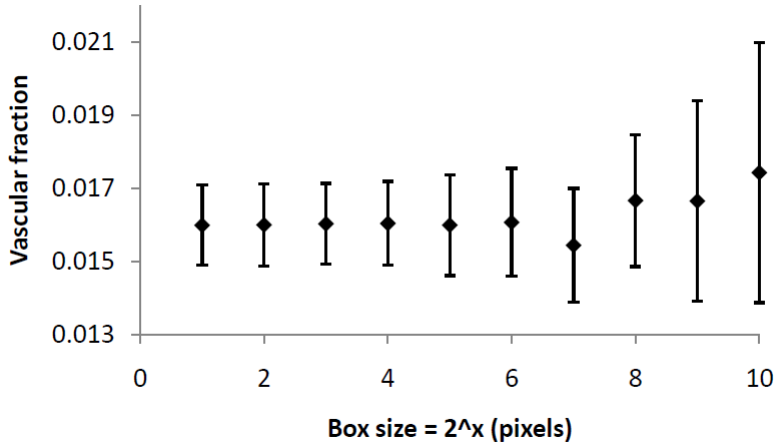

Figure 3.6 The mean vascular fraction and standard deviation bars of 12 randomly chosen samples as function of the box size chosen for the grid-intersection method. For boxes smaller than or equal to box size 16x16 pixels (2^4 = 16 pixels), both the average value and the standard deviation remain stable.

In the box-counting method, as explained in chapter 2, a series of grids of decreasing box size overlays the image ($p^2 = 128^2, 64^2, 32^2$ with p the box size). For each grid, the number of boxes intersected by the structure is counted ($N(p)$) (figure 3.7). An estimate of FD is obtained by taking the negative of the least squares regression slope of the plot of ln($N(p)$) versus ln(p) (Kirchner *et al.*, 1996; Parsons-Wingerter *et al.*, 1998; Sandau and Kurz, 1997). Results depend on the choice of the minimum and maximum box size. Fractals are structures which demonstrate self-similarity to infinity. In nature some structures are 'fractal-like', however there are scale boundaries in which the structure is 'self-similar-like'. Since the self-similarity of a natural structure does not repeat until infinity, the smallest scale at which the structure is fractal is determined by the smallest repeating element in the structure. In this case the smallest detectable blood vessels are around 10 µm, so 4 pixels in width. The smallest distances between two vessels are around 30 to 100 pixels. When looking at a scale smaller than 30 pixels, there will not be any self-similarity in the structure. On very large scales the fractality will also be lost due to the very few, large blood vessels in the network. Moreover, from a specific scale onwards, the blood vessel network, in every image, will always fill all boxes of the grid and no fractality is measured. The blood vessel network of the CAM is a fractal structure from the scale of 32x32 pixels box size (=84 µm) up to the scale of 128x128 pixels box size (=338 µm). The R^2 of the regression slope of the ln-ln plot, in this

scale range, is higher than 0.98 which confirms the fractality (Kirchner *et al.*, 1996; Sandau and Kurz, 1997).

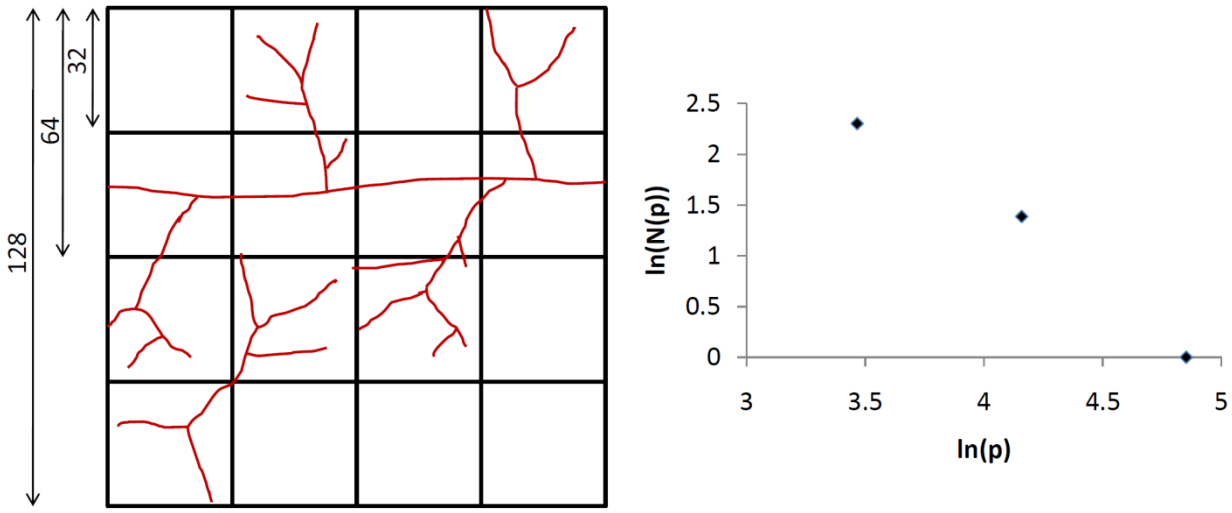

Figure 3.7 An example of the box-counting method. For the largest box size, 1 box contains blood vessels (p = 128, $N(p)$ = 1); for a smaller box size, 4 boxes contain blood vessels (p = 64, $N(p)$ = 4); for the smallest box size, 10 boxes contain blood vessels (p = 32, $N(p)$ = 10). Plotting ln($N(p)$) versus ln(p) leads to a least squares regression slope of -1.66. The fractal dimension (FD) is 1.66. R^2 is 0.986.

3.2.4 Experimental data

3.2.4.1 Repeatability and reproducibility

The automatic determination of the structural parameters is inherently deterministic, however, the results, as part of a measuring system, are subject to measurement error. The different factors which can be a source of undesired, but not excludable variation are the operator, noise of the camera sensor, manual focus variations, and position of the sample under the camera. System capability studies express the precision of the system as a variance or standard deviation of the measurement error, which is modeled as the sum of the repeatability and the reproducibility (R&R). The repeatability describes the variation between different results obtained under the same conditions. The reproducibility describes the variation between different results obtained under different conditions, which are in this case different operators (Borror *et al.*, 1997).

To calculate the reproducibility and repeatability of the new methodology, three persons took pictures of 14 randomly chosen samples. For each sample 4 pictures were taken to measure the possible variations under the same conditions.

3.2.4.2 Validation

Besides defining the precision of a new measurement system, the accuracy of the system should be evaluated. The accuracy is the mean difference between the obtained values and the true values of the parameters. Since there does not exist a golden standard to quantify the angiogenesis, the accuracy cannot be determined. Whereas only the differences between groups have to be investigated, it is not necessary to know the absolute, true values. However, it is still necessary to ensure the validity of the methodology, with or without a systematic bias.

A group of 120 White Leghorn eggs, from the same flock, are incubated in two incubators with the same conditions of temperature and relative humidity (T=37.8°C and RH=45%) but different O_2 concentrations. Control embryos are incubated under normoxic conditions (21% O_2, 0.03% CO_2). Experimental embryos are incubated under normoxic conditions until embryonic day (ED) 5 when eggs are transferred to a second incubator where hypoxic conditions (15.0 ± 0.3% atmospheric O_2, 0.03% CO_2) are maintained (Zoer *et al.*, 2009). From each group 20 eggs per ED are randomly selected, and analyzed on ED 11, 14 and 16. The results are compared with data from literature.

3.2.5 Statistics

3.2.5.1 Repeatability and reproducibility

For the reproducibility and repeatability calculation, the classical gauge R&R is determined via a mixed model, built for the measurements X_{ijk}, so that the effects can be defined as random factors (Borror *et al.*, 1997):

$$X_{ijk} = \mu + P_i + O_j + (OP)_{ij} + R_{k(ij)} \quad \text{(Eq. 3.1)}$$

with i = 1,2,…,m, the number of parts (*i.e.* samples); j = 1,2,..,n, the number of operators, k = 1,2, …,q, the number of replications of measurements per part and per operator; P, the

effect of Parts; *O*, the effect of the Operator; *OP*, the effect of the interaction between Operator and Part; *R*, the Replications of measurements; and μ, the overall mean.

The variance component for reproducibility, $s^2_{reproducibility}$, is defined as the sum of the estimates of the variation due to the operators, s^2_O, and due to the interaction of operator and part, s^2_{OP}:

$$\sqrt{s^2_{reproducibility}} = \sqrt{\left(s^2_O + s^2_{OP}\right)} \quad \text{(Eq. 3.2)}$$

The variance component for repeatability, $s^2_{repeatability}$, is estimated by the variation due to error, in other words, the residual variance in the model, s^2_R:

$$\sqrt{s^2_{repeatability}} = \sqrt{s^2_R} \quad \text{(Eq. 3.3)}$$

The total gauge variation estimate, s^2_{gauge}, is given by the sum of the repeatability and reproducibility:

$$\sqrt{s^2_{gauge}} = \sqrt{\left(s^2_{repeatability} + s^2_{reproducibility}\right)} \quad \text{(Eq. 3.4)}$$

The total variation estimate, s^2_{total}, is given by the sum of the gauge R&R and the parts variation, s^2_P:

$$\sqrt{s^2_{total}} = \sqrt{\left(s^2_{gauge} + s^2_P\right)} \quad \text{(Eq. 3.5)}$$

For all analyses, SAS 9.2 is used (SAS Institute Inc., Cary, North Carolina, USA).

3.2.5.2 Validation

In the validation experiment, the structural parameters are calculated for each band (A, B and C) by taking the average of the 8 pieces of each band. To compare the structural parameters between the groups (hypoxia and control), and bands (A, B and C), an ANOVA model is built for each parameter, treating group, band, embryonic day (ED) and their interactions as possible categorical independent variables. A hierarchical variable selection is performed to eliminate non-significant higher order interactions terms. Linear contrasts are set up in order to estimate differences between the considered settings. The following possible differences are tested: differences between groups over all ED, between bands over

all ED, between groups per ED, between bands per ED and between the ED. The statistical analyses are performed using SAS 9.2 (SAS Institute Inc., Cary, North Carolina, USA).

3.3 Results

3.3.1 Light source test

In figure 3.8 the *p*-values as function of the wavelength are shown which result from a t-test between the intensities at different wavelengths of a group of pixels belonging to the background and a group of pixels belonging to blood vessels. The wavelengths from 450 nm to 590 nm, the blue and green region of the spectrum, give the highest significant differences. Considering these results, the fact that commercial cameras with a Bayer color filter are most sensitive to green light and the availability of Farnell Luxeon Star W/Optic LED's (Farnell In One), with high intensities, a LED with dominant wavelength at 530 nm is chosen.

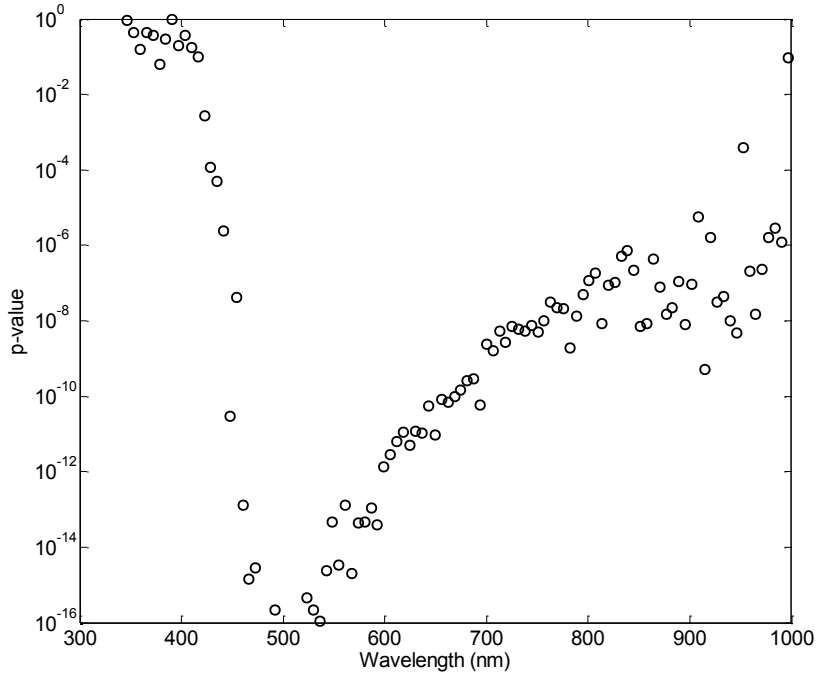

Figure 3.8 The *p*-values as function of the wavelength which result from a t-test between the intensities at different wavelengths of a group of pixels belonging to the background and a group of pixels belonging to blood vessels.

3.3.2 Evaluation of the new methodology: reproducibility and repeatability

The reproducibility and repeatability analysis as described above (*n*=168) results in a model where the interaction between parts and operator is not significant. The variance components are represented in table 3.1. Since there is no interaction, the variance component estimate for reproducibility is the same as the variance component due to the operator (Eq. 3.2). The ratio of the R&R variation, or total gauge variation (Eq. 3.4), compared to the parts variation is 0.32 for VF and 0.21 for FD, and to the total variation 0.30 for VF and 0.21 for FD.

Table 3.1 The variance components: Vs^2_R, square root of the residual variance (repeatability) (Eq. 3.3), Vs^2_O , square root of the operator variation (reproducibility) (Eq. 3.2), Vs^2_P, square root of the parts variation (parts), and Vs^2_{gauge},, square root of the total gauge variation (gauge R&R) (Eq. 3.4).

	Repeatability $\sqrt{s_R^2}$	**Reproducibility** $\sqrt{s_O^2}$	**Parts** $\sqrt{s_P^2}$	**Gauge R&R** $\sqrt{s_{gauge}^2}$
VF	3.09×10^{-4}	3.44×10^{-5}	9.85×10^{-4}	3.11×10^{-4}
FD	8.66×10^{-3}	$< 0.00 \times 10^{-5}$	4.00×10^{-2}	8.66×10^{-3}

3.3.3 Validation of the new methodology: hypoxia versus control

Group, ED, their interaction and band are important as independent variables in the model for VF (*n*=284) as well as in the model for FD (*n*=284). The difference between the groups and bands is tested globally over all ED and per ED (figure 3.9).

Overall, there is no significant difference between the groups. However, on ED 14, VF and FD are significantly higher for the eggs incubated under hypoxic conditions (p = 0.0003 and 0.0011 respectively for VF and FD) (figure 3.9). On ED 16 the control group shows significantly higher VF and FD than the hypoxia group ($p < .0001$ for both parameters). There is no interaction between band and ED. Both parameters of band C, the closest one to the air cell, are significantly higher than those of band A, the most distant one to the air cell (p =

0.0015 for the VF and p = 0.0002 for the FD). The FD also differs between band C and B (p = 0.009).

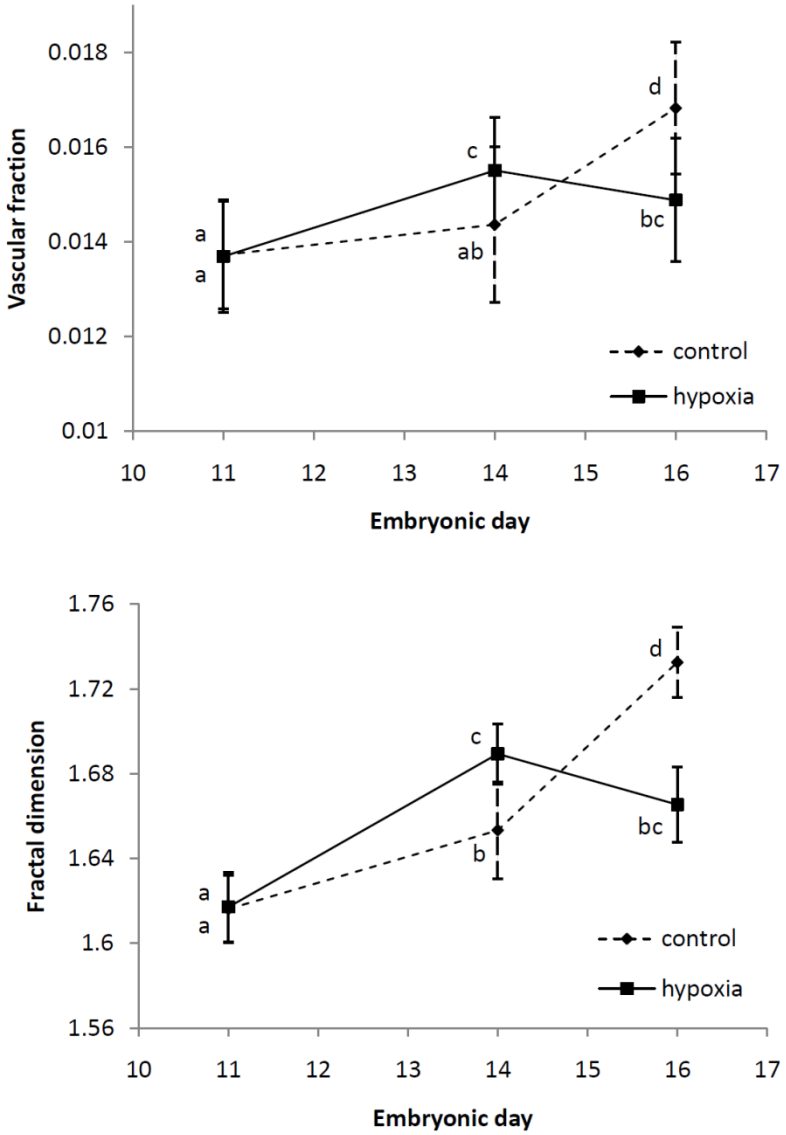

Figure 3.9 Overall mean vascular fraction (top) and fractal dimension (bottom) of the vascular network of the CAM in function of the embryonic day (ED), for embryos incubated under hypoxic (hypoxia) and normal conditions (control) with standard deviation bars (n=284). Diamond symbols and dashed bars represent the control group, square symbols and full bars represent the hypoxia group. Different letters indicate significant differences ($p < 0.01$).

In the control group both parameters are significantly higher at ED 16 as compared to ED 14 (p < .0001), and at ED 16 as compared to ED 11 (p < .0001) (figure 3.9). The FD is also significantly higher at ED 14 as compared to ED 11 (p = 0.007). For the hypoxia group on the

other hand, both parameters are significantly higher at ED 14 as compared to ED 11 (p < .0001), and at ED 16 as compared to ED 11 (p = 0.0036 for VF and p = 0.001 for FD). In this group, there is no significant difference between ED 16 and ED 14. The values (mean ± standard deviation) for VF range from 0.0137 ± 0.0011 on ED 11 to 0.0168 ± 0.0014 on ED 16 for the control group, and from 0.0137 ± 0.0012 on ED 11 to 0.0149 ± 0.0013 on ED 16 for the hypoxia group. The values for FD (mean ± standard deviation) range from 1.616 ± 0.016 on ED 11 to 1.732 ± 0.017 on ED 16 for the control group, and from 1.617 ± 0.016 on ED 11 to 1.665 ± 0.018 on ED 16 for the hypoxia group.

3.4 Discussion

3.4.1 Advantages of the methodology presented

The results described above show that it is possible to quantify the endogenous angiogenesis in the CAM and detect differences due to different environmental conditions. The methodology developed fulfils specific requirements for this kind of research concerning sample preparation, measuring configuration and image processing. The eggs are only handled on the moment of sampling and the latter is also done with minimal disturbance of the CAM. As one spot will not be representative for the whole CAM, different samples of one CAM are taken by dividing the eggshell with attached CAM into three bands, each consisting of 8 pieces which are all measured. To visualize the microvessels of the CAM a sufficiently high actual resolution must be achieved. This actual resolution is determined by a combination of the resolution of the camera and the used magnification. The cameras mounted on microscopes have relatively low resolution (e.g. 1200 x 1600 pixels) compared to commercial cameras (e.g. 4992x3328 pixels). By the magnification of the microscope it is still possible to see small blood vessels, but at the cost of the area pictured, which becomes very small. The high actual resolution (2.64 µm/pixel), combined with the large area pictured (4.4 mm x 6.6 mm) is achieved by the use of a commercial high resolution digital camera, a macro lens which magnifies 5 times, and an extension tube. Both macro lens and extension tube decrease the minimal focus distance (*i.e.* the distance between the object and the sensor) so that a small object can be photographed from a small distance to obtain a frame filling image of the object. Subsequently, with the set-up as described, fewer images have to

be taken from one sample to obtain the same information as with a camera mounted on a microscope, and still a very high resolution is achieved.

The digital pictures are processed automatically to become binary images in which the vessels and the background are well separated. By illuminating the samples using wavelengths for which the discriminating power between object and background is large, the thresholding improves. Every part of the developed measuring system, namely the sample preparation, the photographing of the samples and the analysis, is fast and less-labor-intensive than the existing techniques. Hence, it is possible to analyze the large number of samples necessary for this kind of research. From the egg to the final pictures of the 24 different pieces, it takes 18 minutes of labor (the overnight fixation time excluded). Another 12 minutes are necessary to process the images but this is performed completely automatically.

The sample preparation as proposed results in two disadvantages of this methodology, namely (1) it cannot measure the angiogenesis in the CAM before ED 10 since the CAM is not yet attached to the eggshell, and (2) it is not possible to apply any (anti-)angiogenic test substance on the surface of the CAM in contrast to the traditional CAM assay. Since this methodology is not meant for research on different angiogenic factors, the latter does not pose any problem. Moreover, the methodology can still be used to investigate the angiogenesis under different gaseous conditions, and under malnutrition by removing some of the yolk or albumen (Miller *et al.*, 2002). Furthermore, aspects of the developed methodology, such as the camera with macro lens, the green illumination, and the complete automatic image processing may be implemented in existing CAM assays. The fact that no measurements can be performed before ED 10 is an important drawback. Nevertheless, the period from ED 10 until the moment that maximal vascular development is reached (around ED 15-16) is probably the most important one concerning the gas exchange of the embryo with the environment. After all, the CAM resistance to the gas exchange decreases drastically from ED 10 to 14, and reaches a maximum around ED 15-16 (Bissonnette and Metcalfe, 1978; Rahn *et al.*, 1979).

3.4.2 Capability and validity of the methodology presented

The variation in the obtained results is reduced to a minimum by making most of the methodology automatic. The reproducibility, *i.e.* the variation due to the operator, and the repeatability, *i.e.* the residual variation (table 3.1) are small compared to the measured values (figure 3.9). Nevertheless, the ratio of the gauge R&R to the parts variation, and to the total variation are not very small. Although the parts are chosen randomly, the variation between the parts used for the R&R calculation is relatively small (table 3.1) compared to the measured values over all ED (figure 3.9). This small parts variation increases the ratio of the gauge R&R to the parts and to the total variation.

Qualitatively, the results obtained in the validation experiment agree with those from literature. Both parameters, VF and FD, increase with the embryonic day in the control group until somewhere between ED 14 and 16. No measurements are performed in between those days. These results can be explained by the normal development of the embryo and associated angiogenesis in the CAM to ensure the gas exchange of the embryo with the environment (Romanoff, 1960). Tazawa and Whittow (2000) describe an increase in O_2 diffusing capacity of the CAM until day 16. Strick *et al.* (1991) demonstrate an increase in vessel endpoint density until day 16. Quantitatively, the values obtained with the developed methodology are generally higher compared to the ones in literature. The VF can be transformed into the usually determined vascular density index (VDI), *i.e.* the amount of intersections with a grid per mm grid, and subsequently compared to the values found in literature. Strick *et al.* (1991) report a higher VDI (control group, day 12: about 4.8 intersections/mm) compared to the values found by Dusseau *et al.* (1986) (control group, day 12: about 3.8 intersections/mm). The explanation given is that they see more small blood vessels as they injected pelican ink as contrast agent opposed to Dusseau *et al.* (1986) who only used the red blood cells to visualize the blood vessels. With the newly developed methodology, about 18 intersections per mm grid are found on ED 11 (*i.e.* (incubation) day 12) in the control group. This is 3.75 times higher compared to the values found by Strick *et al.* (1991). No conclusions can be drawn on which of these two values approach most the true values. Their method may underestimate the true values, but our method may equally well overestimate the true values. Nevertheless, considering the high resolution of 2.64

µm/pixel achieved, and the small grid size used, it can be speculated that even more small blood vessels are detected with this methodology compared to the one of Strick *et al.* (1991). Furthermore, it cannot be excluded that, in the study of Dusseau *et al.* (1986), some differences in the density of the vascular network are due to the removal of the eggshell before the actual sampling. Strick *et al.* (1991) neither removed the eggshell or opened the egg before the actual sampling. The FD can be compared to values found by Sandau and Kurz (1997) for windowed CAM on day 15, namely 1.45 - 1.56. The FD in the control group on ED 14 (*i.e.* (incubation) day 15), measured with the developed methodology, is 1.66. The resolution of the imaging set-up of Sandau and Kurz (1997) is 11 µm/pixel. This lower resolution may explain the lower values compared to the ones resulting from the developed methodology. Kirchner *et al.* (1996) report higher values, namely about 1.8. Their results present a difference in FD of the vascular network, both in evolution as in values, between the windowed and the *ex ovo* CAM assay, pointing out the influence of removal of the eggshell on the angiogenesis in the CAM.

Hypoxia has a stimulating effect on angiogenesis in the CAM when applied from day 7 to 14 (Dusseau and Hutchins, 1989). In the performed experiment values for VF and FD are significantly higher on ED 14 for the group incubated under hypoxic conditions compared to normoxic conditions.

The differences between the bands are the same between both groups and can be explained by the normal development of the CAM. The allantois is formed as an appendage of the hind gut. Around ED 4 the allantois fuses with the chorion. It first grows over the embryo to the blunt side of the egg, and later on to the sharp end of the egg. The differences between the bands, as described in the results, seem to reflect this way of growth. At the blunt end of the egg, the vascular network in the CAM is significantly higher developed than at the sharp end, which is the latest to develop (Romanoff, 1960). Additionally, the local differences between VF and FD of the vascular network in the CAM are in line with the local differences in the eggshell conductance and pore density of the shell (Rokitka and Rahn, 1987). The vascular network is the highest developed in these regions where the eggshell conductance and pore density is also the highest, namely at the blunt side of the egg.

3.4.3 Complexities on the influence of hypoxia

On ED 16 the eggs incubated under normoxic conditions show a significantly higher developed vascular network than those under hypoxic conditions, in contrast with the results at ED 14. The CAM arrested its growth after ED 14 for the hypoxia group. This is in accordance with Ruijtenbeek *et al.* (2003) who found that chronic hypoxia has a negative impact on growth and birth weight.

Most likely there is a compensating growth of the blood vessels in the CAM in response to early hypoxia. Hypoxia is a well-known stimulator for angiogenesis, as described in tumor research. It affects angiogenesis through different molecular factors. The most important one is the hypoxia-inducible factor-1 (HIF-1), which upregulates, amongst others, the formation of vascular endothelial growth factor (VEGF), the most studied angiogenesis stimulator (Bradbury, 2001). By increasing the angiogenesis, and so improving the O_2 uptake, the embryo adapts to the hypoxic conditions. However, when the hypoxic conditions are maintained longer, the embryo seems not to be able to cope. The ambient O_2 amount becomes insufficient, affecting the growth of the embryo, and in accordance the development of the CAM.

From studies on developmental origins of health and disease, it is shown that lower birth weight is a predisposition to cardiovascular and metabolic diseases in adult life (Barker, 1995). Chronic hypoxia during prenatal development is one of the possible factors which will lead to intrauterine growth retardation and will influence the susceptibility to cardiovascular diseases (Ruijtenbeek *et al.*, 2003). Even without long-term hypoxic incubation conditions, the chicken embryo may suffer from a period of critical hypoxia in the second half of the incubation. Rahn *et al.* (1979) demonstrate that, although the embryo grows, the O_2 uptake reaches a plateau from around ED 15-16 onwards until internal pipping (figure 2.8). This may lead to hypoxic conditions and therefore to a higher susceptibility for ascites by triggering structural changes in the heart (Decuypere *et al.*, 2000; Villamor *et al.*, 2004). Ascites is a syndrome related to cardiovascular and pulmonary ailments, and the main cause of non-infectious mortality in the broiler sector, leading to economic losses and animal welfare problems. On the other hand, hypoxia during early embryonic development stimulates angiogenesis (see above), and hence the O_2 diffusing capacity of the CAM (Tazawa and

Whittow, 2000). Consequently the limited O_2 uptake during the described plateau phase may be increased. This leads to the hypothesis that the changes early antenatal under influence of temporal hypoxia, may make the natural critical hypoxia later in the incubation less severe, and so lower the ascites sensitivity. This hypothesis can be considered in future research.

3.5 Conclusions and future research

In this chapter, a fast, objective, quantitative methodology to assess changes in the overall vascular development in the CAM of chicken embryos is presented. Samples were taken with minimal disturbance of the CAM by emptying the egg so that the CAM stayed attached to the shell, which was then cut in pieces. A set-up was made with a commercial digital camera and a macro lens set at 5x magnification to take pictures with sufficient contrast and resolution (2.64 μm/pixel). These were processed automatically with computer algorithms to calculate the vascular fraction (VF) and the fractal dimension (FD) automatically on binary images. The ratio of the repeatability and reproducibility variation compared to the parts variation was 0.32 for VF and 0.21 for FD. In a validation experiment (n=284), one group was incubated under hypoxic conditions and a control group under normoxic conditions. It was shown that early hypoxia stimulated the angiogenesis while chronic hypoxia impeded growth with significant differences between both groups. These results were in line with literature data, and therefore supported the validity of the measurement system.

A capable method is developed to assess overall angiogenesis in the CAM. It can now be used to analyze the effects of different incubation conditions on the angiogenesis in the CAM. Since the angiogenesis in the CAM is necessary for the gas exchange of the embryo's metabolism, it also holds information on the development of the embryo. In future research the link with the growth and metabolism of the embryo can be investigated, and additionally the link with health and disease in adult life. It will improve the understanding of the physiology of incubation and embryonic development, and so it will help to optimize incubation conditions in the poultry sector which may have a major impact post hatch (Collin *et al.*, 2007; De Oliveira *et al.*, 2008; Decuypere and Bruggeman, 2007; Hulet, 2007; Yahav, 2000). Ideally, non-destructive measurement systems must be developed to monitor these

changes throughout embryonic development, and their effect on post hatch growth. This destructive method may serve as a reference when developing such a non-destructive technique.

Chapter 4

The Effect of Early Prenatal Hypercapnia on the Angiogenesis in the CAM

(Adapted from Verhoelst *et al.* (in press-b))

4.1 Introduction

As the embryo develops it consumes O_2 and produces CO_2. The brooding hen increases the CO_2 concentrations and lowers the O_2 concentrations around the eggs by sitting on the nest and so limiting the exchange of these gases with the environment. In artificial incubation practice, the incubator is ventilated as to keep the O_2 and CO_2 concentrations to 21% O_2 and 0.1% CO_2. However, recent studies report several beneficial effects of hypercapnia, *i.e.* high CO_2 concentrations, such as higher embryo weights, and earlier hatch (Bruggeman *et al.*, 2007; Buys *et al.*, 1998; De Smit *et al.*, 2006; Everaert *et al.*, 2007). Moreover, both increased levels of CO_2 in the beginning of incubation, and at the end of incubation to stimulate hatch, are becoming common practice in the incubation industry. However, there is still a need for optimization of the dose and the administration window (De Smit *et al.*, 2006). Therefore, a more profound understanding about the physiological changes induced by different hypercapnic regimes is needed. One of the processes in the development which may change under hypercapnic conditions is the angiogenesis in the CAM. In this chapter, the previously developed fast and objective methodology is used to quantify changes in the vascular network of the CAM under hypercapnic conditions, built up gradually during the first ten days of incubation.

4.2 Materials and Methods

4.2.1 Experimental design

4.2.1.1 Experiment 1

For the first experiment 1200 fresh Cobb eggs from a 43-weeks-old broiler breeder flock (*Gallus gallus*) provided by Vervaeke (Tielt, Belgium) are randomly divided equally in two incubators after individual numbering and weighing. One incubator is a standard forced-draft (control) incubator (PasReform, Zeddam, The Netherlands) with a capacity of 600 eggs. The second incubator is an adapted air-tight forced-draft (CO_2) (PasReform, Zeddam, The Netherlands) incubator in which CO_2 (100% CO_2, N25, Air Liquide, Belgium) is automatically injected according to a programmed pattern shown in figure 4.1. After 24 hours of

incubation the CO_2 concentration is gradually increased until 1.5 % is reached at 96 hours. This concentration of CO_2 is maintained until 240 hours. Both groups are incubated at a dry bulb temperature of 37.6 °C and wet bulb temperature of 29.9 °C. The turning frequency of the eggs is set at once an hour over an angle of 90°. On ED 10, all eggs are mixed and randomly distributed in the two incubators which are further normally ventilated, set at 37.6°C and 45% relative humidity. Every day, from ED 10 up to and including ED 14, 10 eggs per group are taken out and the angiogenesis in the CAM is analyzed. All eggs are weighed before the incubation to determine initial egg weight, and egg weight at sample time. The absolute weight loss, and the relative weight loss to the initial egg weight are calculated.

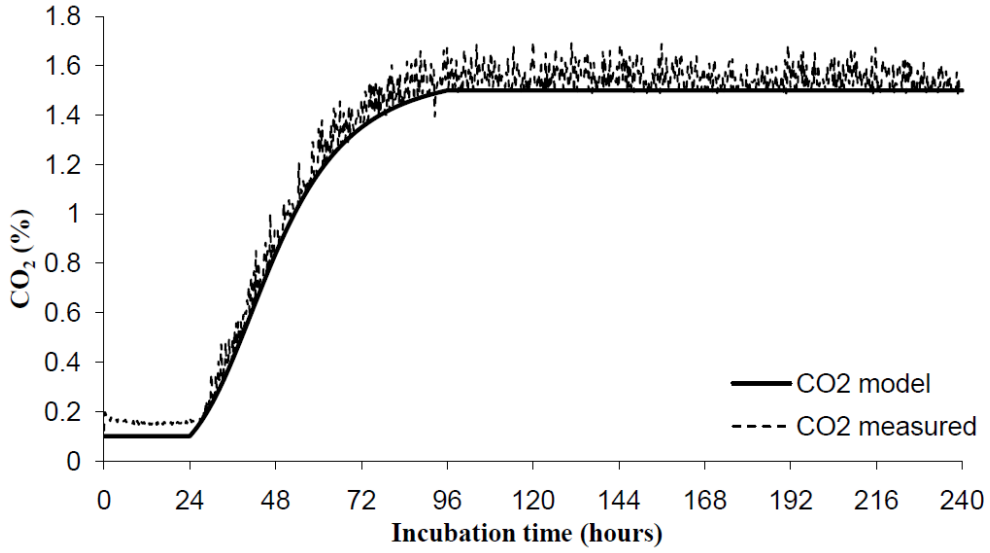

Figure 4.1 Programmed CO_2 pattern, and measured CO_2 pattern for the first ten days after which normal CO_2 concentrations are reestablished.

4.2.1.2 Experiment 2

For the second experiment, 400 fresh Cobb eggs from a 39-weeks-old broiler breeder flock (*Gallus gallus*) provided by Belgabroed (Merksplas, Belgium) are incubated in the same way as the first experiment. The temperature is set at 37.6°C dry-bulb temperature and 29.9°C wet-bulb temperature. The angiogenesis in the CAM of 20 eggs per group, and per ED from ED 10 up to and including ED 16 is analyzed. Moreover, besides the weighing of the eggs before incubation and at sample time to determine initial egg weight and egg weight at sample time, the embryo itself is weighed after removal from the egg to determine absolute

embryo body weight, as well as relative to initial egg weight and relative to egg weight at sample time. The embryo is dried for 24 hours in an oven at 105°C to determine the absolute dry embryo body weight and both relative dry embryo body weights, namely relative dry embryo body weight to initial egg weight, and relative dry embryo body weight to egg weight at sample time.

4.2.2 Sample preparation

The sample preparation is the same as explained in the previous chapter. The eggs are opened at the sharp end, after which yolk, albumen and embryo are carefully removed. The CAM stays attached to the eggshell and the egg is filled with formalin for 24 hours to fixate the erythrocytes in the blood vessels. The eggshell with attached CAM is divided in three bands (A, B, C) and every band is cut into 8 pieces with a diamond blade mounted on a dremel drill (Dremel Multipro, Dremel Europe, Breda, The Netherlands) (figure 3.1).

4.2.3 Measuring Configuration

Pictures are taken of the pieces of CAM attached to the eggshell using the set-up previously developed and described in chapter 3. A CANON EOS-1Ds Mark II commercial digital camera with extension tube EF12 II and macro lens MP-E 65mm f/2.8 1-5x (Canon Inc., Tokyo, Japan), set at magnification 5x is used. The obtained resolution of the combination is 2.64 µm per pixel. So vessels of 10 µm are represented by almost 4 pixels. To ensure a sufficient depth of field, the diaphragm is set at its smallest aperture (f/16) while the shutter time is determined by the camera in the fixed set-up at 8 seconds. The ISO value is set at 100 to minimize the noise. A manual white balance is chosen to increase the contrast between blood vessels and background. The samples are illuminated with two Farnell Luxeon Star W/Optic LED's of 530 nm (Farnell, Grace-Hollogne, Belgium) which are placed at 45 degrees at each side of the sample. The set up is discussed more in detail in the previous chapter (figure 3.2).

4.2.4 Image processing

Pictures of the samples of CAM are processed by algorithms implemented in Matlab 7.5 software (The Mathworks Inc., Natick, USA) as described in the previous chapter. The results

are binary images of the skeleton of the vascular network (figure 3.3) on which two structural parameters are calculated, namely the vascular fraction (VF) as a measure for the density of the vascular network, and the fractal dimension (FD) as a measure for the branching degree of the vascular network.

4.2.5 Statistics

The structural parameters are calculated for each band (A, B and C) by taking the average of the 8 pieces of each band. To test the differences between the groups (hypercapnia and control), the bands (A, B and C), and the ED (10, 11, 12, 13, 14, (15 and 16)), a three way ANOVA is performed. During model building, all main effects as well as all possible interactions are considered as plausible covariates. A hierarchical model building procedure is followed in order to remove non significant terms from the model. Linear contrasts are set up in order to estimate differences between the considered settings. In the same way, models are built for the weights of the eggs and embryos, and for the weight loss as dependent variables. For all analyses SAS 9.2 is used (SAS Institute Inc., Cary, North Carolina, USA).

4.3 Results

4.3.1 Incubation conditions

Until ED 10 the eggs are incubated in different incubators in which temperature, relative humidity (RH) and CO_2 concentrations are controlled. Due to unforeseen circumstances, the average RH in the hypercapnic incubator in the first experiment raised to 70 % during these first 10 days. The RH of the control incubator was increased to minimize the differences in RH between both groups as much as possible. The control incubator had an average RH of 61 % in the first experiment. The regulation of the RH in the hypercapnic incubator in the second experiment was optimized compared to the one in the first experiment which resulted in a RH which reached closer to the set-point compared to the RH in the first experiment. This resulted in an average RH of 63 % in the hypercapnic incubator in the second experiment. The control incubator had an average RH of 56 % in the second experiment. The CO_2 profile was the same for both experiments.

4.3.2 Experiment 1

In the model for the VF (*n*=256) as well as for the FD (*n*=256), group (control, hypercapnia), ED (10, 11, 12, 13, 14), and band (A, B, C) are significant as independent variables. There is no significant interaction between the ED and the bands. The *p*-value of the interaction between ED and group in de model for the VF is 0.0729. This is a borderline case, but is chosen to be included in the model since it seems to reveal a systematic pattern between both groups which is confirmed in the second experiment (see below).

Overall, both the VF and FD are significantly higher in the hypercapnia group compared to the control group (p = 0.0003 and p = 0.0032 respectively) (table 4.1). The structural parameters of band C, the one closest to the air cell, are significantly higher compared to those of band B (p = 0.0049 and p = 0.0003 for VF respectively FD). Additionally, the structural parameters of band B are found to be significantly higher compared to band A (p < .0001 for VF and FD) (table 4.1).

Table 4.1 Overview of significant overall mean differences for vascular fraction (VF) and fractal dimension (FD) in experiment 1 between the groups (control and hypercapnia) and between the bands (A, B, and C). * $p < 0.05$ ** $p < 0.01$ NS = non-significant p values (n=256).

	Control-hypercapnia	bandC-bandB	bandB-bandA	bandC-bandA
VF	-3.45×10^{-4}**	3.71×10^{-4}**	6.49×10^{-4}**	10.20×10^{-4}**
FD	-10.69×10^{-3}**	14.04×10^{-3}**	22.79×10^{-3}**	36.83×10^{-3}**

Both structural parameters increase significantly from ED 10 until ED 13 (figure 4.2). In the control group the VF increases from ED 10 until 14 with one exception, namely from ED 11 to 12 there is no significant increase (figure 4.2). The VF is significantly higher in the hypercapnia group compared to the control group on ED 12 and 13 (p = 0.0255 and p < .0001 respectively). The correlation between VF and FD is 0.94.

The initial egg weight and the egg weight at sample time are not different between both groups. On the other hand, the weight loss, absolute as well as relative, is 0.33 g respectively

0.46 % higher for the control group compared to the hypercapnia group (both $p < .0001$) (n = 100).

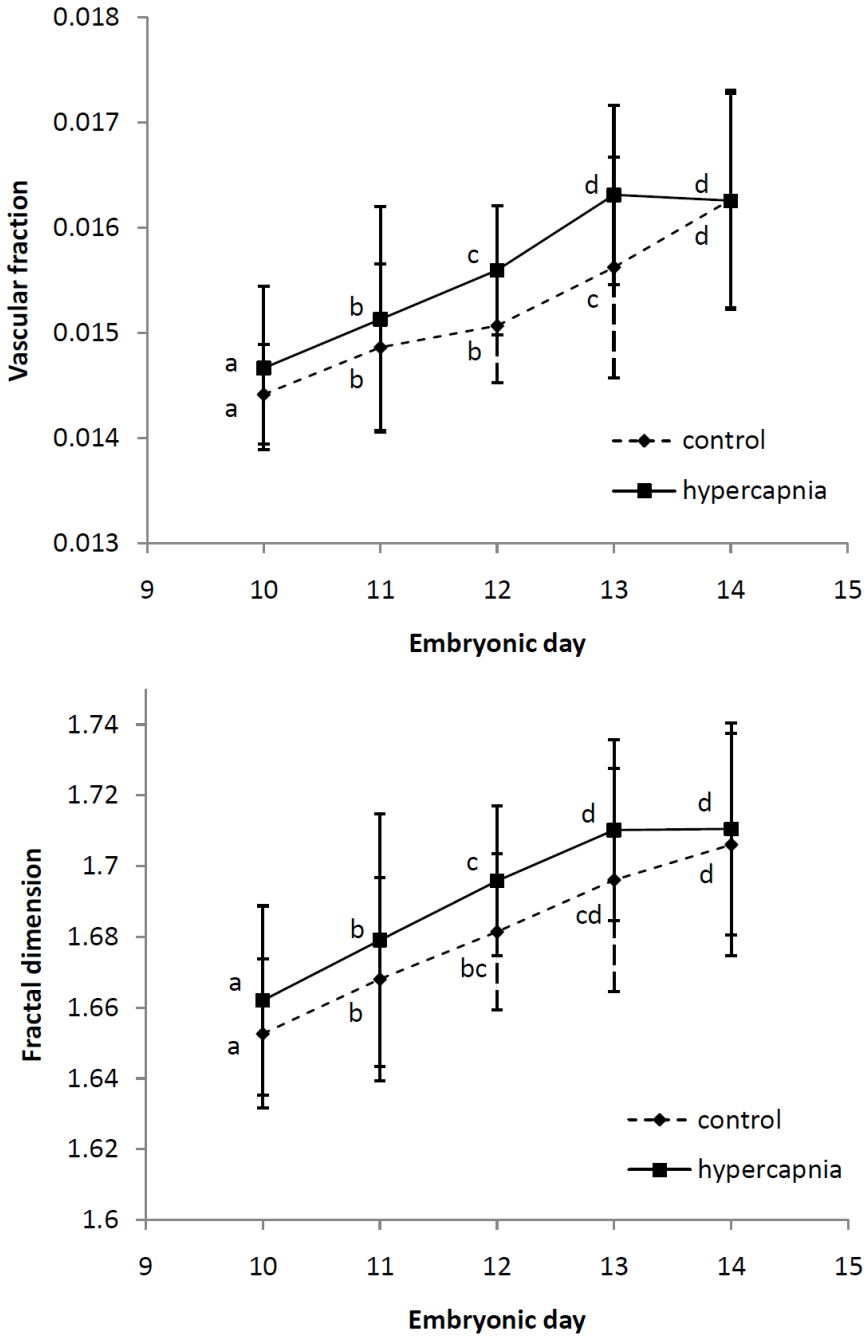

Figure 4.2 Mean values of vascular fraction (VF) (top image) and fractal dimension (FD) (bottom image) for both groups on the measured embryonic days (ED) in the first experiment (n = 256). The control group is marked with diamond symbols and dashed standard deviation bars, and the hypercapnia group with square symbols and full standard deviation bars. Values sharing no common letters are significantly different ($p < 0.05$). For the FD there are no significant differences between

the groups per ED, however, over all ED the hypercapnia group has a higher FD compared to the control group (p = 0.0032).

4.3.3 Experiment 2

In the models (n=728) for VF and FD, built as described in the materials and methods section, the following independent variables are important: ED (10, 11, 12, 13, 14, 15, 16) (p < .0001 for VF and FD), group (control, hypercapnia) (p < .0001 for VF and FD), their interaction (p = 0.0233 and 0.0093 for VF and FD respectively), band (A, B, C) (p < .0001 for VF and FD), and its interaction with ED (p = 0.0145 and 0.0065 for VF and FD respectively).

Overall, both the VF and FD are significantly different between the control group and the hypercapnia group with higher values in the hypercapnia group (p < .0001 for VF and FD) (table 4.2). All three bands, over all ED, are significantly different concerning their structural parameters with the highest ones in band C, the closest to the air cell, and the lowest ones in band A, at the sharp end of the egg (all p < .0001 for VF and FD, except p=0.0303 for the difference in VF between band A and B) (table 4.2).

Table 4.2 Overview of significant overall mean differences for vascular fraction (VF) and fractal dimension (FD) in experiment 2 between the groups (control and hypercapnia) and the bands (A, B, and C). * p < 0.05 ** p < 0.01 NS = non-significant p values (n=728).

	Control-hypercapnia	bandC-bandB	bandB-bandA	bandC-bandA
VF	-2.99×10^{-4}**	2.39×10^{-4}**	1.31×10^{-4}*	3.70×10^{-4}**
FD	-8.77×10^{-3}**	10.50×10^{-3}**	8.53×10^{-3}**	19.03×10^{-3}**

The hypercapnia group has significantly higher structural parameters than the control group from ED 10 up to and including ED 14 (figure 4.3). Both structural parameters increase significantly from ED 10 until 15 in the control group as well as in the hypercapnia group (figure 4.3) with two exceptions. The first exception is the VF in the control group, which does not increase significantly between ED 12 and 13 (p=0.1318). The second exception is the FD in the hypercapnia group, which does not increase significantly anymore between ED 14 and 15 (figure 4.3). The correlation between VF and FD is 0.95.

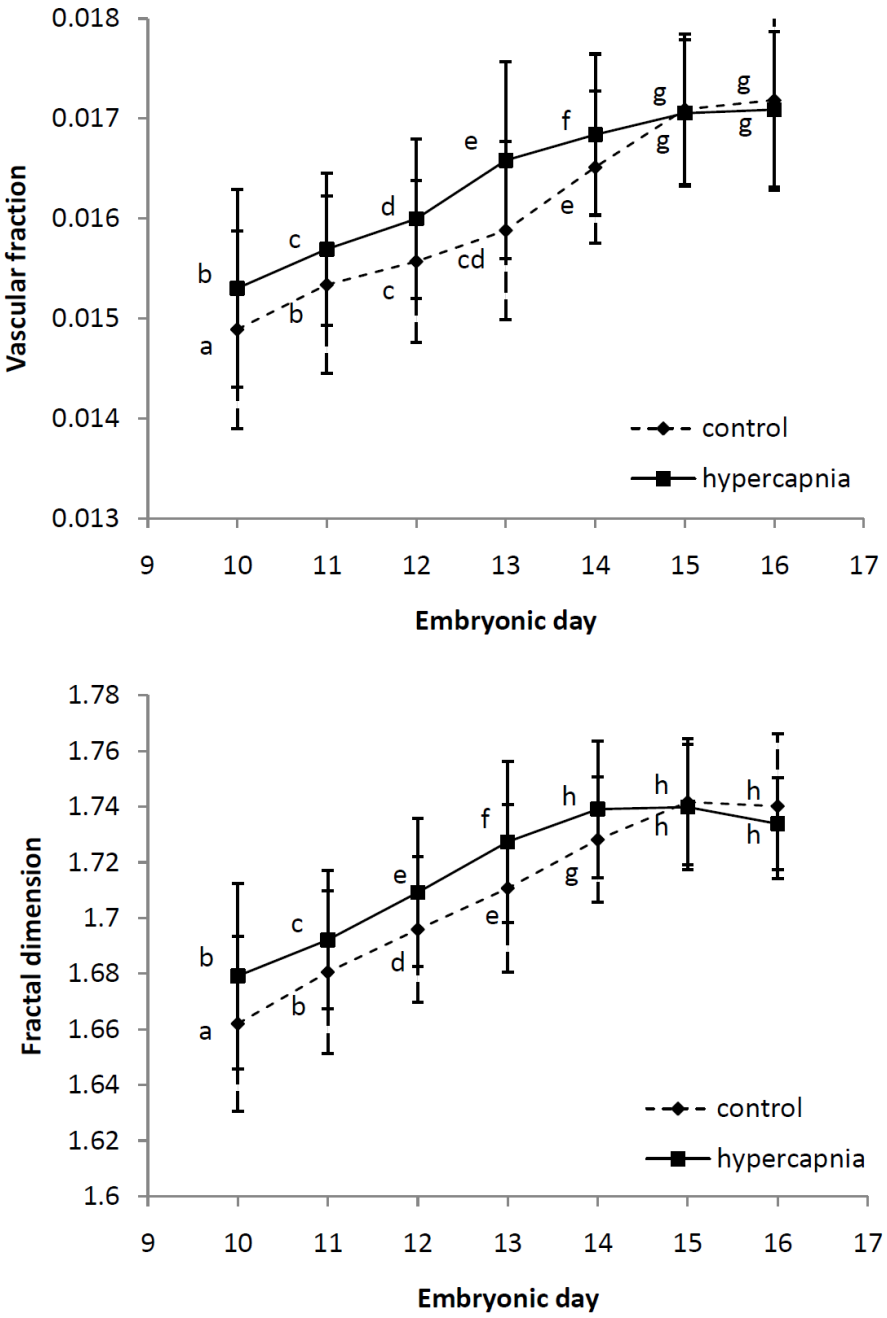

Figure 4.3 Mean values of vascular fraction (VF) (top image) and fractal dimension (FD) (bottom image) for both groups on the measured embryonic days (ED) in the second experiment (n = 728). The control group is marked with diamond symbols and dashed standard deviation bars, and the hypercapnia group with square symbols and full standard deviation bars. Values sharing no common letters are significantly different ($p < 0.05$).

The VF and FD of band C increase both from ED 10 until 14 (table 4.3). In band B, only the VF increases until ED 15, while the FD does not change after ED 14. In band A there is an

increase for both structural parameters until ED 15. Between ED 12 and 13 there is no increase in the VF as well as the FD for band A and B.

Table 4.3 Overview of significant mean differences in experiment 2 between the embryonic days (ED) for vascular fraction (VF) and fractal dimension (FD) per band (A, B, and C). * $p < 0.05$ ** $p < 0.01$ NS = non-significant p values (n=728).

VF	ED11-10	ED12-11	ED13-12	ED14-13	ED15-14	ED16-15
A	5.20×10^{-4}*	5.29×10^{-4}**	(1.73×10^{-4}) NS	6.85×10^{-4}*	5.28×10^{-4}**	(4.68×10^{-4}) NS
B	8.91×10^{-4}**	2.89×10^{-4}*	(1.80×10^{-4}) NS	6.18×10^{-4}**	4.21×10^{-4}*	(2.20×10^{-4}) NS
C	2.89×10^{-4}*	3.47×10^{-4}**	4.12×10^{-4}**	4.23×10^{-4}*	(3.38×10^{-4}) NS	(0.15×10^{-4}) NS

FD	ED11-10	ED12-11	ED13-12	ED14-13	ED15-14	ED16-15
A	18.69×10^{-3}**	19.01×10^{-3}**	(7.54×10^{-3}) NS	26.84×10^{-3}**	7.78×10^{-3}*	(12.4×10^{-3}) NS
B	29.38×10^{-3}**	19.18×10^{-3}**	(8.02×10^{-3}) NS	19.82×10^{-3}**	(7.59×10^{-3}) NS	(-4.29×10^{-3}) NS
C	13.74×10^{-3}**	20.66×10^{-3}**	13.29×10^{-3}**	12.56×10^{-3}*	(6.12×10^{-3}) NS	(-0.36×10^{-3}) NS

Besides the egg weights and the weight losses, also the embryo weights are measured (n=280). The statistical analysis reveals that the initial egg weight and egg weight at sample time do not differ between the groups. Weight loss as well as relative weight loss is 0.41 g respectively 0.64 % higher for the control group compared to the hypercapnia group ($p <$ .0001 and $p = 0.0002$ respectively). The absolute embryo body weight, and relative to the initial egg weight are significantly higher, 0.192 g respectively 0.0040, in the hypercapnia group ($p = 0.0175$ and $p = 0.0142$ respectively) during the measured period from ED 10 to 16. All dry embryo body weights (absolute and both relative ones) are significantly higher, 0.039 g respectively 0.0008 and 0.0007, in the hypercapnia group compared to the control group ($p = 0.02111$, $p = 0.0129$, and $p = 0.0482$ respectively) (figure 4.4).

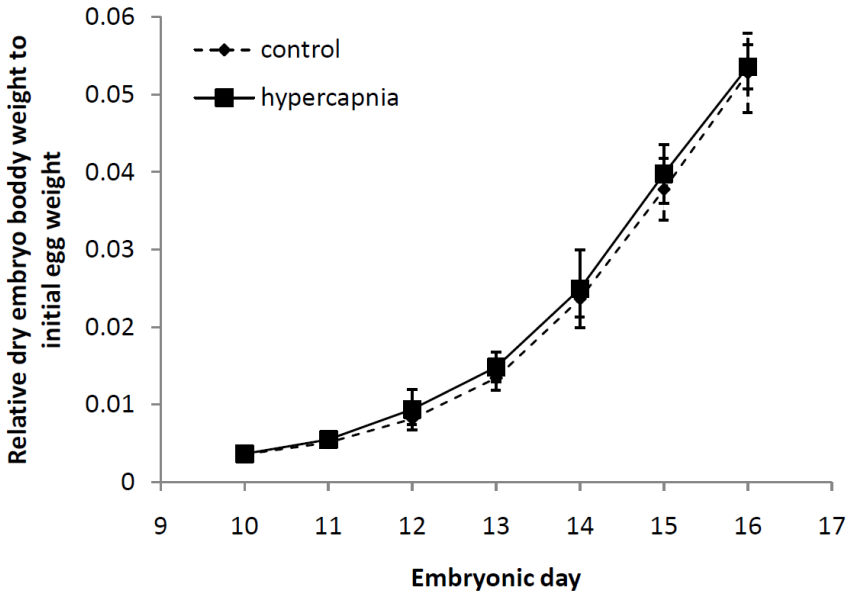

Figure 4.4 Overview of the average relative dry embryo body weight to initial egg weight per group and per embryonic day (ED) with standard deviation bars (*n*=280). Over all ED, the relative dry embryo body weight to initial egg weight is significantly higher in the hypercapnia group than in the control group (p = 0.0129).

4.3.4 Comparison of both experiments

The data of both experiments are compared with each other and the differences between the experiments are tested in the same way the previous differences between the groups are tested per experiment (figure 4.5). For simplicity reasons, first the average of VF and FD per egg over the three bands is calculated. Subsequently, a general linear model is built for the VF as well as the FD with experiment (1, 2), group (hypercapnia or control), and ED (10, 11, 12, 13, 14) as independent categorical variables (*n*=337). None of the interactions terms are significant. Both the VF and the FD are significantly higher in the second experiment compared to the first experiment (p < .0001), and for the hypercapnia group compared to the control group (p < .0001). For both experiments and both groups there is a significant increase in the VF and FD from ED 10 up to ED 14. ED 15 and 16 are not considered in this model since in the first experiment the CAMs of these embryonic days are not measured.

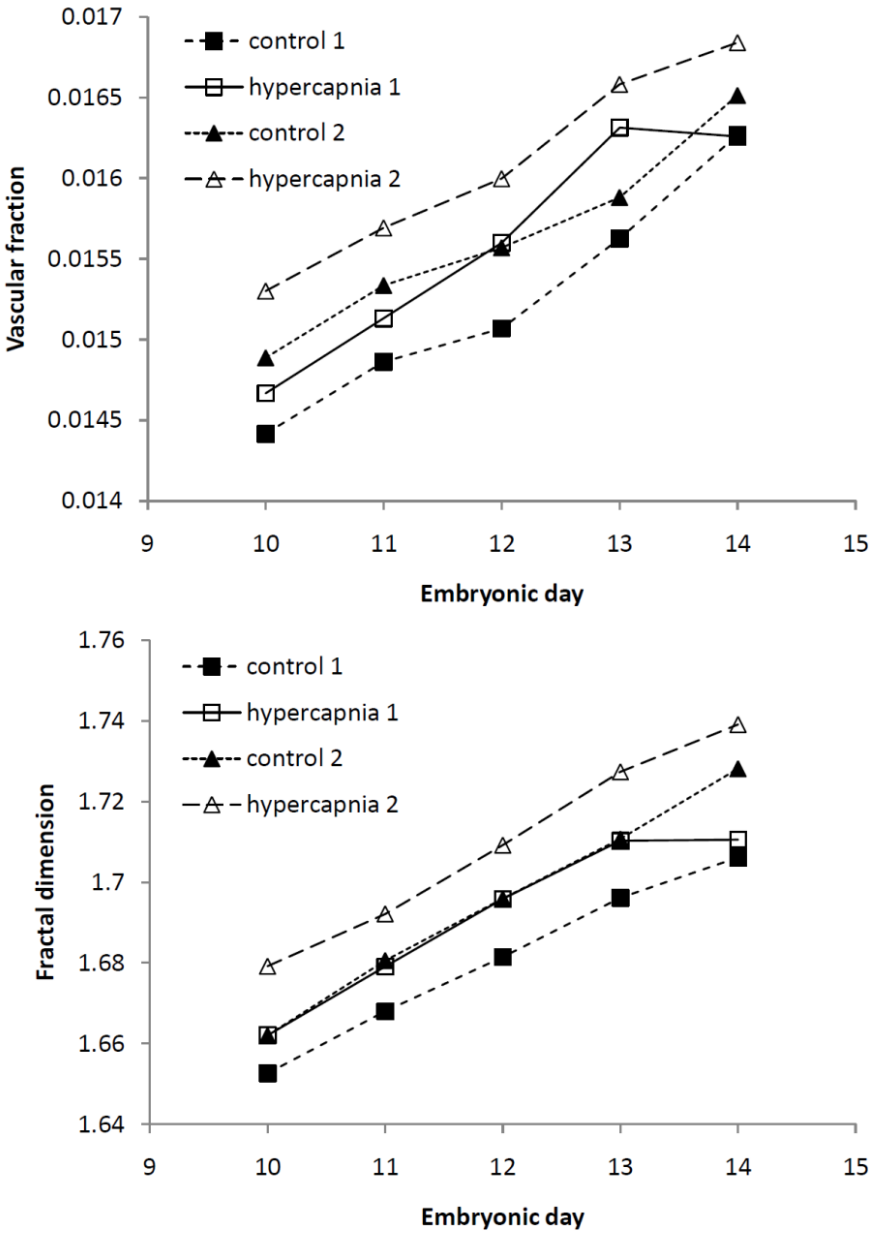

Figure 4.5 Mean values of vascular fraction (VF) (top image) and fractal dimension (FD) (bottom image), averaged over the bands, for both groups and both experiments on the measured embryonic days (ED) (*n* = 337). Experiment 1 is marked with square symbols and experiment 2 with triangle symbols. The filled symbols represent the control groups and the open symbols the hypercapnia groups. No standard deviation bars are shown to keep the figure clear.

The initial egg weight, egg weight at sample time, weight loss, and relative weight loss are also tested for differences between the experiments (*n*=380) (table 4.4). The initial egg weight and egg weight at sample time are significantly higher in the first experiment

compared to the second experiment (both $p < .0001$). The weight loss and relative weight loss are significantly higher in the second experiment ($p < .0001$). In both experiments, the weight loss and relative weight loss are also higher in the control group compared to the hypercapnia group ($p < .0001$).

Table 4.4 Mean values ± standard deviation of the initial egg weight, egg weight at sample time, weight loss, and relative weight loss per experiment, and the differences between both experiments. Per parameter, different letters indicate significant differences (all $p < .0001$).

	Experiment 1		**Experiment 2**	
Initial egg weight (g)	67.04 ± 3.93^{a}		64.10 ± 3.67^{b}	
Egg weight at sample time (g)	64.02 ± 3.91^{a}		60.21 ± 3.85^{b}	
	Control	**Hypercapnia**	**Control**	**Hypercapnia**
Weight loss (g)	2.75 ± 0.71^{a}	2.43 ± 0.65^{b}	4.10 ± 1.15^{c}	3.68 ± 0.94^{d}
Relative weight loss (%)	4.08 ± 1.07^{a}	3.65 ± 0.97^{b}	6.41 ± 1.89^{c}	5.77 ± 1.51^{d}

4.4 Discussion

4.4.1 Growth of the vascular network

As described in chapter 2, there are different mechanisms of angiogenesis, namely sprouting, intussusception, and elongation (Gargett and Rogers, 2001). Intussusception is the formation of transcapillary pillars of interstitial tissue in the vascular lumen (figure 2.2) (Kurz *et al.*, 2003). The more the vascular network in the CAM is developed, the higher the vascular fraction (VF) and fractal dimension (FD) will be. The first parameter is a measure for the density and the second one for the branching degree. The density, and therefore the VF, can increase without an increase in the branching degree, by elongation of the blood vessels. However, an increase in the branching degree by sprouting, measured by the FD, goes along with an increase in density. Intussusception will also increase both the FD and the VF (Kurz *et al.*, 2003).

The growth of the vascular network, observed in our study through an increase in both VF and FD, is in accordance with literature (Kirchner *et al.*, 1996; Nikiforidis *et al.*, 1999; Tazawa

and Whittow, 2000), and adds until now unknown characteristics of the growth of the network in the CAM such as the differences in type of growth which will be explained in what follows.

At the end of the development of the network, an increase in density by elongation seems to be dominant since only VF, and not FD, increases from ED 13 to 14 (control group of first experiment) or from ED 14 to 15 (hypercapnia group of the second experiment) (figure 4.2 and 4.3). Elongation occurs also in the placenta of mammals near the end of the pregnancy, when placental growth factor (PlGF) becomes the dominant vascular growth factor instead of vascular endothelial growth factor (VEGF). This shift causes a decrease in branching angiogenesis (Ancar and Chardonnens, 2003).

The development of the vascular network does not show a pure linear trend with time during incubation for the control group. Indeed, a period of reduced growth is observed from ED 11 to 12 (first experiment) or 12 to 13 (second experiment) in the VF (figure 4.2 and 4.3). After this period of reduced growth, a period of increased growth is observed from ED 12 to 14 (first experiment), or ED 13 to 15 (second experiment) (figure 4.2 and 4.3). This cannot be seen in the FD of both experiments. Hence, it is postulated that the differences in increase in density mainly come from differences in the proportion of the elongation form of angiogenesis in the total expansion of the network. A plausible explanation for this jump in the density of the vascular network around day 13 can be found from data on the acid-base status of the blood of the developing chicken embryo as presented by Dawes and Simkiss (1969) and Boutilier *et al.* (1977). On days 13-14 there is a significant drop in the pH. The strong increase in pCO_2 from day 11-14 due to the metabolism of the embryo, induces a decrease in pH in the blood which is normally compensated by an influx of bicarbonate. However, this influx of bicarbonate to neutralize the low pH, lags around 24 hours behind the rise in pCO_2, which causes a fall in pH from day 11 to 13. From that point onwards the compensation catches up with the increasing pCO_2 in the blood (Boutilier *et al.*, 1977; Bruggeman *et al.*, 2007; Dawes and Simkiss, 1969). The stimulatory effect of vascular endothelial growth factor (VEGF) and basic fibroblast growth factor (bFGF) on angiogenesis is enhanced by low pH (Burbridge *et al.*, 1999). Both vascular growth factors are known regulators of angiogenesis in the CAM (Ribatti and Presta, 2002; Ribatti *et al.*, 1995).

Moreover, the transcription of VEGF is shown to be increased by acidic pH (D'arcangelo *et al.*, 2000; Fukumura *et al.*, 2001; Xu *et al.*, 2002). Subsequently, the sharp increase in the VF of the CAM is believed to be due to the time lag of the compensation by bicarbonate for low pH and the rising pCO_2 in the blood due to the metabolism, resulting in a decreased pH.

4.4.2 Effect of hypercapnia on angiogenesis in the CAM during development

The results described above show, for the first time, that early hypercapnia, without surpassing the physiological limits, has a stimulating effect on the angiogenesis in the CAM during early incubation (table 4.1, and 4.2, figure 4.2 and 4.3). In the end, both groups reach an equally developed vascular network (figure 4.2 and 4.3). The stimulating effect of hypercapnia and systemic acidosis on angiogenesis is already described in other tissue by Howell *et al.* (2004), Holmes *et al.* (1994; 1998), and Irie *et al.* (2005). In analogy with literature data, the stimulating effect of hypercapnia on the angiogenesis found here can be attributed to a lower pH in the eggs and the blood (acidosis) of embryos incubated under hypercapnic conditions. A lower pH enhances the effect of VEGF and bFGF, the main regulators of angiogenesis in the CAM as described above. Bruggeman *et al.* (2007) show that for eggs incubated under identical conditions, albumen pH, measured on ED 0, 3, 4, 5, 6, 7, 8, 9, 10, and 12, is significantly lower in the hypercapnia group from ED 3 to 12 with significant differences at ED 3, 4, 5, 6, 7, and 10. Probably there is also an associated lower blood pH in the beginning of early hypercapnic incubation, which can explain the systematic bias between angiogenesis in the CAM of the hypercapnia group compared to the control group.

In figure 4.2 and 4.3, related to the first respectively the second experiment, a strong increase is seen for the VF of the hypercapnia group between ED 12 and 13, while this is seen from ED 13 to 14 in the control group. Hence, the jump in the VF occurs one day earlier in the hypercapnia group. Bruggeman *et al.* (2007) show that blood pH, measured on ED 10, 11, 12, and 14 does not differ between eggs incubated under identical conditions as described here. In both groups, they report a significant drop in blood pH from ED 12 to 14. However, ED 13 is not measured in the study by Bruggeman *et al.* (2007). Additionally, they report significant higher bicarbonate levels in the hypercapnia group at ED 14. Since bicarbonate levels lag 24 hours behind the decrease in pH (Dawes and Simkiss, 1969), it can

be assumed that there is a significant difference in pH between the hypercapnia and control group on ED 13. This may have caused the difference in angiogenesis in the CAM as explained above, and so caused the shift of the jump in the increase of VF from ED 13-14 to ED 12-13. This needs to be investigated in further research.

The hypercapnic treatment is induced from 24 hours of incubation until 240 hours (ED 10), leading to differences which persist after ED 10. The differences during the hypercapnic treatment itself may be higher, but cannot be measured by the used method. In the second half of incubation, there is still an effect of early hypercapnic incubation besides the difference in offset at ED 10 and the following ED, namely the shift of the jump in the increase of VF between ED 13 and 14 to one between ED 12 and 13. Nevertheless, the differences attenuate when reaching the maximal development of the vascular network. Up to date no suggestions for these persistent effects can be given, except a (partially) sustained difference in metabolism between both groups which causes a difference in acid-base balance after hypercapnic conditions were reset to normal. De Smit *et al.* (2006) report a significant lower *pO2/pCO2* in the air cell of the eggs in the early prenatal hypercapnia group compared to the control group from ED 10 until ED 15-16, due to a significant lower *pO2* and higher *pCO2*, probably as the result of a higher metabolism of the embryos.

4.4.3 Local differences in angiogenesis

The vascular development in the CAM differs locally. The local differences between the bands are independent of the group. In band C, located closest to the air cell, the VF and FD are significantly higher compared to the ones in band B, and the ones in band B compared to the ones in band A (table 4.1 and 4.2). These results are in accordance with the ones in the hypoxia-control experiment of chapter 3. All are in accordance with the normal growth of the CAM, and the local differences in eggshell conductance as explained in chapter 3. In experiment 2, the differences between the bands interact with ED. In band C, the closest one to the air cell, both structural parameters increase from ED 10 until 14 in both groups. In band B and A, at the sharp end of the egg where the CAM develops later, the angiogenesis continues until ED 15, but with no measurable growth from ED 12 to 13 for both groups (table 4.3).

4.4.4 Differences in embryo weights

Part of the wet weight difference in the embryos measured in experiment 2, may have been a result of the differences in weight loss between both groups due to the different RH in the two incubators during the first 10 days (63 % versus 56 % for hypercapnia and control group respectively). Davis and Ackerman (1987) report a relation between the water loss in the egg and the wet embryo mass. Nevertheless, also the dry embryo weights are significantly higher in the hypercapnia group. From this it can be concluded that at least a part of the difference in embryo weight is due to the early hypercapnic treatment, which confirms the results of De Smit *et al.* (2006).

4.4.5 General effect of hypercapnia

The differences in embryo weight, together with the higher developed vascular network in the CAM, and the shift of the jump in increase of VF to one day earlier in the hypercapnia group compared to the control group, confirms the hypothesis that chicken embryos incubated under early hypercapnic conditions develop faster (Bruggeman *et al.*, 2007; De Smit *et al.*, 2006). De Smit *et al.* (2006) conclude that chickens incubated under early prenatal hypercapnia have a higher weight and hatch earlier. Nevertheless, the differences in the structural parameters of the vascular network, measured in this paper, attenuate. This may result in a disadvantage from ED 15 onwards for the embryos of the hypercapnia group since they have a higher weight but an equally developed vascular network in the CAM compared to the ones of the control group. If this results in more severe hypoxia for the embryos in the hypercapnia group must be investigated in further research. Other factors such as the affinity of the red blood cells for oxygen may also play a role (Bissonnette and Metcalfe, 1978; Dragon and Baumann, 2003; Tazawa, 1980).

4.4.6 Differences between the experiments

The angiogenesis is different between both experiments. The progression of both parameters, VF and FD, is very similar between the experiments, for the control group as well as the hypercapnia group. The effect of early hypercapnia is the same in both experiments since there is no significant effect of the interaction between the experiment

and the group on VF or FD. There is only a systematic difference between the values of the structural parameters between both experiments (figure 4.2, 4.3 and 4.5). The vascular network in the CAM of the eggs in the first experiment is less developed compared to the ones in the second experiment. The differences in conditions between both experiments are the flock age, which is 43 weeks in experiment 1 and 39 weeks in experiment 2, and probably differences in the flock management in the breeding farm, which is Vervaeke in experiment 1 and Belgabroed in experiment 2. Moreover, the RH in the incubator is different between both experiments. At last, there is also a significant difference between both experiments concerning the weight loss of the eggs, absolute as well as relative to the initial egg weight. Which of these factors, namely flock age, flock management, RH, or weight loss, is related to the difference in the angiogenesis in the CAM between both experiments is not clear. Moreover, these factors interact with each other.

The RH may have an influence on the angiogenesis in the CAM indirectly via its influence on the embryonic development. Furthermore, there will be some relation between the weight loss and the angiogenesis in the CAM via (1) the eggshell conductance which probably affects both, or (2) via the influence of RH on the weight loss, the embryonic growth, and so indirectly on the angiogenesis in the CAM. Nevertheless, these relations are not unambiguous ones as can be seen from comparison of both tables below (table 4.5 and 4.6). Neither the difference in RH, nor the difference in weight loss is unambiguously related to the differences in the angiogenesis over both experiments and both groups. So, from these data, no conclusions can be drawn on the relation between RH or weight loss and the angiogenesis in the CAM.

Table 4.5 RH, weight loss, and the angiogenesis in the CAM determined by VF and FD compared between the two experiments over both groups.

	Experiment 1		**Experiment 2**
RH	70% & 61%	>	63% & 56%
Weight loss (table 4.4)		<	
VF and FD (figure 4.5)		<	

Table 4.6 RH, weight loss, and the angiogenesis in the CAM determined by VF and FD compared between both groups over both experiments.

	Hypercapnia		Control
RH	70% & 63%	>	61% & 56%
Weight loss (table 4.4)		<	
VF and FD (figure 4.5)		>	

The differences in angiogenesis between both experiments may also be linked to the differences in flock management and/or age and the correlated variations. The initial egg weight is significantly higher in the first experiment in accordance with the higher flock age (67.04 ± 3.93 g in experiment 1 and 64.10 ± 3.67 g in experiment 2) (Peebles and Brake, 1987). These differences in the initial egg weight may also partially be due to differences in the flock management. Furthermore eggshells of eggs from an older flock age normally have a higher eggshell conductance (Peebles and Brake, 1987). These differences in eggshell characteristics with flock age impact the growth of the embryo (Peebles *et al.*, 2001), and therefore may also impact the associated angiogenesis in the CAM. The eggshell conductance may also have a direct effect on the angiogenesis in the CAM (Wagner-Amos and Seymour, 2003). However, the relation between eggshell conductance and the vascular development in the CAM is not unambiguously elucidated (Wagner-Amos and Seymour, 2003). The fact that the angiogenesis in the CAM does not unequivocally match to the development of the embryo is confirmed in this study. Although the eggshell conductance may be assumed to be the highest for the eggs in experiment 1, the vascular network in their CAM is less developed compared to the ones in experiment 2. To elucidate this relation, the eggshell conductance should be determined in future research. Anyhow, the differences in the flock age are very small and their impact may therefore be minimal. Another possible explanation for the differences in angiogenesis is the flock management in the breeding farm. Flock management may change the internal quality of the egg and/or the quality of the eggshell (Renema, 2007). The feeding program for example affects egg quality such as the nutrients in the egg, and subsequently chick quality (Aviagen, 2007; Cobb, 2008).

4.5 Conclusions and future research

In this chapter, the methodology described in chapter 3 is used to quantify the angiogenesis in the CAM under normal and early hypercapnic conditions. Two experiments are conducted in which the same CO_2 profile is applied, namely a gradual increase in CO_2 concentration from 24 hours of incubation to 1.5 % at 96 hours. This concentration is maintained until 240 hours of incubation after which normal values are reestablished. The development of the vascular network is monitored from embryonic day (ED) 10 until ED 14 in experiment 1, and until ED 16 in experiment 2. This development is characterized by two different parameters – the vascular fraction (VF) as a measure for the density of the network, and the fractal dimension (FD) of the vascular network as a measure for the degree of branching. Moreover, in experiment 2, embryo weights are compared between both groups. The results show that differences in the development of the vascular network can be observed across groups, but also as function of the embryonic day. Both VF and FD, and the embryo weight are shown to be higher in the hypercapnia group compared to the control group. The period between ED 12 and 14 seems to be important with respect to angiogenesis. This period is characterized by a relatively higher increase of VF in the CAM compared to the increase between the other ED. This relatively higher increase occurs one day earlier under hypercapnic conditions during incubation. It seems plausible that the differences in angiogenesis come from differences in the acid-base balance caused by the hypercapnic conditions, and subsequently the effect of the pH on the binding activity and expression of VEGF and bFGF, the main regulators of angiogenesis in the CAM.

From these results, new hypotheses arise for which no literature data is available, namely that flock age or/and management influence the angiogenesis in the CAM, and that the acid-base balance in the blood of the embryo has an effect on the angiogenesis in the CAM. Therefore, in future research, the influence of flock age and management on angiogenesis in the CAM may be investigated. Moreover, the pH, pCO_2 and bicarbonate levels in the chorioallantoic blood should be measured every day during incubation, and especially at ED 12, 13, and 14 together with the angiogenesis in the CAM. VEGF and bFGF in the CAM should be measured as well, in order to correlate them with the angiogenesis, and to check if there are differences in their concentrations at ED 13.

Chapter 5

Investigations on the Use of SRS to Measure Angiogenesis in the CAM

5.1 Introduction

To monitor the angiogenesis in the chorioallantoic membrane (CAM) throughout its development and to correlate it with health and disease in adult life, non-destructive techniques must be developed. This makes that one individual can be followed during its whole life and long-term effects can be identified. Additionally, it enables the elimination of the inter-individual variability. This chapter describes a method which has theoretically the potential of measuring the angiogenesis in the CAM non-invasively. However, in this first study, the eggshell is still removed since it poses some practical problems which should be addressed in further research. So, although the described method is still destructive, it constitutes the first step towards a non-invasive and non-destructive measurement of the angiogenesis in the CAM.

As described in chapter 2, CT, MR, PET, and ultrasound in clinical settings do not reach the resolution necessary to visualize the pre- and postcapillary blood vessels in the CAM (10 µm). Higher resolutions are achieved with these techniques in research settings. However, the dose of radiation would become lethal to the embryo (De Clerck, 2005). Additionally, the injection of a contrast agent makes these methods invasive. Optical measurements do not have these disadvantages. Moreover, blood has a very typical light absorption spectrum. Therefore, spectral measurements are chosen to follow up the angiogenesis in the CAM non-destructively. The strong absorption of light by the growing embryo in the egg from ED 10 onwards, imposes a restriction to the use of transmission spectroscopy (Kemps *et al.*, 2010). Since the CAM is in close contact with the eggshell, only the subsurface blood has to be measured, which may be achieved using reflectance spectroscopy. Not only the amount of blood in the CAM is an important parameter, the structure of the network contains information too as it changes with incubation time and conditions.

Spatially resolved spectroscopy (SRS) is a technique based on Near Infrared Spectroscopy (NIRS), but instead of one source and one detector, multiple detectors are used at different distances from the source. In combination with light propagation models, the absorption and scattering coefficients of the tissue can be estimated. Since scattering arises from relative refractive index differences between the different structures in the tissue, SRS thus

provides information on both the composition and the microstructure of the tissue (Lu, 2004; Pogue *et al.*, 2004; Srinivasan *et al.*, 2003). The technique has applications both for the determination of the optical properties of biological tissue as of those of agricultural products. SRS with large source-detector distances is used to investigate tissue volumes of several cm^3. More local and less deep tissue measurements can be performed with smaller source-detector distances (Bevilacqua and Depeursinge, 1999).

In this chapter, a spatially resolved spectroscopy set-up with small source-detector distances is elaborated and used to measure differences in the angiogenesis in the CAM. The eggshell causes different problems for the use of spatially resolved spectroscopy to measure the angiogenesis in the CAM. The eggshell of broilers contains protoporphyrin, which colors the shell (partially) brown. The absorption peaks of protoporphyrin (539, 589 and 643 nm) are very close to the ones of hemoglobin (542 and 577 nm) since their chemical structure is very similar. Moreover, the eggshell strongly scatters the light, making it difficult to distinguish the signal from inside the egg from the one from the eggshell. For these reasons, in this first study, the eggshell is removed and measurements are performed directly on the CAM. In future research, the problems with the shell should be addressed to come to a really non-destructive technique. In a first analysis, the blood value based on the spectral information of the first collection fiber is used to determine the amount of blood. Next, the spectra are evaluated without estimation of the optical properties. Finally, the light propagation in the tissue is modeled using the most simple approximation, namely the diffusion theory. This leads to a preliminary estimation of the absorption and scattering coefficients. In what follows, first some information on the diffusion theory is given. Subsequently the experimental part is described.

5.2 The Diffusion Theory

5.2.1 Definitions

Before giving an overview of the important literature on the topic, some terms concerning the tissue optical properties are explained for understanding the theory of light propagation in tissue. The light, when entering the tissue, interacts with this tissue in different ways

(figure 5.1). It can be absorbed or scattered in a single scattering event or in multiple scattering events. The first phenomenon is described by the absorption coefficient μ_a (mm^{-1}), which is the ratio between the power absorbed in a unit volume and the power incident per unit area (Martelli *et al.*, 2009). Absorption of light in tissue is due to endogenous chromophores such as hemoglobin and melanin. The second phenomenon, scattering, is described by the scattering coefficient μ_s (mm^{-1}) and the phase function $p(\hat{s}',\hat{s})$. The scattering coefficient μ_s is the ratio between the power scattered in a unit volume and the power incident per unit area (Martelli *et al.*, 2009). The reciprocal describes the mean free path of scattering (Wilson and Jacques, 1990). The phase function $p(\hat{s}',\hat{s})$ is the angular scattering probability function for scattering from direction $\hat{s}'$ to $\hat{s}$ (Cheong *et al.*, 1990; Martelli *et al.*, 2009). At the boundaries of the tissue, refraction or reflection can occur (figure 5.1). The first phenomenon is a change in the direction of light propagation when the light enters or leaves the tissue. The second phenomenon occurs when the light at the boundary is reflected back into the medium from where it comes. If the light is reflected back into the observed tissue, it is called internal reflection. This light propagation in and out the tissue is influenced by the relative refractive index differences between the tissue and the surrounding medium. The refractive index of a medium is given by $n = c/v$ with *c*, the speed of light in vacuum, and *v*, the speed of light in the medium. The refractive index of the tissue changes according to its water content (Wilson and Jacques, 1990): $n = 0.53 - 0.2 * W$ with *W*, the water content in percentage of the total mass, and *n*, the refractive index.

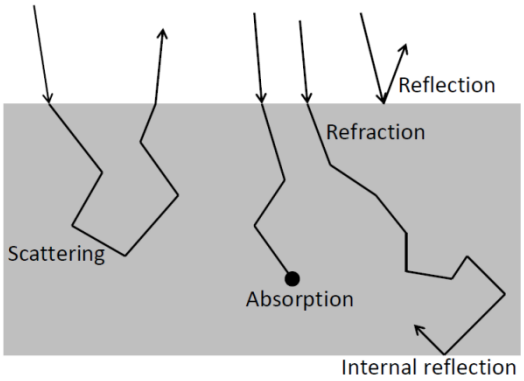

Figure 5.1 The basic interactions of light with a biological tissue

Typical values for these parameters for soft tissue in the 600-1000 nm range, the most used window for VIS-NIR Spectroscopy, range for μ_a from 0.005 mm^{-1} (Contini *et al.*, 1997) to 0.05

mm^{-1} or 1 mm^{-1} (Wilson and Jacques, 1990), for μ_s from 10 mm^{-1} (Wilson and Jacques, 1990) or 50 mm^{-1} until 200 mm^{-1} (Contini *et al.*, 1997), and for *n* from 1.38 to 1.41 (Wilson and Jacques, 1990). Subsequently, the ratio of scattering to absorption $N = \mu_s / \mu_a$ has a value from 10 to 40 000, showing that biological tissue is dominated by scattering in the VIS-NIR region.

When the thickness of the sample is relatively low compared to the mean free path of scattering, only single scattering will occur. The optical parameter which can be measured is the total attenuation coefficient $\mu_t = \mu_a + \mu_s$. The reciprocal is called the mean free path (*mfp*), describing the average distance traveled by a photon before a scattering or absorption event, and ranges from 5 to 100 µm (Wilson and Jacques, 1990). Very often however, in spectroscopic measurements, multiple scattering occurs. To fully describe these scattering phenomena in tissue, the phase function must be modeled. The function can be expanded in a series of Legendre polynomials (Bevilacqua and Depeursinge, 1999). In most practical cases, the scattering can be described sufficiently by the first order moment of the phase function, namely the mean cosine of the scattering angle θ, *i.e.* the anisotropy factor *g* = mean(cos(θ)) (Bevilacqua, 1998). When the scattering is mostly in the forward direction, *i.e.* forward-peaked scattering, as normally occurs in biological tissue, *g* tends to 1 (Hollis, 2002), with typical values of 0.8 - 0.95 in the 600-1000 nm range (Wilson and Jacques, 1990). This restricted anisotropy can be modeled by isotropic scattering via the application of the similarity relations (Hemenger, 1977; Wilson and Jacques, 1990). These state that the light propagation will be the same for different values of *g* and different values of μ_s as long as $\mu_s' = \mu_s(1-g)$ is the same. This coefficient μ'_s is called the reduced or transport scattering coefficient. In this way, linearly anisotropic material can be modeled with an isotropic scattering coefficient μ'_s. This gives rise to the definition of the effective or transport mean free path (*mfp'*) $1/\mu_t' = 1/(\mu_a + \mu_s')$, and the corresponding ratio of the transport scattering to absorption $N' = \mu_s'/\mu_a$, called the diffuseness by Doornbos *et al.* (1999).

All these optical properties determine the outcome of transmission or reflection measurements. In transmission, the light which has gone through the sample is detected. In reflection, the backscattered light is detected on the same side as the light is directed

towards the sample. The total reflectance of a tissue increases as *N'* increases (Wilson and Jacques, 1990).

5.2.2 A literature overview

In this paragraph, an overview will be given of the literature about light propagation modeling and measuring techniques in tissue. A crucial event in the history of VIS-NIR spectroscopy was the discovery of the differences in visible (VIS) and near-infrared (NIR) absorption spectra of deoxyhemoglobin (Hb) and oxyhemoglobin (HbO_2), giving rise to quantitative measurements of the O_2 saturation of blood, namely oximetry. Blood oximetry was then expanded to tissue oximetry giving information about the metabolic state of the tissue. Especially the 600-1000 nm light was able to penetrate relatively deep in the tissue. Therefore, the region of 600-1000 nm was called the therapeutical window and the field of investigations using this technique, Visual-Near InfraRed Spectroscopy (VIS-NIRS) of tissue. The technique was also used in agriculture for the determination of molecule concentrations in food. Via the Lambert-Beer law, a simple model could be used to link the concentration of a chromophore in a solution to the absorption of light by this solution. However, in tissue, the main challenge was light scattering due to the complex structures giving rise to differences in refractive indices. VIS-NIRS is also used in medical imaging. But due to the high scattering of VIS-NIR light in tissue, the contrast of the image decreases drastically, and VIS-NIR imaging cannot compete with existing X-ray-based techniques or Magnetic Resonance Imaging (MRI). Nevertheless, optical techniques have the advantage of being non-invasive (no contrast agent), they can provide metabolic information, they do not require ionizing radiation, and they are relatively cheap (Bevilacqua, 1998).

Until some decades ago, the main attempt was to correct for this light scattering. Recently, interest has grown in determining the scattering coefficient too, aside from the absorption coefficient, since it contains information about the structure of the tissue. Different techniques are developed, and different models of light propagation in tissue are proposed for quantifying both the scattering and the absorption properties of tissue. Additionally, knowledge about the propagation of photons in tissue has also applications in the field of therapeutic use of lasers, such as the photodynamic treatment of cancer, or the treatment of port wine stains (Bevilacqua, 1998). The techniques can be divided into three main

categories, namely time-resolved (Patterson *et al.*, 1989), frequency-domain (Patterson *et al.*, 1991), and steady state techniques such as spatially resolved spectroscopy (Groenhuis *et al.*, 1983a; Groenhuis *et al.*, 1983b). The instrumentation of the first two is expensive and more complex compared to the steady-state technique (Qin and Lu, 2006).

The radiation of light in tissue can be described in different ways. Analytical solutions for the light propagation can be obtained through the radiative transfer equation which is based on the preservation of energy. Numerical solutions can be obtained through Monte Carlo simulations, which are based on stochastic modeling of the random walks that photons make as they travel through the tissue. Although these numerical solutions are less restricting in the conditions for which they are appropriate, they require more computational time. The radiative transfer equation can yield rather simple solutions when different assumptions are made. The most widely used approximation is the diffusion approximation, and the radiative transfer equation is transformed into the diffusion equation (Farrell *et al.*, 1992a; Groenhuis *et al.*, 1983a; Kienle and Patterson, 1997; Martelli *et al.*, 2009). This theory is expected to be valid in diffusive media. These are turbid media in which the light propagation is dominated by scattering, *i.e.* the scattering coefficient is much larger than the absorption coefficient, in the order of 10 (Doornbos *et al.*, 1999; Martelli *et al.*, 2009), or even 40 times (Hielscher *et al.*, 1998), making the light propagation a diffusive phenomenon. Biological tissues behave as diffusive media in the near-infrared region and in part of the visual region depending on the amount of absorbing components present in the tissue. Even a material with lower scattering properties can be a diffusive medium whenever the measured volumes are large, so the light propagation becomes a diffusive process too. When measuring very close to the source, the light propagation is often not yet diffuse (Groenhuis *et al.*, 1983a). Therefore, if the source-detector distance of the measuring set-up is too short compared to the effective mean free path of the photons, diffusion theory may give deviating estimates of the optical properties of the tissue (Martelli *et al.*, 2009). Farrell *et al.* (1992a) and Doornbos *et al.* (1999) show that the diffusion theory is adequate at distances greater than 1 *mfp*', although, Kienle *et al.* (1996) report larger distances. Moreover, the sampled tissue should be homogeneous and semi-infinite, *i.e.* having a slab thickness >> 1 *mfp*', and the optical properties should be isotropic (Doornbos *et al.*, 1999; Hemenger, 1977). Due to the formulation of the reduced scattering coefficient, restricted

anisotropy, as found in highly forward-peaked scattering in most biological tissue, can be modeled as explained before (Hemenger, 1977).

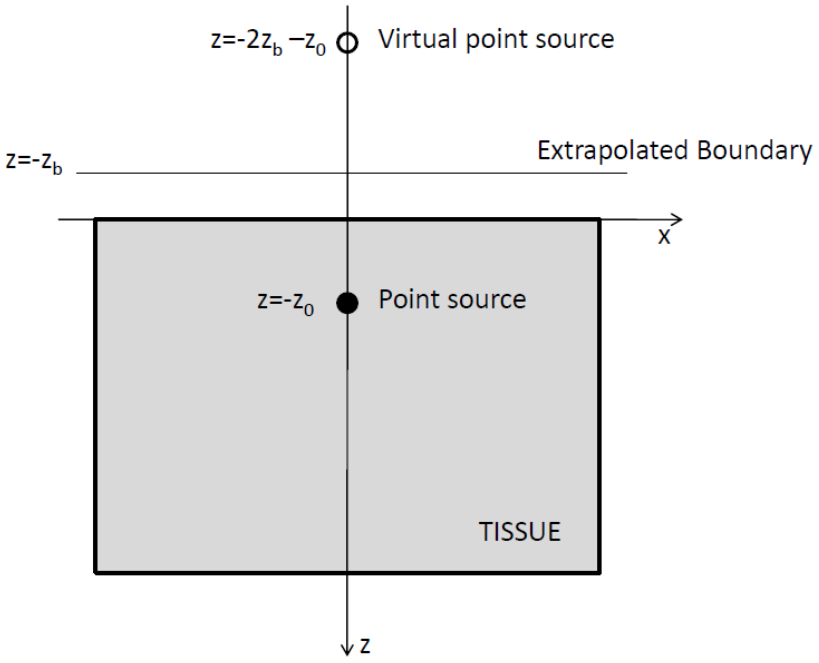

Figure 5.2 Modeling the light propagation from a pencil beam normal to the tissue surface. The source is represented by an isotropic point source at ($0,z_0$) and the boundary conditions are taken into account by introducing the concept of an extrapolated boundary at a height z_b above the surface, and a virtual negative isotropic point source at an additional distance above this extrapolated plane (Farrell *et al.*, 1992a).

The steady-state solution to the diffusion equation for the fluence Φ, *i.e.* the total number of photons that intersect a unit area, at distance (ρ,z) from an isotropic point source at ($0,z_0$) in an infinite turbid medium is (with x- and z-axis as presented in figure 5.2) (Farrell *et al.*, 1992a) (the dependencies of Φ, D, and μ_{eff} on the wavelength λ are omitted for clarity):

$$\Phi(\rho,z)=\frac{1}{4\pi D}\frac{\exp(-\mu_{eff}r)}{r} \quad \text{(Eq. 5.1)}$$

with D, the diffusion coefficient:

$$D=\frac{1}{3\left(\mu_a+\mu_s'\right)} \quad \text{(Eq. 5.2)}$$

r, the distance of the isotropic point source at depth z_0 to the point (ρ,*z*):

$$r = \sqrt{(z - z_0)^2 + \rho^2} \quad \text{(Eq. 5.3)}$$

and μ_{eff}, the effective attenuation coefficient (with *D* see Eq. 5.2):

$$\mu_{eff} = \sqrt{3\,\mu_a\left(\mu_a + \mu_s'\right)} = \sqrt{\frac{\mu_a}{D}} \quad \text{(Eq. 5.4)}$$

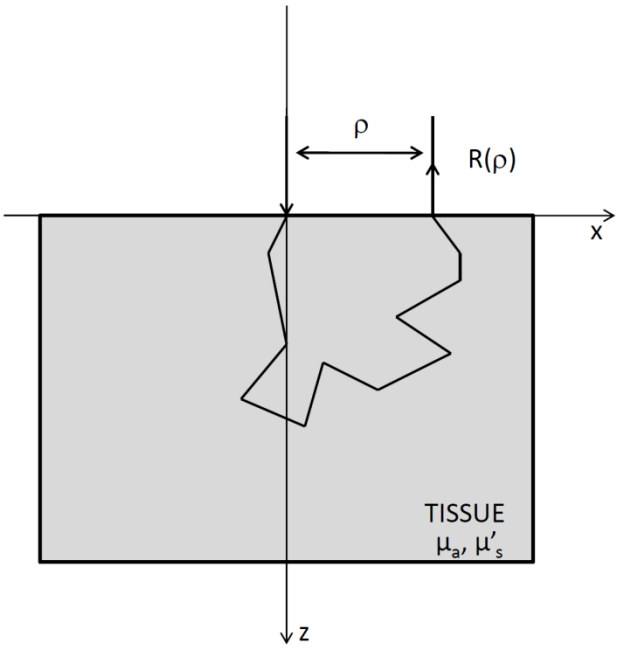

Figure 5.3 The reflectance $R(\lambda,\rho)$ when light from a pencil beam source passes through the tissue with $\mu_a(\lambda)$ and $\mu'_s(\lambda)$.

For practical situations, the fluence from a pencil beam source leaving the tissue at *z*=0, *i.e.* the reflectance $R(\lambda,\rho)$ must be calculated (figure 5.3). This reflectance $R(\lambda,\rho)$ is dependent on ρ, the distance between the measurement point on the tissue surface and the point where the light beam enters the tissue, and on the wavelength λ. To calculate this reflectance the formulation of boundary conditions is necessary. Different solutions of the diffusion equation are proposed in literature depending on the approximations made regarding the boundaries. The zero boundary condition solution assumes that there is no photon current back into the scattering medium at the boundary, which is true when there is no refractive index mismatch between the scattering and the non-scattering medium. To find the solution, the source beam is modeled by an isotropic point source at a depth z_0

below the boundary (figure 5.2). This distance z_0 is equal to μ'^{-1}_s or μ^{-1}_t depending on the definition of the source term (Contini *et al.*, 1997; Farrell *et al.*, 1992a). However, under the conditions for which the diffusion theory is appropriate, namely $\mu_a << \mu'_s$, the difference between assuming z_o to be μ'^{-1}_s or μ^{-1}_t is very small (Hollis, 2002). Furthermore, the fluence at an extrapolated boundary at height $z_b=2D$, is set equal to zero. To achieve this, besides the isotropic point source at a depth z_0, a virtual negative isotropic point source is modeled at an additional distance above the extrapolated plane (figure 5.2). The resulting equation is called the *zero boundary condition* (ZBC) solution for a slab geometry (Farrell *et al.*, 1992a) (the dependencies of R, μ_{eff}, and μ'_t on the wavelength λ are omitted for clarity):

$$R(\rho) = \frac{z_0}{2\pi}(\mu_{eff} + \frac{1}{r})\frac{\exp(-\mu_{eff} r)}{r^2} \quad \text{(Eq. 5.5)}$$

with $R(\rho)$, the relative reflectance in function of the source-detector distance $(\rho,0)$ from an isotropic point source at $(0,z_0)$; z_0, the depth of the isotropic point source in the tissue:

$$z_0 = \frac{1}{\mu'_s} \; or \; \frac{1}{\mu'_t} \quad \text{(Eq. 5.6)}$$

r, the distance of the isotropic point source at depth z_0 to the point $(\rho,0)$:

$$r = \sqrt{z_0^2 + \rho^2} \quad \text{(Eq. 5.7)}$$

and μ_{eff}, the effective attenuation coefficient (see Eq. 5.4).

If there is a refractive index mismatch at the boundary, the fluence is also set equal to zero at an extrapolated boundary. The position of this extrapolated boundary is given by $z_b = 2AD$, where D is the diffusion coefficient, and A is the internal reflection parameter, which is dependent on the relative refractive indices of the media. A is equal to 1 for a matched boundary in the zero boundary condition solution. For unmatched boundaries, A can be calculated by:

$$A = \frac{1 + r_d}{1 - r_d} \quad \text{(Eq. 5.8)}$$

with $r_d = -1.440 n_{rel}^{-2} + 0.710 n_{rel}^{-1} + 0.668 + 0.0636 n_{rel}$ and $n_{rel}=n_t/n_v$, the relative refractive index of the tissue-air boundary with n_t, the refractive index of the tissue and n_v, the

refractive index of air (Farrell *et al.*, 1992a; Groenhuis *et al.*, 1983a). The solution then found, is called the *extrapolated boundary condition* (EBC) solution for a slab geometry (Farrell *et al.*, 1992a; Kienle and Patterson, 1997) (the dependencies of *R*, μ_{eff}, and μ'_t on the wavelength λ are omitted for clarity):

$$R(\rho) = \frac{1}{4\pi}(z_0\,(\mu_{eff} + \frac{1}{r_1})\frac{\exp(-\mu_{eff} r_{1)})}{r_1^2} + (z_0 + 2z_b)(\mu_{eff} + \frac{1}{r_2})\frac{\exp(-\mu_{eff} r_2)}{r_2^2} \quad \text{(Eq. 5.9)}$$

with $R(\rho)$, the relative reflectance in function of the source-detector distance (ρ,0) from an isotropic point source at ($0,z_0$); z_0, the depth of the isotropic point source in the tissue (see Eq. 5.6); z_b, the height of the extrapolated boundary:

$$z_b = 2AD \quad \text{(Eq. 5.10)}$$

with *A*, the internal reflection coefficient (see Eq. 5.8); *D*, the diffusion coefficient (see Eq. 5.2); μ_{eff}, the effective attenuation coefficient (see Eq. 5.4); r_1, the distance of the isotropic point source at depth z_0 to the point (ρ,0):

$$r_1 = \sqrt{z_0^2 + \rho^2} \quad \text{(Eq. 5.11)}$$

r_2, the distance of the virtual isotropic point source above the extrapolated plane at a height $z_b + z_0$ to the point (ρ,0):

$$r_2 = \sqrt{(z_0 + 2z_b)^2 + \rho^2} \quad \text{(Eq. 5.12)}$$

In literature, there are two definitions of *D*, namely $D = 1/(3\,(\mu_a + \mu_s'))$ as used in the previous equations (see Eq. 5.2), and $D = 1/3\,\mu_s'$. As for the differences in the definition of z_0, the differences here are also negligible under the assumption of the diffusion theory, namely $\mu_a << \mu'_s$ (Martelli *et al.*, 2009).

An important parameter which can be calculated from diffusion theory solutions is the penetration depth of light, which is the depth at which the photon flux falls by e^{-1}. This is an important parameter in clinical dosimetry for photodynamic therapy of tumors, and in laser treatments of skin problems. The penetration depth δ (mm) is given by (Patterson *et al.*, 1995):

$$\delta = \frac{1}{\mu_{eff}} = \frac{1}{\sqrt{3\,\mu_a\left(\mu_a + \mu_s^{'}\right)}} \quad \text{(Eq. 5.13)}$$

From this equation it follows that the penetration depth increases as μ_a or μ'_s decreases. The latter happens when μ_s decreases or when g increases due to more forward-peaked scattering. From this characteristic, the average photon depth into the tissue can be calculated for the photons reaching a detector at distance ρ from the source (Patterson *et al.*, 1995):

$$< z >= \frac{1}{2}\sqrt{\rho\,\delta} \quad \text{(Eq. 5.14)}$$

For practical use of the above described ZBC and EBC solutions under the diffusion assumptions, the inverse problem should be solved. By fitting, per wavelength (λ), the equations to the measured reflectance (R) as function of the source-detector distance (ρ), estimates of μ_a and μ'_s per wavelength can be obtained. This inverse problem can be solved by nonlinear least squares curve fitting or by neural networks (Farrell *et al.*, 1992a; Farrell *et al.*, 1992b).

The model of light propagation gives the absolute radial reflectance, $R_{Theoretical}(\lambda,\rho)$, as a function of the optical properties (see Eq. 5.5, the ZBC solution, and Eq. 5.9, the EBC solution). The measured reflectance, $R_{Measured}(\lambda,\rho)$, is the ratio of the detected intensity and the input intensity, both corrected for the dark current and converted to equal integration times. Doornbos *et al.* (1999) use the measurements in an integrating sphere as the input intensity:

$$R_{Measured}(\lambda,\rho) = \frac{I_{Tissue}(\lambda,\rho)}{I_{Integrating\ sphere}(\lambda,\rho)} \quad \text{(Eq. 5.15)}$$

with $R_{Measured}(\lambda,\rho)$, the measured reflectance at wavelength λ and distance ρ from the source; I_{Tissue}, the intensity detected from the tissue; and $I_{Integrating\ sphere}$, the intensity measured in the integrating sphere, both corrected for the dark current, or dark reference, and converted for the integration times. The use of the integrating sphere as the white reference allows one to correct for the spectral shape of the source lamp emission, and the

wavelength-dependent efficiencies of each fiber, and of the detector (Doornbos *et al.*, 1999; Hollis, 2002; Qin and Lu, 2006).

Small changes in the measured reflectance are possible due to changes in the optical coupling between the detector and the tissue, such as thin layers of dirt or fluid on the surface of the tissue, the pressure exerted, the diameter of the fiber, and the numerical aperture of the fiber which characterizes the range of angles from which the light can enter the fiber. These are difficult to remove or to correct for, so that in most practical cases only the relative reflectance can be obtained and a scaling factor is introduced (Doornbos *et al.*, 1999; Farrell *et al.*, 1992a; Qin and Lu, 2006):

$$R_{Measured}(\lambda,\rho) = s\ R_{Theoretical}(\lambda,\rho) \quad \text{(Eq. 5.16)}$$

with $R_{Measured}(\lambda,\rho)$, the measured radial reflectance, $R_{Theoretical}(\lambda,\rho)$, the theoretical reflectance from the model of light propagation, and s, the scaling factor.

After the curve fitting algorithm of $R_{Theoretical}(\lambda,\rho)$ to $R_{Measured}(\lambda,\rho)$, the optical properties of the tissue, $\mu_a(\lambda)$ and $\mu'_s(\lambda)$ are estimated.

5.3 Materials and Methods

5.3.1 Experiment design

The same incubation experiment as described in experiment 2 of chapter 4 is used. Fresh Cobb eggs of a 39-weeks-old broiler breeder flock (*Gallus gallus*) provided by Belgabroed (Merksplas, Belgium) are randomly divided equally in two incubators after individual numbering and weighing. One incubator is a standard forced-draft (control) incubator (PasReform, Zeddam, The Netherlands) with a capacity of 600 eggs. The second incubator is an adapted air-tight forced-draft (CO_2) (PasReform, Zeddam, The Netherlands) incubator in which CO_2 (100% CO_2, N25, Air Liquide, Belgium) is automatically injected according to a programmed pattern shown in figure 4.1. Both groups are incubated at a dry bulb temperature of 37.6 °C and wet bulb temperature of 29.9 °C. The turning frequency is set at once an hour over an angle of 90°. On ED 10, all eggs are mixed and randomly distributed in the two incubators which are further normally ventilated, set at 37.6°C and 45% relative

humidity. Per day, on ED 10, 13, and 16, five eggs per group are taken out for analysis, and the light propagation in the CAM is measured with the SRS set-up.

5.3.2 SRS set-up

The SRS set-up in this study is elaborated as proposed by Thueler (2000), who uses the technique for gastro-intestinal measurements as 'optical biopsy'. The SRS optical probe has been designed and assembled at the Micro-engineering Department of the Swiss Federal Institute of Technology (EPFL Lausanne, France) and is provided by the Advanced Photonics Laboratory of Professor Depeursinge (EPFL Lausanne, France). It consists of 8 multimode quartz fibers (FVP-200 PF, Thorlabs, New Jersey, USA), 1 illumination and 7 collection fibers, with a numerical aperture of 0.22 and a core diameter of 200 µm which are glued together with black epoxy resin in the pattern presented in figure 5.4, and inserted in a polyamide tube (Thueler, 2000). At the front face of the probe the fibers are polished. Short source-detector distances are chosen to be able to analyze superficial small volumes of the tissue. After all, the CAM is only 50-110 µm in thickness (Reizis *et al.*, 2005). The fibers are separated 278.11 µm, 395.29 µm, 543.58 µm, 650.88 µm, 786.87 µm, 920.68 µm, and 1185.25 µm from the source.

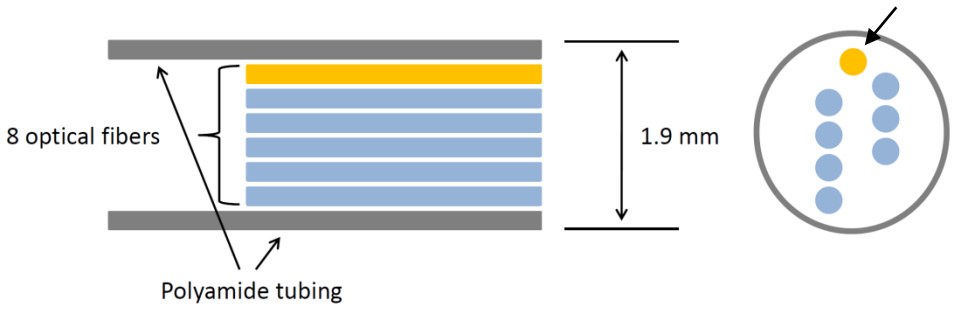

Figure 5.4 The optical probe (Thueler, 2000): left image: scheme of the fiber positions in the probe; right image: *en face* image of the probe with the illumination fiber indicated by an arrow.

In figure 5.5 a general scheme of the set-up with all its components is shown. The light of a tungsten halogen light source (AvaLight-HAL, Avantes, Eerbeek, The Netherlands) is coupled into one 200 µm fiber (FVP-200 PF, Thorlabs, New Jersey, USA) and transported to a source selector using a rotating wheel system. Here, the light is distributed over two 200 µm fibers (FVP-200 PF, Thorlabs, New Jersey, USA), namely the illumination fiber of the SRS probe, and

a reference fiber which is directly coupled into the spectrograph (CP140-1824 Horiba Jobin Yvon, Kyoto, Japan). The light exiting the illumination fiber of the SRS optical probe interacts with the tissue in contact with the probe and the diffusely reflected light is collected by 7 collection fibers of the SRS optical probe. The spectrograph splits the light from each of the collection fibers and that from the reference fiber in different wavelengths from 400 to 1100 nm, and focuses this on a cooled CCD camera (C7041, S7031-1008 Hamamatsu Photonics, Hamamatsu, Japan). This results in a spectral resolution of 0.7 nm/pixel. The exposure time of the CCD camera is set by a mechanical shutter. The mechanical shutter and the CCD camera are coupled to a computer and controlled with LabView 6.0 software (National Instruments, Austin, TX, USA).

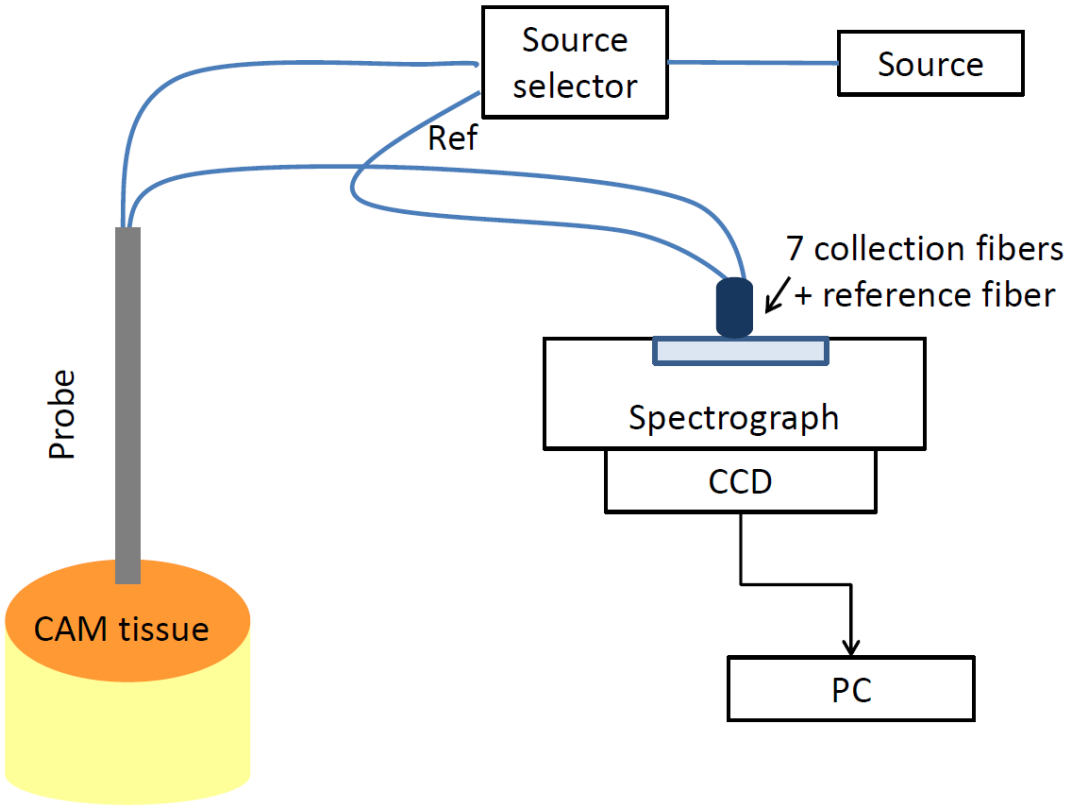

Figure 5.5 General set-up for the SRS measurements

5.3.3 Sample preparation and measurement procedure

The CAM is a well vascularized membrane which lies just underneath the eggshell. As explained in the introduction of this chapter, the first measurements are made directly on this CAM in this first study on the potential of SRS for angiogenesis monitoring, in order to avoid complication by the presence of the eggshell. Therefore, the eggshell and the outer shell membrane at the blunt side over the air cell are removed, while the inner shell membrane stays attached to the CAM. Subsequently, the SRS probe is placed perpendicular on the CAM (figure 5.6). To avoid measuring one blood vessel, the probe is carefully placed in a region of vessel endpoints. Besides this limitation, the probe is placed randomly on the CAM. SRS measurements are performed at eight different spots on the CAM of every egg. Before every measurement on the CAM , the dark current is measured. The integration time is optimized for every measurement. Furthermore, every day (ED 10, 13, and 16), a measurement is performed in an integrating sphere (AvaSphere-50-IRRAD, Avantes, Eerbeek, The Netherlands) after stabilization of the light source, and before the actual measurements on the CAM.

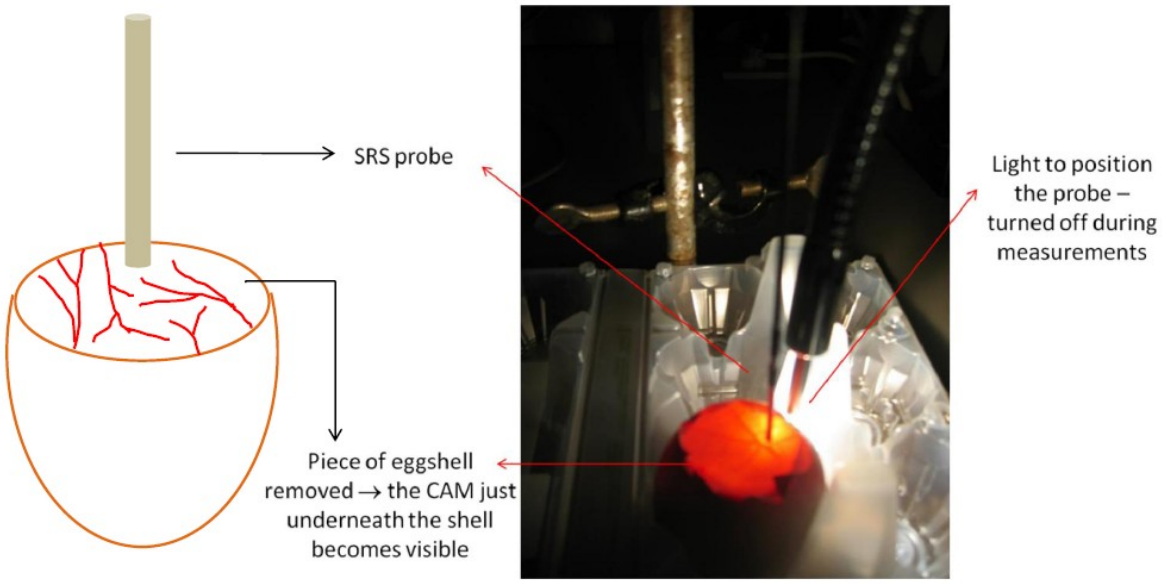

Figure 5.6 Positioning of the probe on the CAM after removal of the eggshell at the blunt side of the egg over the air cell. The light on the right side of the picture is used to position the probe on the CAM, but is turned off during measurements.

5.3.4 Feature extraction

The intensity spectra acquired for each of the collection fibers are corrected for the dark current and converted to intensity per ms by dividing by the integration time. The measurements with the probe inserted in the integrating sphere allow for correction of the wavelength-dependent efficiencies of every fiber. The relative reflectance values for each of the seven collection fibers are thus calculated using the following equation in which the dependencies of *R*, *I*, and *B* on the wavelength λ are omitted for clarity:

$$R_{CAM,f} = \frac{\left(I_{CAM,f} - B_{CAM,f}\right)/T_{CAM}}{\left(I_{sphere,f} - B_{sphere,f}\right)/T_{sphere}} \left(f = 1-7\right) \quad \text{(Eq. 5.17)}$$

with $R_{CAM,f}$ the relative reflectance of the measurement on the CAM for fiber *f*; $I_{CAM,f}$ the measured intensity spectrum of the CAM for fiber *f*; $B_{CAM,f}$ the dark current measured every time before the spectral measurement on the CAM for fiber *f*; T_{CAM} the integration time of the measurement on the CAM (the signal of all fibers is measured simultaneously); $I_{sphere,f}$ the measured intensity spectrum in the integrating sphere for fiber *f*; $B_{sphere,f}$ the dark current measured before the spectral measurements in the integrating sphere for fiber *f*; and T_{sphere} the integration time of the measurement in the integrating sphere. Moreover, these relative reflectance spectra are smoothed by a savitsky-golay filter (degree 2, span 11). Only the range of 450 to 1000 nm is used.

From these smoothed relative reflectance spectra for the seven collection fibers, different parameters are determined to describe the optical properties in the CAM and the age-related changes, as well as the differences between both groups, hypercapnia and control. A blood value (*BV*) is calculated for the first collection fiber, the one closest to the source, as a measure for the amount of blood in the CAM:

$$BV = \frac{R_{CAM,1}\left(577\ nm\right)}{R_{CAM,1}\left(610\ nm\right)} \quad \text{(Eq. 5.18)}$$

It should be noted that this blood value is calculated from relative reflectance values instead of the commonly used transmittance values (Gielen *et al.*, 1979). The blood value decreases with increasing blood concentration as more light is absorbed by the blood.

Besides the absorption of the blood, differences in light propagation due to differences in both the absorption and scattering properties in the CAM are investigated. For this purpose, an exponential function is fit to the profile of the relative reflectance $R_{CAM,f}$ as function of the source-detector distance ρ per wavelength. This is the most simple function which gives a reasonable description of the decay of the reflectance with increasing distance to the illumination fiber. This function can be transformed into a linear one which can then be used in a linear least squares regression algorithm:

$$\ln(R(\rho)) = c_1 + c_2\rho \quad \text{(Eq. 5.19)}$$

with c_1 and c_2, constants, ρ, the source-detector distance, and $R(\rho)$, the relative reflectance. The parameters c_1 and c_2 are analyzed per wavelength. They contain information both on the absorption coefficient as well as on the scattering coefficient. This regression is performed in Matlab 7.5 software (The Mathworks Inc., Natick, USA).

More physically meaningful parameters can be obtained, not by fitting just a simple exponential function to the reflectance decay, but through the application of the diffusion theory to model the light propagation in the tissue.

5.3.5 Inverse optical properties estimation

After data preprocessing as described above, the ZBC solution equation of Farrell *et al.* (1992a) (Eq. 5.5), multiplied by a scaling factor (Eq. 5.16), is used to fit the reflectance $R_{CAM,f}$ (Eq. 5.17) per wavelength λ. A nonlinear least squares curve fitting algorithm is implemented using the Matlab 7.5 Curve Fitting Toolbox (The Mathworks Inc., Natick, USA) to estimate μ_a and μ'_s per wavelength λ. To increase the performance, the curve fitting process is divided into three steps as proposed by Doornbos *et al.* (1999) and Qin and Lu (2006; 2007). In the first step μ_a, μ'_s and the scaling factor s are free parameters of the fitting. An average scaling factor per measurement is determined in the wavelength range of 630-900 nm, where this scaling factor is most stable. This average scaling factor is introduced in the ZBC solution equation. Again the curve fitting algorithm is implemented, but now only with μ_a and μ'_s as free parameters. The resulting scattering coefficient spectra $\mu'_s(\lambda)$ approximate a decreasing exponential with increasing wavelength in the range of 630-900 nm. Therefore, the

estimated $\mu'_s(\lambda)$ spectrum for each SRS measurement is fit to a simple wavelength-dependent function derived from Lorenz-Mie theory as proposed by Doornbos *et al.* (1999):

$$\mu_s^{'} = a\,\lambda^{-b} \qquad (\lambda \; in \; \mu m) \quad \text{(Eq. 5.20)}$$

with *a* and *b* constants. In a third fitting step, the resulting μ'_s spectra, extrapolated over the entire wavelength range, are reintroduced in the ZBC solution equation, and the fitting is repeated with only μ_a as a free parameter.

5.3.6 Statistics

For the *BV* (Eq. 5.18) as well as for the parameters of the exponential fit c_1 and c_2 (Eq. 5.19), per wavelength λ, a mixed ANOVA model is built treating ED, group, and egg nested in the interaction of group and ED, as independent categorical variables. Egg is treated as a random variable. A hierarchical model building procedure is followed in order to remove non-significant terms from the model. Linear contrasts are set up in order to estimate differences between the considered settings. For all analyses SAS 9.2 is used (SAS Institute Inc., Cary, North Carolina, USA).

5.4 Results

5.4.1 The measured spectra

The mean spectra of all the measurements per ED in the useful range of 450 to 1000 nm are shown in figure 5.7.

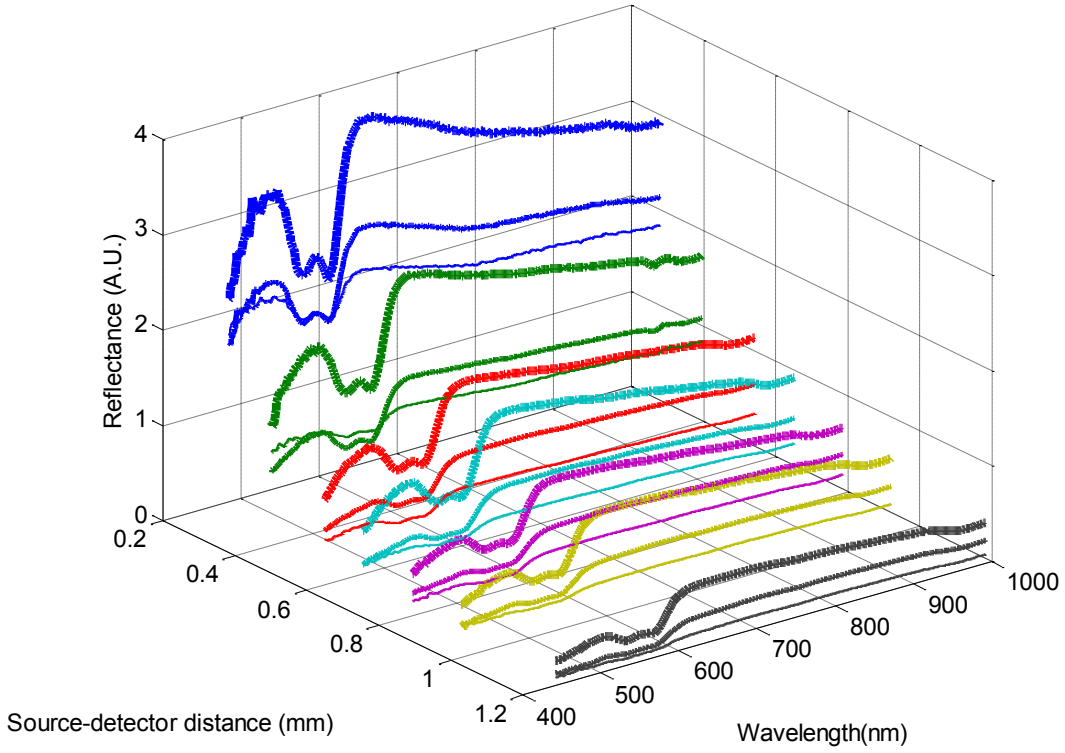

Figure 5.7 Mean spectra of all the measurements per collection fiber (7 fibers) at different source-detector distances indicated by different colors, and per embryonic day (ED) with linewidth 1 = ED 10, linewidth 2 = ED 13, and linewidth 3 = ED 16.

As an example, the mean relative reflectance profile versus the source-detector distance at 610 nm, for each ED, is shown in figure 5.8. The same graph but in a semi-log plot is added to show the differences in intercept and decay of the relative reflectance versus source-detector distance.

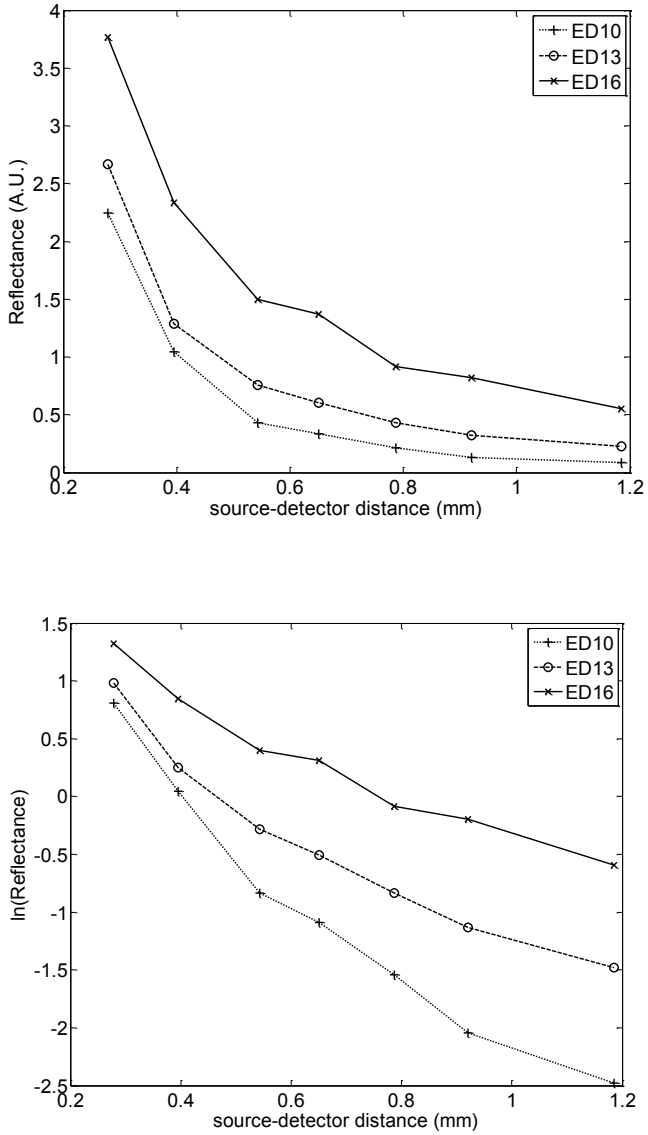

Figure 5.8 Top graph: relative reflectance versus source-detector distance at 610 nm per ED. Bottom graph: ln(relative reflectance) versus source-detector distance at 610 nm per ED. Plus symbols (+) and dotted lines indicate ED 10, circle symbols (o) and dashed lines indicate ED 13, and cross symbols (x) and full lines indicate ED 16.

5.4.2 Blood value

In the model for the blood value (*BV*) (Eq. 5.18) (*n*=131), built as described in the materials and methods section, only ED (10, 13, and 16) is significant as independent variable ($p < 0.0004$). Group or the interaction between group and ED are not significant. The *BV* is

significantly lower on ED 13 and on ED 16 compared to ED 10, p = 0.0013 respectively 0.0001 (figure 5.9).

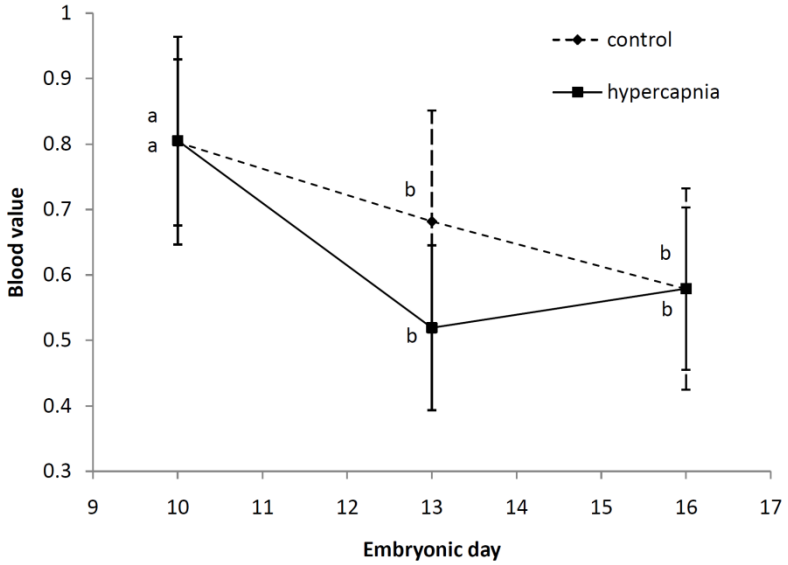

Figure 5.9 Mean blood value (*BV*), measured in reflectance mode, per embryonic day (ED) and per group with standard deviation bars. Diamond symbols, dashed lines and dashed bars indicate the control group. Square symbols, full lines and full bars indicate the hypercapnia group. Different letters indicate significant differences.

As can be seen on figure 5.9, the *BV* on ED 10 and 16 is not different between both groups. On ED 13 there is a small difference with a higher value for the *BV* in the control group compared to the hypercapnia group, but this is not significant.

5.4.3 Simple exponential approximation of the reflectance

In figure 5.8 the decay of the relative reflectance versus source-detector distance seems to behave as an exponential function. Therefore, the data is fitted to a simple exponential model (Eq. 5.19).

The extrapolated results of the estimated mean natural logarithm of the reflectance values versus the source-detector distance and the wavelength are shown in figure 5.10 per ED and per group, namely the control group in the top row and the hypercapnia group in the bottom row of graphs.

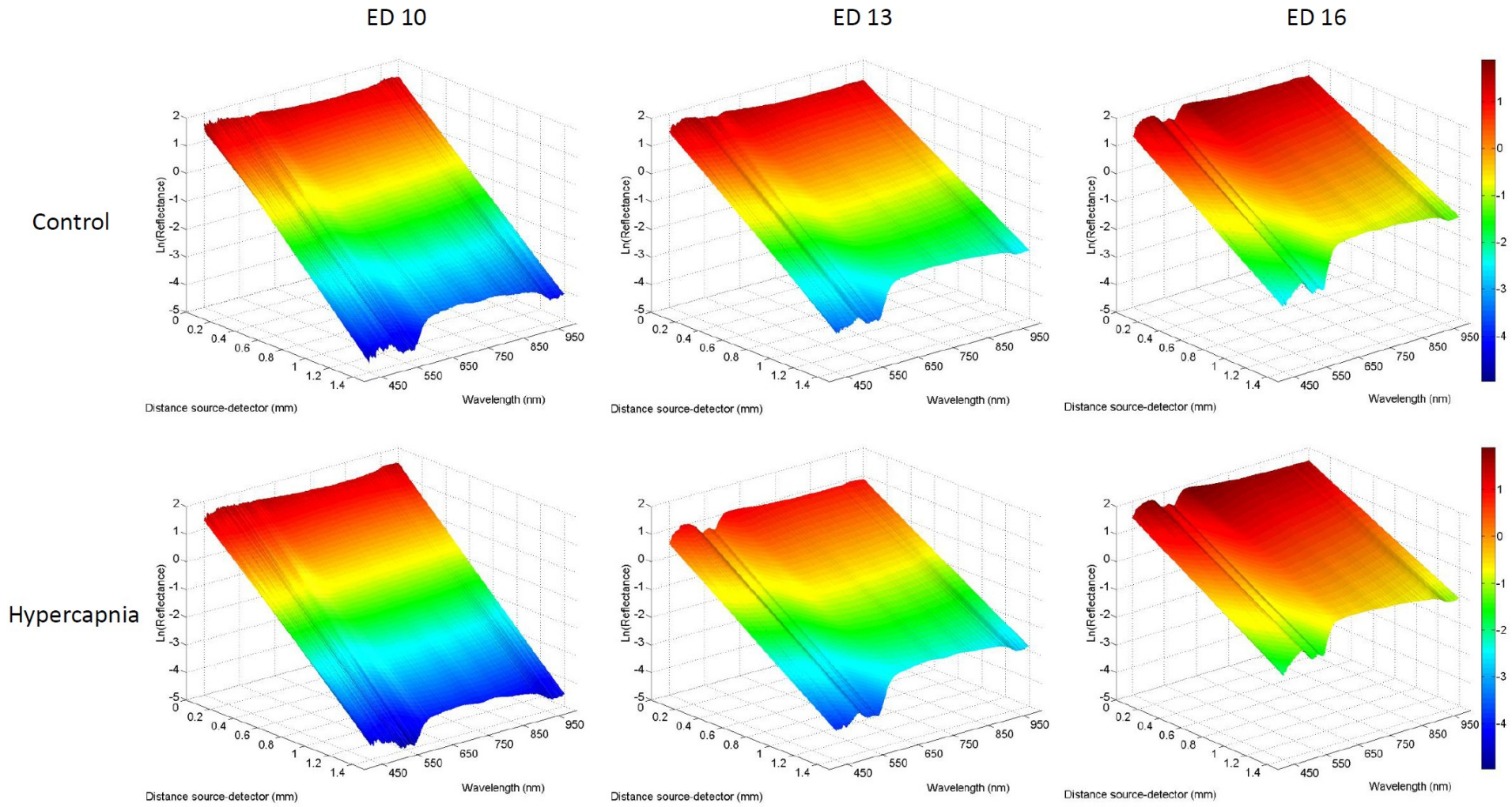

Figure 5.10 The extrapolated mean estimated ln(reflectance) versus wavelength and source-detector distance obtained via a simple exponential model per ED, namely ED 10 (left), 13 (center), and 16 (right), and per group, namely the control (top) and hypercapnia group (bottom).

The goodness of fit can be evaluated by the R^2 values. An overview of the mean R^2 value per wavelength and per ED is given in figure 5.11. The mean estimated reflectance spectra based on the estimates of c_1 and c_2, the constants in the linear form of the simple exponential model (Eq. 5.19) are represented in figure 5.12.

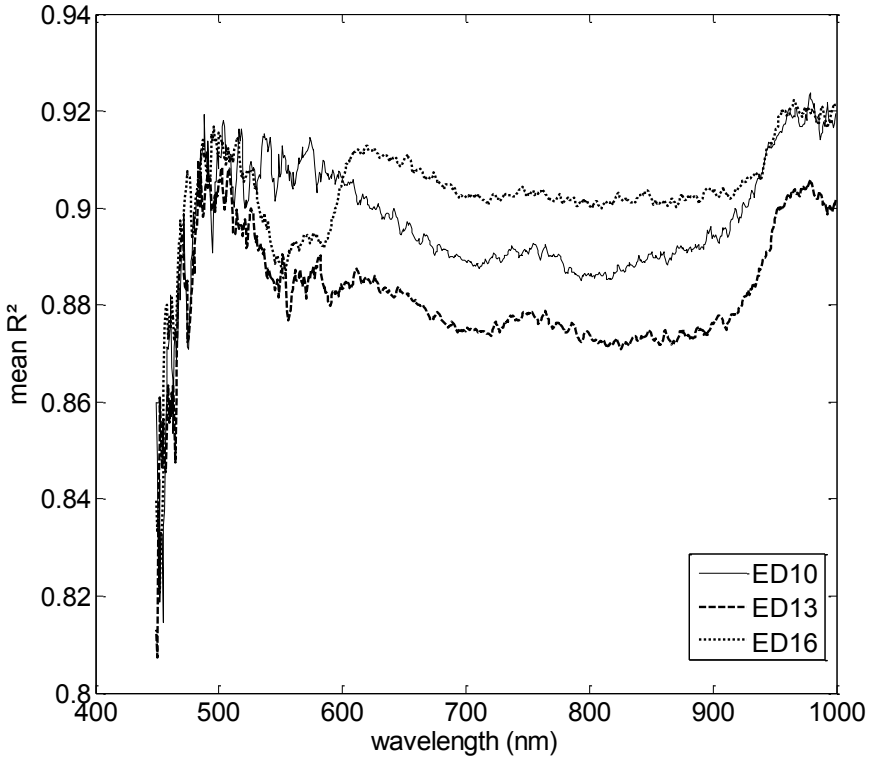

Figure 5.11 Mean R^2 values per wavelength and per ED for a simple exponential fit of the reflectance data. Full line = ED 10, dashed line = ED13, dotted line = ED 16.

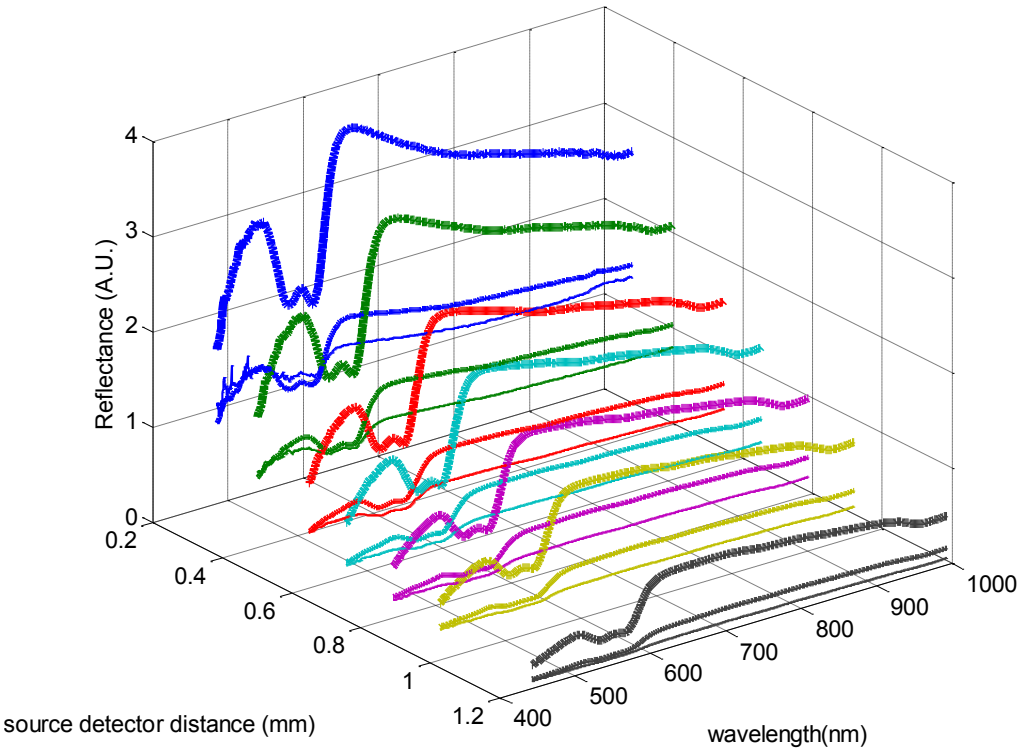

Figure 5.12 The mean reflectance spectra based on the estimates of c_1 and c_2, the constants of the linear form of a simple exponential model (Eq. 5.19). The different source-detector distances are indicated by different colors. The different embryonic days (ED) are indicated by linewidth: linewidth 1 = ED 10, linewidth 2 = ED 13, linewidth 3 = ED 16.

As for the *BV*, both parameters c_1 and c_2 are tested for their differences between the measured ED and the groups at wavelength 610 nm, a blood neutral wavelength, after building a mixed model (n=131) as explained in the materials and methods section. For c_1 no significant model is found. In the model for c_2, only ED is a significant variable ($p < .0001$). The decay of the reflectance versus source-detector distance is larger at ED 10 compared to ED 13 ($p = 0.0027$), and at ED 13 compared to ED 16 ($p = 0.0005$) (figure 5.13).

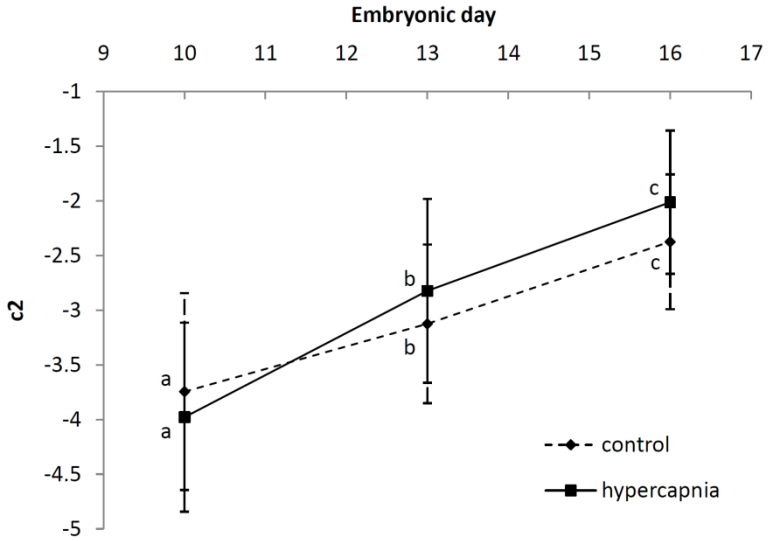

Figure 5.13 Mean coefficient c_2 of the linear fit (Eq. 5.19) of ln(Reflectance) versus source-detector distance per ED and per group with standard deviation bars. Diamond symbols and dashed bars indicate the control group. Square symbols and full bars indicate the hypercapnia group. Different letters indicate significant differences.

5.4.4 Diffusion approximation of the reflectance

All results described in this section are based only on these measurements that resulted in a good fit of the ZBC diffusion solution (Eq. 5.5) to the data. Only 5 measurements at ED 10 can be retained. At ED 13 and 16, respectively 17 and 45 measurements are retained. The mean R^2 values of the fitting over all measurements per ED are shown in the left top image of figure 5.14. The corresponding mean estimates of the absorption coefficients μ_a over all these measurements per ED are presented in the right top image. The mean reduced scattering coefficients μ'_s of the model $\mu'_s = a\lambda^{-b}$ are given in the left bottom image. With these estimated coefficients, the effective attenuation coefficient μ_{eff} spectra (Eq. 5.4) are rebuilt, as well as the reflectance spectra (Eq. 5.5) which are presented in the right bottom image of figure 5.14, respectively figure 5.15.

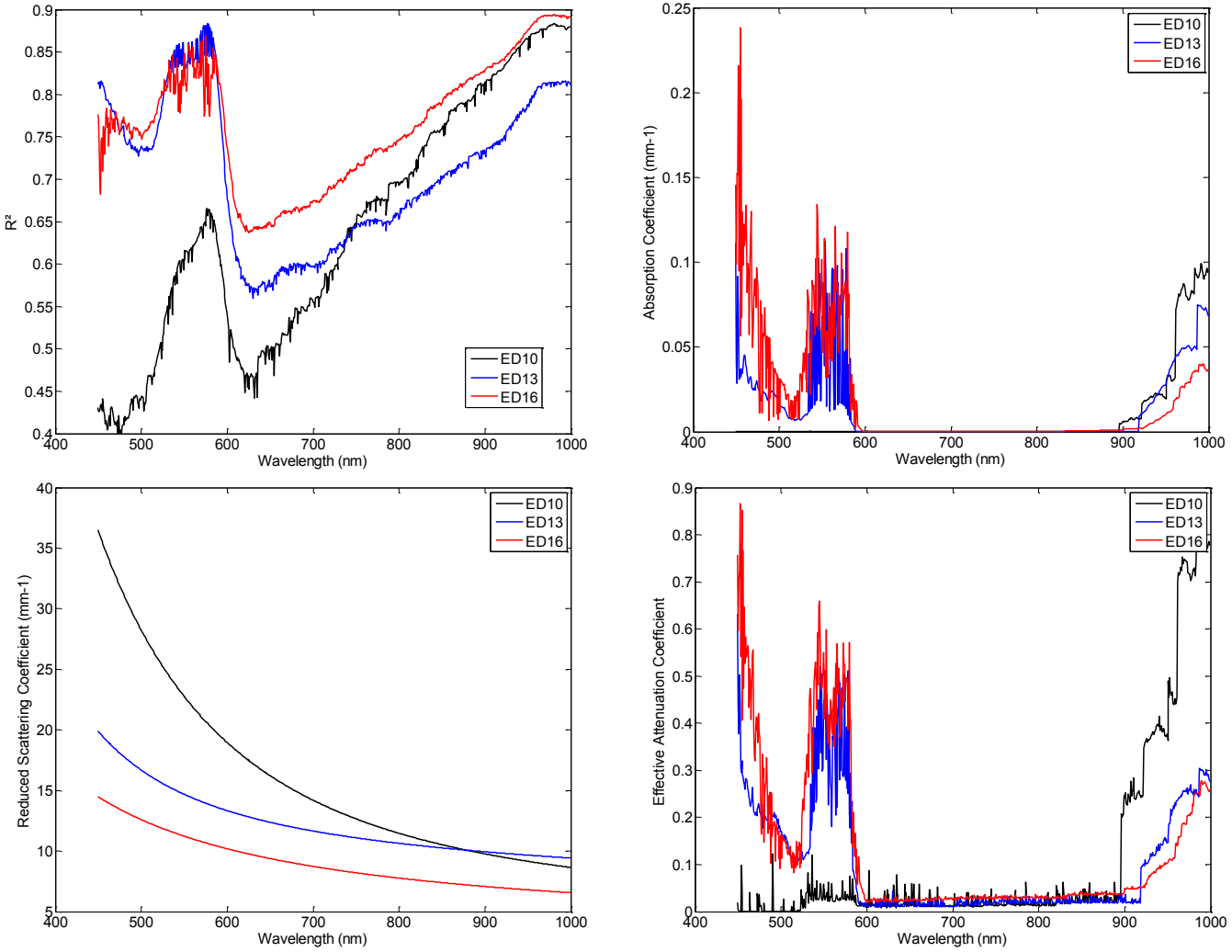

Figure 5.14 The results of the curve fitting to the ZBC diffusion solution (Eq. 5.5) of light propagation. Left top image: mean R^2 values of the curve fitting. Right top image: mean absorption coefficient estimates (μ_a). Left bottom image: mean modeled reduced scattering coefficients (μ'_s). Right bottom image: mean effective attenuation coefficients (μ_{eff}).

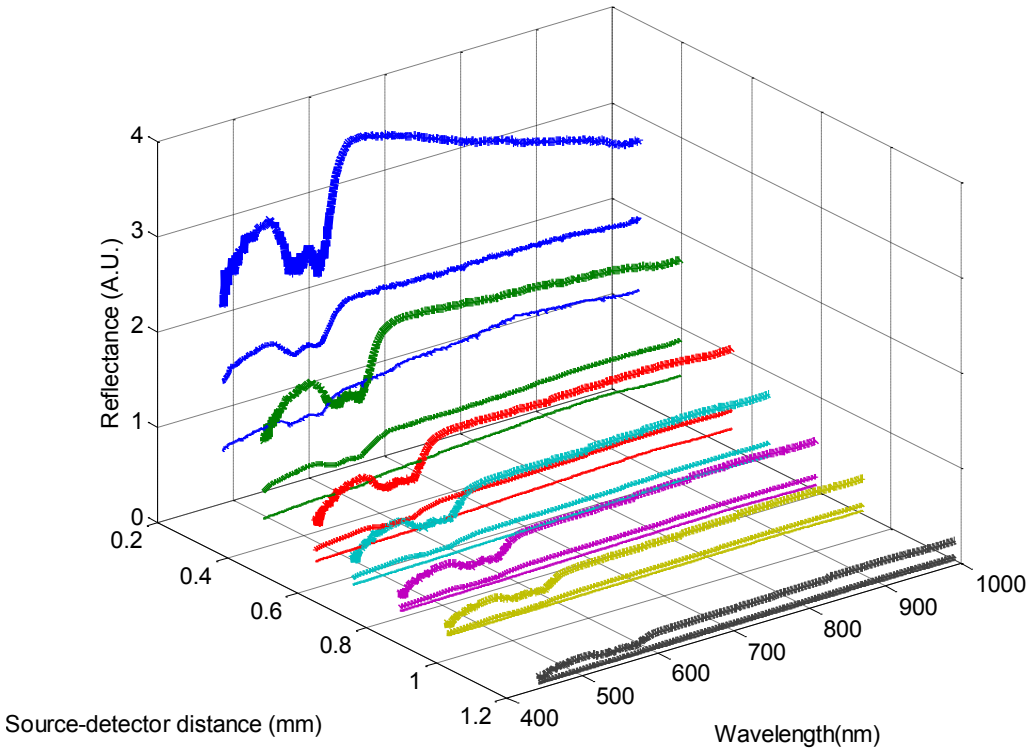

Figure 5.15 The mean reflectance spectra based on the estimates of the optical properties via the ZBC diffusion solution (Eq. 5.5). The different source-detector distances are indicated by different colors. The different embryonic days (ED) are indicated by linewidth: linewidth 1 = ED 10, linewidth 2 = ED 13, linewidth 3 = ED 16.

The light propagation at the typical blood absorption wavelength 577 nm is worked out. All mean optical properties are given in table 5.1. In addition, based on the diffusion theory, the penetration depth is calculated (Eq. 5.13) and the average photon depth (Eq. 5.14) into the tissue for the photons reaching the most distant detector (ρ = 1.2 mm) (Patterson *et al.*, 1995). Furthermore, $\rho\,\mu'_s$ is given for the most and the least distant detector (ρ = 0.3 mm) since it is an indicator for how many terms of the phase function must be included into the model as will be explained below in the discussion section.

Table 5.1 The light propagation in the tissue at 577nm, the typical blood absorption wavelength described by the mean optical properties: absorption coefficient μ_a, reduced scattering coefficient μ'_s, reduced total attenuation coefficient μ'_t, effective mean free path *mfp'*, diffuseness *N'*, diffusion coefficient *D*, effective attenuation coefficient μ_{eff}, penetration depth δ, the average photon depth into the tissue for the photons reaching the most distant detector (ρ = 1.2 mm) <*z*> , and $\rho\mu'_s$ for the most and the least distant detector.

	ED 10	**ED 13**	**ED 16**
μ_a **(mm^{-1})**	6.0 x 10^{-5}	0.0148	0.0884
μ'_s **(mm^{-1})**	20.54	13.89	10.63
μ'_t **(mm^{-1})**	20.54	13.91	10.72
mfp' **(mm)**	0.049	0.072	0.093
N'	3.4 x 10^{+5}	939	120
D **(mm)**	0.021	0.033	0.049
μ_{eff} **(mm^{-1})**	0.037	0.26	0.49
δ**(mm)**	27	3.8	2.0
<*z*> **(mm)**	2.8	1.1	0.8
$\rho\mu'_s$ **(ρ = 1.2 mm)**	24.6	16.7	12.8
$\rho\mu'_s$ **(ρ = 0.3 mm)**	6.2	4.2	3.2

5.5 Discussion

5.5.1 Measuring angiogenesis with SRS

The absorption spectrum of oxygenated hemoglobin is clearly recognizable in the tissue spectra with two absorption peaks at 542 nm and 577 nm (figure 5.7) (Johnson *et al.*, 2007). Furthermore, the absorption band of water at 970 nm is detectable.

In the previous research on the same incubation (see chapter 4 experiment 2), it is observed that the density of the vascular network in the CAM, measured by the vascular fraction (VF), increases from ED 10 to 13, and from ED 13 to 16 (table 5.2). Moreover, on ED 10 and 13,

the hypercapnic group has a denser vascular network compared to the control group (table 5.3).

Table 5.2 Overview of significant mean differences between the ED (10, 13, and 16) for the vascular fraction (VF) over both groups (*n*=728). ** $p < 0.01$, NS = non-significant *p* values.

	ED 10-13	ED 13-16	ED 10-16
VF	-1.24×10^{-3}**	-1.06×10^{-3}**	-2.30×10^{-3}**

Table 5.3 Overview of significant mean differences between the groups, control and hypercapnia, for the vascular fraction (VF) per ED (*n*=728). ** $p < 0.01$, NS = non-significant *p* values.

	ED 10	ED 13	ED 16
VF Control-hypercapnia	-0.41×10^{-3}**	-0.70×10^{-3}**	(-0.03×10^{-3}) NS

So, from the comparison of the results obtained in the previous chapter (table 5.2 and 5.3), and the ones described above in the results section on the *BV* (figure 5.9), it can be concluded that the differences in the BV are consistent with the increase in amount of blood due to a denser vascular network in the CAM. However, the *BV* measurement based on the first fiber of the SRS set-up is not as sensitive as the destructive measurements previously developed since it cannot detect the small differences between ED 13 and 16, and the ones between both groups. This may be due to a too small amount of data, a hypothesis which should be tested in future research.

The information obtained from the measurements with all collection fibers at specific distances from the source reveals also changes with increasing ED. The differences in the decay of the reflectance (c_2) are significant, showing that the light propagates further into the tissue at ED 13 compared to ED 10, and at ED 16 compared to ED 13 (figure 5.10 and 5.13). However, the separate contributions of scattering and absorption in this light propagation cannot be estimated from this simple exponential model.

5.5.2 Use of the diffusion theory to estimate optical properties

The diffusion theory is used to estimate the absorption and reduced scattering coefficient based on the reflectance profiles. When holding the probe in contact with the tissue, the mismatch between the refractive index of the tissue and of the air has a negligible effect (Bevilacqua *et al.*, 1999; Farrell *et al.*, 1992a). Therefore, the ZBC solution equation (Eq. 5.5) is used in the curve fitting algorithm. After the first fitting procedure, for each measurement the mean scaling factor is determined over a wavelength range in which there is little variation, namely from 630-900 nm. The variations of the scaling factor with the wavelength are an artefact of the fitting procedure (Doornbos *et al.*, 1999). After the second fitting it becomes clear that the nonlinear least-squares fitting does not always separate μ_a and μ'_s well, especially in the VIS region with wavelengths smaller than 630 nm. Therefore, μ'_s is modeled in the region where it follows an exponential decay with the wavelength, namely 630-900 nm. Subsequently, the model for μ'_s is extrapolated to the whole wavelength range of 450-1000 nm. Finally, the resulting μ'_s are used in a third fitting to estimate μ_a.

Many measurements had to be excluded due to a bad fit. The remaining R^2 values are still rather low on ED 10 (top left image of figure 5.14). The diffusion theory is only appropriate when the light propagation in the tissue is a diffuse process. Consequently, only when this assumption is fulfilled, the diffusion solution will fit the data well. Different parameters are proposed to check this assumption, although all are derived from the estimates of the diffusion solution itself. Therefore, they can only confirm the consistency of the method (Doornbos *et al.*, 1999). The different parameters are summarized below:

- High scattering compared to absorption: Diffuseness = $N' > 10$ (Doornbos *et al.*, 1999) or > 40 (Hielscher *et al.*, 1998)
- Semi-infinite geometry: Slab thickness >> 1 *mfp*' (Doornbos *et al.*, 1999)
- Measurements far from source: $\rho > 1$ *mfp*' (Doornbos *et al.*, 1999; Farrell *et al.*, 1992a)
- Only the first order moment, *g*, of the phase function necessary to describe the scattering (see below): $\rho\,\mu'_s > 10$ (Bevilacqua and Depeursinge, 1999)

When these parameters are checked for the example given in table 5.1, the diffuseness is fulfilled. The thickness of the CAM tissue, 0.05-0.11 mm (Reizis *et al.*, 2005) together with

the inner shell membrane, 0.03-0.036 mm (Moran and Hale, 1935) ranges from 0.08 to 0.146 mm. In consequence, compared to the *mfp'*, the tissue cannot be considered as a semi-infinite geometry and the underlying tissue will have an influence on the measurements. The source-detector distances are larger than 1 *mfp*'. However the $\rho\,\mu'_s$ are not larger than 10 for all ρ. As a result, not only the first order moment of the phase function will be important to describe the scattering but also higher order moments (see below).

The estimates of μ_a and μ'_s are in normal ranges for soft tissue. All be it with a lot of variation in the estimates, the mean μ_a spectra do clearly demonstrate the absorption profile of blood, except on ED 10 (figure 5.14). The mean μ_a in the VIS region is higher at ED 16 compared to ED 13, and at ED 13 compared to ED 10 which confirms the presence of more blood in the CAM at a later ED. In addition, the absorption of water is shown in the 900-1000 nm region. The egg loses water and therefore, the mean μ_a at ED 10 is higher in this region compared to ED 13, and at ED 13 compared to ED 16. The mean μ'_s is lower at ED 16 compared to ED 13, and at ED 13 compared to ED 10. This may be explained by a lower μ_s or by a higher *g*, since μ'_s is determined by both these variables. A lower μ_s is unlikely since, due to the denser vascular network, the light will most probably be more scattered. A higher *g* results from scattering which is more forward-peaked. Due to the higher density of the vascular network, forming cylinders, the light may be less isotropic. The same phenomenon is found in tendon tissue and in tooth, due to the collagen fibers respectively the dental tubules (Martelli *et al.*, 2009). Nevertheless, the blood vessels in the CAM are not aligned and therefore, up to date, no sure conclusions can be drawn. In addition, the profile of the mean μ'_s versus wavelength is different at ED 10 compared to ED 13 and 16. However, since the measurements at ED 10 are the less well fitted, this may be an artefact. The same is true for the μ_a profile at ED 10 in which no blood spectrum can be recognized. In the mean μ_{eff} profile however, the blood absorption peaks can be recognized. From this it seems plausible that the separation of μ_a and μ'_s failed while fitting the data at ED 10: μ'_s is probably overestimated and μ_a underestimated leading to the same μ_{eff}.

The mean *D* is larger at ED 16 compared to ED 13, and at ED 13 compared to ED 10 (table 5.1) resulting in higher reflectance values in the farthest detector with increasing age (figure 5.10). Since μ_a increases with ED, the higher *D* at later ED is a result of the decrease in μ'_s.

The penetration depth of the light, δ, reported in table 5.1 is large due to the rather low μ_a. The membrane tissue between the blood vessels contributes to the light propagation. This is a matrix that does not significantly absorb or scatter light (Nowak-Sliwinska *et al.*, 2010), leading to the rather low μ_a values.

5.5.3 Limitations of the diffusion theory

The diffusion theory to model the light propagation in tissue is used as a first approach to estimate the optical properties of the CAM tissue. However, the tissue and set-up used in this study do not completely fulfill the assumptions of the diffusion theory as partially described in the previous section. Therefore, the determined optical properties should be interpreted with caution. The different assumptions which need a thorough consideration in further research are summarized below.

(1) The source-detector distances are chosen very small as to probe a small volume of the tissue. After all, the chorioallantois is a very thin membrane, and to obtain only information from this membrane, only a very small volume should be measured. However, the diffusion theory may not be used for source-detector distances smaller than one effective mean free path (*mfp'*) since close to the source the light propagation is not randomized enough by multiple scattering. In addition, the tissue is very often not homogeneous on such a small scale (see also point (2)), and the anisotropy of the scattering can very often not be reduced to one moment of the phase function (see also point (3)) (Bevilacqua and Depeursinge, 1999; Doornbos *et al.*, 1999; Farrell *et al.*, 1992a).

(2) The measured tissue is not homogenous, not only close to the source but also more in general as it consists of more than one layer, namely the inner shell membrane, the chorioallantois, and the content under the chorioallantois which probably influences the measurements too. Moreover, the layers themselves are not homogeneous, especially the CAM layer. The blood vessels in the CAM will absorb the light strongly, and will probably also scatter the light, but the non-vascularized parts are almost transparent, with very low absorption and low scattering, or highly forward scattering properties (Nowak-Sliwinska *et al.*, 2010). Niedorf *et al.* (2005) describe a possible theory to take these different compartments in a tissue into account. The light reflected at the surface or only passing

through absorption free parts of the tissue form a different compartment, called the white fraction (Niedorf *et al.*, 2005). As such, the different optical properties of each layer should be taken into account, the optical properties of every compartment in each layer, as well as the properties of the boundaries between the layers and the compartments. Due to the inner shell membrane on top of the CAM, and the differences in its hydration state, large differences arise in the reflectance. The internal reflection changes with the relative refractive index of the tissue, and therefore with the water content of the tissue. Moran and Hale (1935) report a refractive index of the inner shell membrane of freshly laid eggs of 1.36. Due to the water loss in the inner shell membrane with incubation time (Ackerman and Rahn, 1981), the refractive index increases over time. The CAM may be assumed to have a higher water content due to the higher blood content. The refractive index of the CAM therefore decreases. So, the light propagating from the inner shell membrane to the CAM will probably be internally reflected, and more at a later time in incubation. This internal reflection at the boundary between the inner shell membrane and the CAM should be taken into account in the light propagation modeling.

(3) The anisotropy level of the scattering in the tissue is unknown. Possibly, more terms of the phase function are necessary to describe the scattering events in the tissue, especially so close to the source. Bevilacqua and Depeursinge (1999) show that the first two moments of the phase function have a significant effect on the reflection profile at small source-detector separations, namely when $0.5 < \rho\,\mu'_s < 10$. The scattering in tissue is a combination of Mie scattering due to the larger particles, which is highly forward-peaked, and Rayleigh scattering due to the smaller particles, with a low anisotropy, and therefore more equal contribution to forward and backward scattering. Bevilacqua and Depeursinge (1999) introduce parameter γ to be able to predict the reflectance curve more correctly:

$$\gamma = \frac{1-g_2}{1-g_1} \quad \text{(Eq. 5.21)}$$

with g_1 and g_2, respectively, the first and second moment of the phase function (Bevilacqua *et al.*, 1999). The first moment g_1 equals g, the anisotropy factor. The second moment g_2 describes the influence of small particles compared to the wavelength (Thueler, 2000). In other words, γ decreases when g_2 increases, *i.e.* when the proportion of backward scattering

increases. In biological tissue γ varies between 0.9 (Rayleigh-type scattering) and values larger than 2 (Mie-type scattering). Due to the similarity relations, the light propagation in a tissue can be described by only three parameters μ_a, μ'_s and γ. In solving the inverse problem, an error in the latter parameter will have an impact on both other optical parameters, and especially on the estimation of μ_a (Bevilacqua and Depeursinge, 1999). At smaller distances ($\rho\,\mu'_s < 0.5$), even more moments of the phase function must be taken into account (Bevilacqua and Depeursinge, 1999). Moreover, for the diffusion approximation the phase function is assumed to be only dependent on the scattering angle θ. Nevertheless, the scattering may also be dependent on the photon's direction like in tendon tissue or tooth where cylindrical particles, respectively dental tubules and collagen fibers, give rise to scattering instead of spherical particles (Martelli *et al.*, 2009).

All these deviations from the assumptions of the diffusion theory may make the light propagation far from a diffuse process and therefore, estimates obtained from diffusion theory may be erroneous.

5.6 Conclusions and future improvements

A spatially resolved spectroscopy device, already partially constructed at the Advanced Photonics Laboratory (EPFL, Lausanne), was further completed, and for the first time spatially resolved measurements were conducted on the CAM tissue. The measurements showed age-related differences in three different parameters, namely (1) the blood values calculated from the signal of the fiber closest to the source, (2) the power of a simple exponential model fitted to the reflectance data versus the different source-detector distances of the seven fibers, and (3) the absorption and reduced scattering coefficients estimated via the diffusion approximation for the light propagation in the tissue. These differences confirmed the ones measured by the previously developed destructive method which are due to the normal development of the CAM. Nevertheless, both the measurements themselves as well as the light propagation modeling can be further improved. Suggestions to improve both are summarized below.

Since the probe makes contact with the tissue, specular reflection will be absent in ideal situations. However, in non-ideal circumstances, the differences in specular reflection can be reduced by the use of water or a mineral oil on top of the inner shell membrane to make the boundary more uniform (Wilson and Jacques, 1990).

More consistent measurements can be obtained by using a Universal Tensile and Compression Test machine to position the probe on the CAM. With this set-up a pressure can be fixed at which lowering of the probe is stopped. A preliminary study must determine the pressure at which the probe makes contact with the tissue, but does not rupture the membranes.

Due to the short source-detector distances in the set-up and the properties of the tissue, the diffusion theory may give deviating estimates of the optical properties. Using Monte Carlo simulations for the light propagation modeling, and then solving the inverse problem, will yield more accurate optical properties. Monte Carlo simulations, like the radiative transfer theory, treat the photons as particles. The propagation of light is modeled as probability distributions, which are based on the geometry and optical properties of the tissue. In short, the paths of photons are simulated taking into account the probabilities of scattering, absorption, and internal reflection. To achieve a high accuracy, an adequate amount of photons should be simulated, normally around 10^6-10^9 photons (Prahl, 1988). After developing the Monte Carlo models for monolayers (Thueler *et al.*, 2003), they must be expanded for mulitlayered tissues (shell membranes, CAM, material under the CAM). It will be important to use an appropriate phase function for the scattering for every layer, and to take enough moments into account. In a first approach only the inner shell membrane, the CAM, and the material just underneath the CAM should be modeled. Finally, also the eggshell, with a significant higher scattering coefficient than other biological tissues normally measured with SRS, should be taken into account, and measurements must be performed through the eggshell. The estimated scattering and absorbing properties can then be used to understand physiological and structural variations in the CAM tissue.

Chapter 6

General Conclusions and Perspectives

6.1 General conclusions

In the poultry sector more and more attention is paid at optimizing the incubation period to obtain healthy and well developed chicken. Due to the selection of the modern broiler, it has a high potential for rapid growth, however only if optimal management conditions are established. The latter must not only be controlled post hatch, but also during the incubation period (Hulet, 2007). In human medicine, as well as in veterinary sciences, it becomes increasingly clear that the conditions during embryonic development may predispose the embryo to diseases in adult life (Barker, 1995; Decuypere *et al.*, 2000; Decuypere *et al.*, 2005; Gluckman *et al.*, 2005). In addition the incubation period becomes a larger portion of the life of a broiler since slaughter age has decreased drastically (De Oliveira *et al.*, 2008; Hulet, 2007). Therefore, knowledge is needed about the optimal conditions during incubation for economical as well as welfare reasons, and consequently, also knowledge about the influence of these conditions on the physiology of the embryo. It may, on the one hand, lead to an optimization of the incubation conditions so the embryo does not develop any predisposition to a disease, or, on the other hand, it may lead to the use of deviating incubation conditions in sensitive periods to establish beneficial long-term changes. The latter may increase the coping of the embryo to possible stressful events later in the development, pre- and/or post hatch.

Recent research points out that hypercapnia, *i.e.* high levels of CO_2 during specific periods of incubation, may have beneficial effects on the growth and health of the embryo. It influences different physiological processes in the embryo which are not yet all understood (Buys *et al.*, 1998; De Smit *et al.*, 2006; Tona *et al.*, 2007; Witters, 2009). One of the possible processes which is influenced, is the angiogenesis in the chorioallantoic membrane (CAM) of the embryo. It is the principal organ for gas exchange during most of the incubation (Romanoff, 1960). Hypoxia, *i.e.* reduced levels of O_2, is known to influence the angiogenesis in the CAM (Dusseau and Hutchins, 1989) and hypercapnia is known to influence angiogenesis in tissue (Holmes *et al.*, 1994; Irie *et al.*, 2005). It seems plausible that hypercapnia will also influence the angiogenesis in the CAM and subsequently the gas exchange, and associated metabolism, growth and health of the embryo.

Although the CAM is an often used assay in studies on the different regulators of angiogenesis, the existing techniques to quantify the angiogenesis are time-consuming, labor-intensive, subjective, and in general not appropriate to monitor overall endogenous changes in the vascular network of the CAM during development. Moreover, to allow monitoring long-term effects and eliminate inter-chicken variability, non-destructive methods should be developed.

The search in this work for such techniques resulted, firstly, in a new objective destructive method, and secondly, the primary steps towards a non-destructive spectroscopic technique. In addition, the destructive technique was used to measure changes in the angiogenesis in the CAM due to early prenatal hypercapnic conditions during incubation.

The destructive methodology consists of an easy and fast sample preparation, a high resolution imaging set-up and automatic image processing computer algorithms for quantifying the angiogenesis in the CAM from embryonic day (ED) 10 onwards. This allows for fast collection of large amounts of data, sensitive to endogenous changes in the angiogenesis, and with a low repeatability and reproducibility variation. For each egg about 18 minutes of labor (the overnight fixation time excluded) are necessary to obtain the final pictures of the 24 different pieces. Afterwards, 12 minutes are used to process the images but this proceeds completely automatically. The developed methodology was validated in an experiment with a hypoxic incubation and a normoxic incubation (ED 11, 14, and 16). The hypoxia group had significantly higher angiogenesis at ED 14 compared to the control group which is in accordance with literature data (Dusseau and Hutchins, 1989). Nevertheless, persistent hypoxic conditions resulted in a less developed vascular network at ED 16 compared to normoxic incubation. This is assumed to arise from a halt in the development of the embryo due to the limited O_2 supply.

The newly developed methodology was used to quantify, for the first time, the changes in the angiogenesis in the chicken CAM during hypercapnic incubation. Two experiments were conducted and samples were taken on ED 10, 11, 12, 13, 14, 15, and 16. The embryo weight was measured too, and served as a parameter to follow up the development under hypercapnic conditions. Gradually built up hypercapnia during the first ten days of chicken development had a stimulating effect on the angiogenesis in the CAM and on the embryo

weight. The effects were revealed immediately after the hypercapnic conditions at ED 10, the first measured day. Moreover, the normal development of the vascular network showed a nonlinear increase with a higher increase of density and branching degree between ED 13 and 14. This higher increase was observed one day earlier in the hypercapnia group. Finally, at ED 15, the effect of hypercapnia was equalized and there were no differences between the hypercapnic and the control group. The most plausible explanation of the stimulating role of hypercapnia on the angiogenesis is via its acidification effect (Bruggeman *et al.*, 2007). A lower pH enhances the stimulating role of VEGF and bFGF, two important angiogenic factors (Burbridge *et al.*, 1999). This may lead to the systematic bias measured between the structural parameters of the vascular network in the control and the hypercapnia group. The nonlinear increase in the degree of development of the vascular network between ED 13 and 14 during normal incubation coincides with a drop in blood pH reported by Dawes and Simkiss (1969) and Boutilier *et al.* (1977). Assumably, this drop in blood pH occurs one day earlier in the hypercapnia group. This indicates persistent effects of the hypercapnic treatment during the first ten days. Nevertheless, the maximum density which was reached around ED 15 was not affected by the hypercapnic conditions. Differences found in the embryonic weights were explained partially by the differences in weight loss due to a lack of complete equalization of the relative humidity (RH) in the hypercapnic and control incubators. However, part of the differences could only be explained by the early prenatal hypercapnic conditions. The differences in embryo weight were not dependent on the ED. Therefore, the hypercapnic embryos seem to have a slight disadvantage from ED 15 onwards by having a slightly higher weight but an equally developed vascular network compared to the control group. It is not known if the embryos will therefore experience more severe hypoxia near the end of the incubation.

In the hypoxia-control validation experiment, as well as both the hypercapnia-control experiments, the local differences of the angiogenesis were studied by dividing the egg in three bands. In all groups and all experiments the vascular network in the band closest to the air cell was the most developed and in the band closest to the sharp end the least developed. This is in accordance with the normal development of the CAM which grows over the embryo to the blunt end, and later on to the sharp end of the egg. It is also in

accordance with the local differences in the eggshell conductance (Rokitka and Rahn, 1987). For the first time such local differences in the angiogenesis in the CAM were detected.

The final goal of this kind of research is the non-destructive and non-invasive measurement of parameters of the chicken development. Therefore, the first steps were taken in the development of a technique which has the potential of measuring the angiogenesis in the CAM non-destructively. Since blood has a very characteristic light absorption spectrum, an optical technique was chosen, namely spatially resolved spectroscopy (SRS). In combination with light propagation modeling, the absorption and scattering coefficient of the tissue can be determined separately, providing information on the concentrations of blood in the tissue as well as on the tissue structure. A reflectance SRS set-up, which was already partially assembled at the Advanced Photonics Laboratory in Lausanne, was further completed. It measured the reflectance at 7 distances from the source ranging from 0.3 to 1.2 mm. These small source-detector distances allowed the measurement of superficial tissue such as the CAM. In these early tests, the eggshell was removed to eliminate its signal since it is a highly scattering material and it contains protoporphyrin, a pigment with similar absorption characteristics to hemoglobin.

The results were promising as the measurements showed a clear blood spectrum with an increasing amount of blood in time (ED 10, 13, and 16), and significant differences in the reflectance profiles as function of the source-detector distances. The light propagates further in the tissue with increasing age. Differences between the hypercapnia and the control group could not be detected due to either a lack of sensitivity of the measurements, or a too small amount of data. A curve fitting to the diffusion approximation of light propagation modeling was used to determine the absorption and reduced scattering coefficients. The absorption coefficient increased with incubation time in the VIS region due to the higher blood content, and decreased between 900 and 1000 nm due to the lower water content. The reduced scattering coefficient decreased with incubation time. It seemed more plausible this was caused by an increase in scattering anisotropy rather than by a decrease in the scattering coefficient with incubation time. Unfortunately, the assumptions of the diffusion theory, namely large source-detector distances, tissue homogeneity and scattering isotropy, were not completely met. The estimates of the optical properties should

therefore be interpreted with caution. Other factors such as the internal reflection between the different layers, namely the inner shell membrane, the CAM, and the material under the CAM may have an influence on the reflectance profile.

In conclusion, a destructive method is developed with many advantages compared to the existing ones for quantifying angiogenesis in the CAM during development. It can be used to improve insight in both embryonic development and angiogenesis of chicken, and more in general of mammals. Secondly, early prenatal hypercapnia, similar to the natural conditions in chicken embryonic development, is shown to increase the angiogenesis in the CAM. At last, spatially resolved spectroscopic measurements are performed on the CAM tissue as first steps towards a non-destructive measuring technique. Significant differences in the light propagation in the CAM tissue with incubation time are detected.

6.2 Perspectives

The next major steps directly emerging from this research are twofold.

On the one hand, the effect of hypercapnia on the angiogenesis in the CAM should be further elucidated. The results in this dissertation lead to the suggestion that VEGF and bFGF should be monitored in conjunction with the angiogenesis in the CAM, and the pH, pCO_2 and bicarbonate levels in the chorioallantoic blood. It will be important to measure all possible days, and especially ED 12, 13 and 14. This research might be done with the developed destructive method. On the other hand, a more correct light propagation model for this specific application should be build. Monte Carlo simulations are proposed due to their flexibility for different conditions, such as multilayered tissue and a higher level of anisotropy (Bevilacqua, 1998). The resulting estimates of the optical properties can then be correlated to measurements with the destructive reference method. However, the development of such a model will be highly complex and will need high amounts of computation time.

Is future investment in such a complex model reasonable and justifiable?

Before investing in such a complex model, it seems appropriate to first investigate the angiogenesis in the CAM, while also measuring, in the same experiment, other parameters

of embryonic development. It is interesting to measure the angiogenesis in the CAM to broaden our physiological knowledge, but differences in the angiogenesis in the CAM may have too little influence, or may be too independent from the embryonic development, to be an interesting parameter for production and/or welfare reasons. It is hypothesized that differences in the angiogenesis may affect the gas exchange of the embryo, and as a consequence the metabolism, growth and health of the embryo, but this is not yet elucidated. If it is possible to link the angiogenesis in the CAM and important aspects of the development of the embryo unambiguously, investing time, money and knowledge in the non-destructive SRS technique is very useful. Indeed, the angiogenesis in the CAM can then be used to follow up the important aspects of development of the embryo. In our research, no unambiguous relation between the embryo weight, one of the possible parameters to characterize embryo development, and the angiogenesis in the CAM is found. First, the eggs, and therefore normally also the embryo's, in experiment 1 of chapter 4 are heavier compared to the ones in experiment 2, but the vascular network in the CAM is less developed in experiment 1 compared to experiment 2. Secondly, in experiment 2 no correlation was found between the embryo weight profile in function of the ED, and the structural parameters of the vascular network in function of the ED. This may be due to the fact that the extraembryonic membranes in the egg develop semi-autonomous from the embryo (Romanoff, 1960; Witters, 2009), although the angiogenesis in the CAM is assumed to be (partially) tuned to the embryonic development (Wagner-Amos and Seymour, 2003). The angiogenesis in the CAM increases with embryonic development to ensure the necessary gas exchange. When the embryonic development stops, the angiogenesis in the CAM probably also stops, as seen on ED 16 in the hypoxia experiment in chapter 3. Nevertheless, the angiogenesis in the CAM will most probably be partially influenced directly by the gaseous conditions without interfering with the growth of the embryo. As a consequence, it will be difficult, when measuring the angiogenesis, to distinguish between the direct effects of the gaseous environment and the indirect effects via the influence on the growth of the embryo. It will be important to determine if differences in certain parameters of the embryonic development are consequences of differences in the angiogenesis in the CAM, or strongly correlated with differences in the angiogenesis in the CAM. If so, investments in the non-destructive technique are highly useful.

Weighing out costs and benefits in assessing the influence of hypercapnic incubation?

One of the more general goals to which this research contributes, is the elucidation of the effect of hypercapnia on the embryonic development. Early prenatal hypercapnic incubation has an effect on the angiogenesis in the CAM, as hypothesized. However, the differences level out when reaching the maximal development of the vascular network in the CAM (ED 15). From this research, it is impossible to determine if this affects the embryo in such a way that it will alter the post hatch growth, or the predisposition to diseases, which are the important parameters for production and welfare. Therefore, other parameters, besides the angiogenesis in the CAM, should be measured too under hypercapnic incubation to clearly sort out the most important ones. This may lead to the conclusion that it is worth the costs to develop a model for light propagation in the CAM tissue inasmuch as the angiogenesis is a crucial parameter, or it may just as well lead to the conclusion that investments have to be made in other parameters which provide more profound insight in the role of hypercapnia on the chicken embryonic development and health. Additionally, it should be assessed if there are any effects of the interaction between hypercapnia and the embryronic temperature. After all, the interaction between gas concentrations and embryonic temperature may have an effect on the embryonic development (Molenaar *et al.*, 2010), and may also have an effect on the angiogenesis in the CAM. Therefore, in future research, the eggshell temperature, as a measure for embryonic temperature, should be included as factor.

How can the SRS measurements be improved?

All the considerations above do not alter the fact that the SRS set-up is able to measure differences in the angiogenesis, and changes can be followed throughout the incubation. It can be tested if changes between a hypercapnic incubation and a control incubation can be detected if more measurements are taken, and if the measurements themselves are made more uniform as proposed in chapter 5. Moreover, it should be examined if the SRS set-up can detect these differences through the eggshell as well. Even without the estimation of the optical properties, the reflectance profiles may provide information which enables to distinguish between different grades of vascular development in the CAM. This simplification may still provide researchers with a non-destructive technique to follow-up the angiogenesis

in the CAM. Obviously this has the advantage of enabling the monitoring of the same individual throughout its life. In a societal context of growing concern about animal welfare, it has the advantage of the abolition of sacrificing the embryos.

How should the suggested research be organized in time?

Different types of research are suggested above, namely (1) further investigations on the effect of hypercapnia on the angiogenesis in the CAM, (2) ruling out if there is an unambiguous relation between important aspects of the development of the embryo and the angiogenesis in the CAM, (3) evaluating other parameters of chicken development which are influenced under hypercapnia, (4) testing the SRS set-up for its ability to detect differences between the hypercapnia and the control group, (5) testing the SRS set-up for measurements through the eggshell, and (6) building more correct models for the light propagation through the eggshell and in the CAM. The first five ones can coexist, but the preferred chronological order is: 2, 3, 1, 4, and 5. The research mentioned as number 6 is conditional. Only after the previous research (number 1 to 5), if the importance of measuring the angiogenesis in the CAM appears to be very high, as a parameter for development, or as a crucial parameter altered under hypercapnia, time and knowledge can be invested in building complex Monte Carlo models for the light propagation through the eggshell and in the CAM to determine the optical properties of the CAM.

Are there any other possible applications of the research presented in this dissertation that enhance its investment value?

The set-ups constructed in this dissertation may serve other research. The SRS set-up can be used for measuring animal tissue or agricultural products to obtain information about the chromophore concentration and the structure of the tissue. The destructive methodology as well may be useful in more general physiology studies besides in the poultry research itself. The chicken embryo is often used as a model to investigate the different mechanisms in the developmental origins of health and disease in humans, since early development of mammalian and bird embryos is very similar. The advantage of working with chicken embryos is the feasibility of development independent of the mother, in incubators in which the environmental parameters can be controlled (Ruijtenbeek *et al.*, 2003). The developed

methodology might be useful in for example studies investigating the mechanisms of placental hyperoxia which causes intrauterine growth retardation (Ancar and Chardonnens, 2003). Furthermore, it may provide clues for improving the existing techniques of quantifying the angiogenesis in the CAM assay, such as the camera that was used without a microscope, the green illumination to enhance the contrast, and the fully automatic image processing based on adaptive thresholding.

APPENDIX

Table: Overview of the important studies in which pre- and postcapillary blood vessels in the CAM were analyzed. If no resolution is given in the table, it was not mentioned in the article.

Author	Test	Sampling	Imaging system	Quantification	Parameter
Dusseau *et al.* 1986	Test substance Hypoxia	-Windowed CAM -Fixation, dissection and mounting on glass slide	Microscope 20x (blood vessels > 10 µm)	Manual counting of intersections with 4-,5-,6-,8-mm diameter concentric circles (72 mm total circumference)	Vascular density index (Intersections/mm)
Strick *et al.* 1991	Hypoxia and hyperoxia	-Egg is opened and emptied -Injection of pelican ink -Fixation, dissection and mounting on glass slide	Video microscope (40x, 80x, 200x)	-Image processing -Manual counting of intersections with 3 concentric circles of 2.06, 2.54, 3.01 mm (2309 mm total circumference)	-Vascular density index (Intersections/mm) at 40x -Vessel length density $L_A=(\pi*\text{intersections})/(2*\text{length of grid})$ (mm/mm²) at 80x -Vessel endpoint density (number/mm²) at 200x
Kurz *et al.* 1995	Test substance	-Windowed CAM -Fixation, dissection, staining and mounting on glass slide	CCD camera with macro lens (11 µm/pixel (Kurz *et al.* 1998))	Manual counting of intersections with 1 mm square grid	-Vessel length density (mm/mm²) -Fractal dimension (Sandau and Kurz, 1997)

Kirchner *et al.* 1996	Tumor grafts	-*Ex ovo* and windowed CAM	Video microscope (574x489 pixels) 20x	-Image processing -Manual tracing of vasculature -Automatic counting	-Vessel density (number of intersected boxes/ area) -Fractal dimension
Vico *et al.* 1998	/	-Windowed CAM	CCD camera (640 x 480 pixels) with macrolens	- Manual tracing of vasculature -Automatic counting	-Fractal dimension
Nikiforidis *et al.* 1998	/	-Windowed CAM -Injection of contrast medium	X-ray Angiography (blood vessels > 50 µm)	-Image processing -Binary image via user-defined threshold	- Classification into three categories (50-100, 100-200, >200 µm) -Blood vessel diameter (via X-ray opaque ruler placed beside the egg -Blood vessel length (= total amount of white pixels)
Parsons-Wingerter *et al.* 1999 (Quail CAM)	Different solutions pipetted onto the CAM	-*Ex ovo* CAM -Fixation, dissection and mounting on glass slide	CCD camera (640 x 480 pixels) mounted on a microscope 10x (13 µm/pixel)	-Image processing -Binary image via user-defined threshold -Grid of 32x32 pixels	- Vessel density (intersections/cm²) - Fractal dimension
Maas *et al.* 1999	Different test tissues	-Windowed CAM	CCD camera mounted on a microscope 42x (blood vessels > 10 µm)	-Image processing -Manual counting with a grid of 5 concentric circles: first circle 2 mm in diameter and subsequent circles 0.25 mm apart	-Vascular density index
Gu *et al.* 2001	Ethanol injected in the air cell	-Egg is opened and emptied -CAM fixed *in situ*	CCD camera mounted on a microscope 25x	-Image processing -Binary image via user-defined threshold -Automatic counting	Vessel length density (mm/mm²)

Okamoto *et al.* 2002	Test substance	-Eggshell above air cell removed -Fixation and dissection	CCD camera to take macroscopic images (only large blood vessels)	-Binary image via fixed threshold -Automatic counting	Fractal dimension
Hazel *et al.* 2002	Test substance	-*Ex ovo* -Injection of contrast agent	CCD camera (768 494 pixels) mounted on a microscope 5x (only large blood vessels)	-Image processing -Manual tracing of vasculature	-CAM area -Vessel length
Wagner-Amos and Seymour, 2003	Local hypoxia by sealing part of the eggshell with wax	-Dissection, fixation, staining and mounting on glass slide	Microscope 40x	-Manual counting of intersections (unknown grid size)	Vessel length density (mm/mm^2)
Miller *et al.* 2004	Test substance	-Windowed CAM -Injection of fluorescent dextran -Dissection and fixation	-Light microscope -Fluorescent microscope	-Image processing -Scoring of response on 0-4 grading scale -Intensity measurements through the fluorescent microscope	-Qualitative score via light microscopy -Fluorescent vascular density index via fluorescent microscopy
Blacher *et al.* 2005	Test substance	-*Ex ovo* CAM -Injection of fluorescent dextran	-CCD camera mounted on a microscope 24x	-Image processing - Binary image via automatic thresholding	-Vessel area density (number of pixels that belong to the vascular network divided by the total area of the image) -Vessel length density (number of pixels that belong to the skeleton of the vascular network divided by the total area of the image)

					-Vessel endpoint density (number of vessel endpoints divided by the total area of the image)
Reizis *et al.* 2005	/	-Dissection, fixation, paraffin embedding, sectioning, staining	-Microscope 20x (detection limit of 8 µm) -Microscope 40x to determine thickness of the CAM	-Manual counting (unknown grid)	-Vessel (numerical) density: N_A(intersections/mm²) -Vessel area fraction -Thickness of CAM: D_{CAM} -Total length of vessels $L=2*N_A*V$ with V the volume of the CAM: $V=S_{CAM}*D_{CAM}$
Parsons-Wingerter *et al.* 2006	Test substance	-*Ex ovo* CAM -Fixation, dissection and mounting on glass slide	CCD camera mounted on a microscope 10x (13 µm/pixel; improvement to 7.32 µm/pixel in McKay *et al.* 2008)	-Image processing -Binary image via user-defined threshold -VESGEN to determine different parameters via the binary morphological operators of the Image Processing Toolbox of Matlab	- Vessel density with 32x32 pixel grid (intersections/cm²) - Fractal dimension image -Classification into 5 generations -Vessel length density L_V (mm/mm²) -Vessel area density A_V (mm²/mm²) -Vessel number density N_V (intersections/mm²) -Average vessel diameter $D_V = A_V/L_V$
Doukas *et al.* 2008	Test substance	-Windowed CAM -Dissection and fixation	CCD camera (7.1 Mpixels) mounted on a microscope	-Image processing -Automatic counting (automatic thresholding but based on user predefined parameters such as the size of the neighborhood used)	-Vessel length (number of pixels belonging to a skeletonized vessel) -Vessel density (vessel length divided by the total number of image pixels)

REFERENCE LIST

Ackerman, R.A. and Rahn, H. (1981). In vivo o-2 and water-vapor permeability of the hens eggshell during early development *Respiration Physiology* 45 (1), 1-8.

Adams, R.H. and Alitalo, K. (2007). Molecular regulation of angiogenesis and lymphangiogenesis. *Nature Reviews Molecular Cell Biology* 8 (6), 464-478.

Ancar, B. and Chardonnens, D. (2003). Main regulators of angiogenesis and their role in preeclampsia and intrauterine growth restriction. A bibliographic review. http://www.gfmer.ch/Endo/Fellows_10/Main_regulators_angiogenesis.htm (15/03/2005).

Auerbach, R., Akhtar, N., Lewis, R.L. and Shinners, B.L. (2000). Angiogenesis assays: Problems and pitfalls. *Cancer and Metastasis Reviews* 19 (1-2), 167-172.

Ausprunk, D.H., Knighton, D.R. and Folkman, J. (1974). Differentiation of vascular endothelium in chick chorioallantois - structural and autoradiographic study. *Developmental Biology* 38 (2), 237-248.

Aviagen (2007). Feeding broiler breeders for chick quality. http://www.thepoultrysite.com/articles/793/feeding-broiler-breeders-for-chick-quality (17/05/2010).

Bacud, L. (2007). Fluorescein angiography of the retina. http://en.wikipedia.org/wiki/File:Fluorescein_angiography.jpg (07/06/2010).

Baker, W.M. and Harris, V.D. (1892). Kirkes' handbook of physiology. P. Blakiston's Son & Co., Philadelphia, 804 p.

Bamelis, F. (2003). Non invasive assessment of eggshell conductance and different developmental stages during incubation of eggs. Katholieke Universiteit Leuven, Department of Biosystems, 206 p.

Bamelis, F.R., Tona, K., De Baerdemaeker, J.G. and Decuypere, E.M. (2002). Detection of early embryonic development in chicken eggs using visible light transmission. *British Poultry Science* 43 (2), 204-212.

Barker, D.J.P. (1995). Intrauterine programming of adult disease. *Molecular Medicine Today* 1 (9), 418-423.

Bennet, T.J. (2001). The ophtalmic photographers. http://www.opsweb.org/index.htm (02/09/2004).

Bevilacqua, F. (1998). Local optical characterization of biological tissues *in vitro* and *in vivo*. École Polytechnique Fédérale de Lausanne (EPFL), Département de Microtechnique, 203 p.

Bevilacqua, F. and Depeursinge, C. (1999). Monte carlo study of diffuse reflectance at source-detector separations close to one transport mean free path. *Journal of the Optical Society of America a-Optics Image Science and Vision* 16 (12), 2935-2945.

Bevilacqua, F., Piguet, D., Marquet, P., Gross, J.D., Tromberg, B.J. and Depeursinge, C. (1999). In vivo local determination of tissue optical properties: Applications to human brain. *Applied Optics* 38 (22), 4939-4950.

Bissonnette, J.M. and Metcalfe, J. (1978). Gas-exchange of fertile hens egg - components of resistance. *Respiration Physiology* 34 (2), 209-218.

Blacher, S., Devy, L., Hlushchuk, R., Larger, E., Noel, L., Burri, P., Corvoll, P., Djonov, V., Foidart, J.-M. and Noël, A. (2005). Quantification of angiogenesis in the chick chorioallantoic membrane (cam). *Image Analysis & Stereology* 24 169-180.

Blacher, S. (2007). Image processing and measurements in the material sciences and biology. Workshop on multivariate imaging analysis. Gembloux, belgium.

Blatt, R.J., Clark, A.N., Courtney, J., Tully, C. and Tucker, A.L. (2004). Automated quantitative analysis of angiogenesis in the rat aorta model using image-pro plus 4.1. *Computer Methods and Programs in Biomedicine* 75 (1), 75-79.

Borror, C.M., Montgomery, D.C. and Runger, G.C. (1997). Confidence intervals for variance components from gauge capability studies. *Quality and Reliability Engineering International* 13 (6), 361-369.

Boutilier, R.G., Gibson, M.A., Toews, D.P. and Anderson, W. (1977). Gas-exchange and acid-base regulation in blood and extraembryonic fluids of developing chicken-embryo. *Respiration Physiology* 31 (1), 81-89.

Bradbury, J. (2001). Breathing hard to keep up with hif-1. *Lancet* 358 (9294), 1704-1704.

Brat, D.J., Kaur, B. and Van Meir, E.G. (2003). Genetic modulation of hypoxia induced gene expression and angiogenesis: Relevance to brain tumors. *Frontiers in Bioscience* 8 D100-D116.

Brownuniversity (2009). Development of the vascular system. http://www.brown.edu/Courses/BI0032/stemcell/vascu.htm (15/11/2009).

Bruggeman, V., Witters, A., De Smit, L., Debonne, M., Everaert, N., Kamers, B., Onagbesan, O.M., Degraeve, P. and Decuypere, E. (2007). Acid-base balance in chicken embryos (gallus domesticus) incubated under high co2 concentrations during the first 10 days of incubation. *Respiratory Physiology & Neurobiology* 159 (2), 147-154.

Burbridge, M.F., Tucker, G.C., West, D.C. and Atassi, G. (1999). The role of extracellular ph in the regulation of in vitro angiogenesis. *Journal of Vascular Research* 36 (2), 159-159.

Burt, D.W. (2007). Emergence of the chicken as a model organism: Implications for agriculture and biology. *Poultry Science* 86 (7), 1460-1471.

Burton, G.J. and Palmer, M.E. (1992). Development of the chick chorioallantoic capillary plexus under normoxic and normobaric hypoxic and hyperoxic conditions - a morphometric study. *Journal of Experimental Zoology* 262 (3), 291-298.

Buys, N., Dewil, E., Gonzales, E. and Decuypere, E. (1998). Different co2 levels during incubation interact with hatching time and ascites susceptibility in two broiler lines selected for different growth rate. *Avian Pathology* 27 (6), 605-612.

Carmeliet, P. (2000). Mechanisms of angiogenesis and arteriogenesis. *Nature Medicine* 6 (4), 389-395.

Carmeliet, P. (2003). Angiogenesis in health and disease. *Nature Medicine* 9 (6), 653-660.

Cheong, W.F., Prahl, S.A. and Welch, A.J. (1990). A review of the optical-properties of biological tissues. *Ieee Journal of Quantum Electronics* 26 (12), 2166-2185.

Chu-Charroll, M.C. (2007). Fractal curves and coastlines. http://scienceblogs.com/goodmath/2007/07/fractal_curves_and_coastlines_1.php (24/08/2010).

Clipart, E. (2009). Vascular area in the chick. http://etc.usf.edu/clipart/51200/51286/51286_chick.htm (20/08/2009).

Cobb (2008). Breeder management guide. http://www.cobb-vantress.com/contactus/brochures/Breeder_guide_2008.pdf (27/05/2010).

Collin, A., Berri, C., Tesseraud, S., Rodon, F.E.R., Skiba-Cassy, S., Crochet, S., Duclos, M.J., Rideau, N., Tona, K., Buyse, J., Bruggeman, V., Decuypere, E., Picard, M. and Yahav, S. (2007). Effects of thermal manipulation during early and late embryogenesis on thermotolerance and breast muscle characteristics in broiler chickens. *Poultry Science* 86 (5), 795-800.

Contini, D., Martelli, F. and Zaccanti, G. (1997). Photon migration through a turbid slab described by a model based on diffusion approximation .2. Theory. *Applied Optics* 36 (19), 4587-4599.

D'arcangelo, D., Facchiano, F., Barlucchi, L.M., Melillo, G., Illi, B., Testolin, L., Gaetano, C. and Capogrossi, M.C. (2000). Acidosis inhibits endothelial cell apoptosis and function and induces basic fibroblast growth factor and vascular endothelial growth factor expression. *Circulation Research* 86 (3), 312-318.

Davis, T.A. and Ackerman, R.A. (1987). Effects of increased water-loss on growth and water-content of the chick-embryo. *Journal of Experimental Zoology* 357-364.

Dawes, C. and Simkiss, K. (1969). Acid-base status of blood of developing chick embryo. *Journal of Experimental Biology* 50 (1), 79-86.

De Clerck, N. (2005). Micro-ct to visualize the cam vasculature (personal communication).

De Oliveira, J.E., Uni, Z. and Ferket, P.R. (2008). Important metabolic pathways in poultry embryos prior to hatch. *Worlds Poultry Science Journal* 64 (4), 488-499.

De Smit, L., Bruggeman, V., Tona, J.K., Debonne, M., Onagbesan, O., Arckens, L., De Baerdemaeker, J. and Decuypere, E. (2006). Embryonic developmental plasticity of the chick: Increased co2 during early stages of incubation changes the developmental trajectories during prenatal and postnatal growth. *Comparative Biochemistry and Physiology a-Molecular & Integrative Physiology* 145 (2), 166-175.

Decuypere, E., Buyse, J. and Buys, N. (2000). Ascites in broiler chickens: Exogenous and endogenous structural and functional causal factors. *Worlds Poultry Science Journal* 56 (4), 367-377.

Decuypere, E., Hassanzadeh, M. and Buys, N. (2005). Further insights into the susceptibility of broilers to ascites. *Veterinary Journal* 169 (3), 319-320.

Decuypere, E. and Bruggeman, V. (2007). The endocrine interface of environmental and egg factors affecting chick quality. *Poultry Science* 86 (5), 1037-1042.

Decuypere, E. (2010). Natural build-up of co_2 concentrations (personal communication).

Defouw, D.O., Rizzo, V.J., Steinfeld, R. and Feinberg, R.N. (1989). Mapping of the microcirculation in the chick chorioallantoic membrane during normal angiogenesis. *Microvascular Research* 38 (2), 136-147.

Defouw, L.M. and Defouw, D.O. (2000). Vascular endothelial growth factor fails to acutely modulate endothelial permeability during early angiogenesis in the chick chorioallantoic membrane. *Microvascular Research* 60 (3), 212-221.

Dinkel, H.P., Moll, R. and Debus, S. (2001). Colour flow doppler ultrasound of the carotid bifurcation: Can it replace routine angiography before carotid endarterectomy? *British Journal of Radiology* 74 (883), 590-594.

Djonov, V., Schmid, M., Tschanz, S.A. and Burri, P.H. (2000). Intussusceptive angiogenesis - its role in embryonic vascular network formation. *Circulation Research* 86 (3), 286-292.

Donati, M.B. and Gozdzikiewicz, J. (2008). Angiogenesis and the progress of vascular and tumor biology: A tribute to judah folkman. *Thrombosis and Haemostasis* 99 (4), 647-650.

Doornbos, R.M.P., Lang, R., Aalders, M.C., Cross, F.W. and Sterenborg, H. (1999). The determination of in vivo human tissue optical properties and absolute chromophore concentrations using spatially resolved steady-state diffuse reflectance spectroscopy. *Physics in Medicine and Biology* 44 (4), 967-981.

Doukas, C.N., Maglogiannis, I. and Chatziioannou, A.A. (2008). Computer-supported angiogenesis quantification using image analysis and statistical averaging. *Ieee Transactions on Information Technology in Biomedicine* 12 (5), 650-657.

Dragon, S. and Baumann, R. (2003). Hypoxia, hormones, and red blood cell function in chick embryos. *News in Physiological Sciences* 18 77-82.

Dusseau, J.W., Hutchins, P.M. and Malbasa, D.S. (1986). Stimulation of angiogenesis by adenosine on the chick chorioallantoic membrane. *Circulation Research* 59 (2), 163-170.

Dusseau, J.W. and Hutchins, P.M. (1989). Microvascular responses to chronic hypoxia by the chick chorioallantoic membrane - a morphometric analysis. *Microvascular Research* 37 (2), 138-147.

Eichmann, A., Yuan, L., Moyon, D., Lenoble, F., Pardanaud, L. and Breant, C. (2005). Vascular development: From precursor cells to branched arterial and venous networks. *International Journal of Developmental Biology* 49 (2-3), 259-267.

Elert, G. (2007). Fractal dimension. http://hypertextbook.com/chaos/33.shtml (19/05/2007).

Everaert, N., Kamers, B., Witters, A., De Smit, L., Debonne, M., Decuypere, E. and Bruggeman, V. (2007). Effect of four percent carbon dioxide during the second half of incubation on embryonic development, hatching parameters, and posthatch growth. *Poultry Science* 86 (7), 1372-1379.

Everaert, N., De Smit, L., Debonne, M., Witters, A., Kamers, B., Decuypere, E. and Bruggeman, V. (2008). Changes in acid-base balance and related physiological responses as a result of external hypercapnia during the second half of incubation in the chicken embryo. *Poultry Science* 87 (2), 362-367.

Fan, T. (2009). Angiogenesis: A brief introduction. http://www.med.unibs.it/~airc/angiogen.html (05/10/2009).

Farrell, T.J., Patterson, M.S. and Wilson, B. (1992a). A diffusion-theory model of spatially resolved, steady-state diffuse reflectance for the noninvasive determination of tissue optical-properties invivo. *Medical Physics* 19 (4), 879-888.

Farrell, T.J., Wilson, B.C. and Patterson, M.S. (1992b). The use of a neural network to determine tissue optical-properties from spatially resolved diffuse reflectance measurements. *Physics in Medicine and Biology* 37 (12), 2281-2286.

Ferrara, N. (2004). Vascular endothelial growth factor: Basic science and clinical progress. *Endocrine Reviews* 25 (4), 581-611.

Flamme, I., Schulzeosthoff, K. and Jacob, H.J. (1991). Mitogenic activity of chicken chorioallantoic fluid is temporally correlated to vascular growth in the chorioallantoic membrane and related to fibroblast growth-factors. *Development* 111 (3), 683-690.

Foster, F.S. (2002). Medical and biological imaging with high frequency ultrasound. http://medbio.utoronto.ca/faculty/foster.html (07/06/2004).

Frame, M., Mandelbrot, B. and Neger, N. (2010). Fractals: Box counting dimension. http://classes.yale.edu/fractals/FracAndDim/BoxDim/BoxDim.html (17/02/2010).

Fukumura, D., Xu, L., Chen, Y., Gohongi, T., Seed, B. and Jain, R.K. (2001). Hypoxia and acidosis independently up-regulate vascular endothelial growth factor transcription in brain tumors in vivo. *Cancer Research* 61 (16), 6020-6024.

Gargett, C.E. and Rogers, P.A.W. (2001). Human endometrial angiogenesis. *Reproduction* 121 (2), 181-186.

Genetech (2009). Research vegf. http://www.researchvegf.com/researchvegf/vegf/vegf-pathway/signaling/index.m (11/09/2009).

George, D.J. and Kaelin, W.G. (2003). The von hippel-lindau protein, vascular endothelial growth factor, and kidney cancer. *New England Journal of Medicine* 349 (5), 419-421.

Gielen, R., Dejong, L.P. and Kerkvliet, H.M.M. (1979). Electrooptical blood-spot detection in intact eggs. *Ieee Transactions on Instrumentation and Measurement* 28 (3), 177-183.

Giussani, D.A., Salinas, C.E., Villena, M. and Blanco, C.E. (2007). The role of oxygen in prenatal growth: Studies in the chick embryo. *Journal of Physiology-London* 585 (3), 911-917.

Glazer, O. (2006). Magnetic resonance angiography. http://en.wikipedia.org/wiki/Magnetic_resonance_angiography (02/06/2010).

Gluckman, P.D., Hanson, M.A. and Pinal, C. (2005). The developmental origins of adult disease. *Maternal and Child Nutrition* 1 (3), 130-141.

Goerges, A.L. and Nugent, M.A. (2003). Regulation of vascular endothelial growth factor binding and activity by extracellular ph. *Journal of Biological Chemistry* 278 (21), 19518-19525.

Green, E. (1998). Fractal dimension. http://pages.cs.wisc.edu/~ergreen/honors_thesis/dimension.html (11/06/2004).

Groenhuis, R.A.J., Ferwerda, H.A. and Tenbosch, J.J. (1983a). Scattering and absorption of turbid materials determined from reflection measurements .1. Theory. *Applied Optics* 22 (16), 2456-2462.

Groenhuis, R.A.J., Tenbosch, J.J. and Ferwerda, H.A. (1983b). Scattering and absorption of turbid materials determined from reflection measurements .2. Measuring method and calibration. *Applied Optics* 22 (16), 2463-2467.

Gu, J.W., Elam, J., Sartin, A., Li, W., Roach, R. and Adair, T.H. (2001). Moderate levels of ethanol induce expression of vascular endothelial growth factor and stimulate angiogenesis. *American Journal of Physiology-Regulatory Integrative and Comparative Physiology* 281 (1), R365-R372.

Harvey, R.P. and Rosenthal, N. (1999). Heart development. Academic Press, San Diego, 530 p.

Hassanzadeh, M., Buyse, J. and Decuypere, E. (2002). Further evidence for the involvement of cardiac beta-adrenergic receptors in right ventricle hypertrophy and ascites in broiler chickens. *Avian Pathology* 31 (2), 177-181.

Hassanzadeh, M., Fard, M.H.B., Buyse, J., Bruggeman, V. and Decuypere, E. (2004). Effect of chronic hypoxia during embryonic development on physiological functioning and on hatching and post-hatching parameters related to ascites syndrome in broiler chickens. *Avian Pathology* 33 (6), 558-564.

Hazel, S.J. (2003). A novel early chorioallantoic membrane assay demonstrates quantitative and qualitative changes caused by antiangiogenic substances. *Journal of Laboratory and Clinical Medicine* 141 (3), 217-228.

Hemenger, R.P. (1977). Optical-properties of turbid media with specularly reflecting boundaries - applications to biological problems. *Applied Optics* 16 (7), 2007-2012.

Hielscher, A.H., Alcouffe, R.E. and Barbour, R.L. (1998). Comparison of finite-difference transport and diffusion calculations for photon migration in homogeneous and heterogeneous tissues. *Physics in Medicine and Biology* 43 (5), 1285-1302.

Hollis, V. (2002). Non-invasive monitoring of brain tissue temperature by near-infrared spectroscopy. University College London, Department of Medical Physics and Bioengineering, 262 p.

Holmes, J.M., Duffner, L.A. and Kappil, J.C. (1994). The effect of raised inspired carbon-dioxide on developing rat retinal vasculature exposed to elevated oxygen. *Current Eye Research* 13 (10), 779-782.

Holmes, J.M., Zhang, S.C., Leske, D.A. and Lanier, W.L. (1998). Carbon dioxide-induced retinopathy in the neonatal rat. *Current Eye Research* 17 (6), 608-616.

Howell, K., Ooi, H., Preston, R. and Mcloughlin, P. (2004). Structural basis of hypoxic pulmonary hypertension: The modifying effect of chronic hypercapnia. *Experimental Physiology* 89 (1), 66-72.

Hulet, R.M. (2007). Managing incubation: Where are we and why? *Poultry Science* 86 (5), 1017-1019.

Irie, H., Tatsumi, T., Takamiya, M., Zen, K., Takahashi, T., Azuma, A., Tateishi, K., Nomura, T., Hayashi, H., Nakajima, N., Okigaki, M. and Matsubara, H. (2005). Carbon dioxide-rich water bathing enhances collateral blood flow in ischemic hindlimb via mobilization of endothelial progenitor cells and activation of no-cgmp system. *Circulation* 111 (12), 1523-1529.

Jensen, P.K. (2004). Resolution of retinal images. http://www.cafia.org/cafia2000/public_html/fullpaper/koch_jensen.htm (02/09/2004).

Johnson, W.R., Wilson, D.W., Fink, W., Humayun, M. and Bearman, G. (2007). Snapshot hyperspectral imaging in ophthalmology. *Journal of Biomedical Optics* 12 (1), 7.

Kahn, J. (1994). Pet-blood flow of brain. http://commons.wikimedia.org/wiki/File:PET-blood_flow_of_brain.gif (02/06/2010).

Kemps, B.J., Bamelis, F.R., Mertens, K., Decuypere, E.M., De Baerdemaeker, J.G. and De Ketelaere, B. (2010). Assessment of embryonic growth in chicken eggs by means of visible transmission spectroscopy. *Biotechnology Progress* 26 (2), 512-516.

Keywestdiagnostics (2007). Services. http://www.keywestcommunitydiagnostics.com/services.htm (02/06/2010).

Kienle, A., Lilge, L., Patterson, M.S., Hibst, R., Steiner, R. and Wilson, B.C. (1996). Spatially resolved absolute diffuse reflectance measurements for noninvasive determination of the optical scattering and absorption coefficients of biological tissue. *Applied Optics* 35 (13), 2304-2314.

Kienle, A. and Patterson, M.S. (1997). Improved solutions of the steady-state and the time-resolved diffusion equations for reflectance from a semi-infinite turbid medium. *Journal of the Optical Society of America a-Optics Image Science and Vision* 14 (1), 246-254.

Kirchner, L.M., Schmidt, S.P. and Gruber, B.S. (1996). Quantitation of angiogenesis in the chick chorioallantoic membrane model using fractal analysis. *Microvascular Research* 51 (1), 2-14.

Kolkman, R.G.M., Huisjes, A., Siphanto, R.I., Steenbergen, W. and Van Leeuwen, T.G. (2004). Photoacoustic imaging of blood vessels in the chorioallantoic membrane of a chicken embryo. In Photons plus ultrasound: Imaging and sensing. Spie-Int Soc Optical Engineering, Bellingham. 16-20.

Konerding, M.A., Fait, E. and Gaumann, A. (2001). 3d-morphometry of the microvascular unit in tumors and normal tissues: Quantitative studies on microvascular corrosion casts. In Vascular endothelium - source and target of inflammatory mediators. I O S Press, Amsterdam. 151-165.

Kurz, H., Ambrosy, S., Wilting, J., Marme, D. and Christ, B. (1995). Proliferation pattern of capillary endothelial-cells in chorioallantoic membrane-development indicates local growth-control, which is counteracted by vascular endothelial growth-factor application. *Developmental Dynamics* 203 (2), 174-186.

Kurz, H. (2000). Physiology of angiogenesis. *Journal of Neuro-Oncology* 50 (1-2), 17-35.

Kurz, H., Burri, P.H. and Djonov, V.G. (2003). Angiogenesis and vascular remodeling by intussusception: From form to function. *News in Physiological Sciences* 18 65-70.

Le Noble, F., Moyon, D., Pardanaud, L., Yuan, L., Djonov, V., Matthijsen, R., Breant, C., Fleury, V. and Eichmann, A. (2004). Flow regulates arterial-venous differentiation in the chick embryo yolk sac. *Development* 131 (2), 361-375.

Leske, D., Wu, J.M., Mookadam, M., Chen, Y., Fautsch, M.P., Holmes, J.M. and Lanier, W.L. (2006). The relationship of retinal vegf and retinal igf-1 mrna with neovascularization in an acidosis-induced model of retinopathy of prematurity. *Current Eye Research* 31 (2), 163-169.

Li, W.W. (2002). Tumor angiogenesis: Molecular pathology, therapeutic targeting, and imaging. http://www3.cancer.gov/bip/AimCIPWEB.pdf (03/02/2005).

Lourens, A., Van Den Brand, H., Meijerhof, R. and Kemp, B. (2005). Effect of eggshell temperature during incubation on embryo development, hatchability, and posthatch development. *Poultry Science* 84 (6), 914-920.

Lourens, A., Van Den Brand, H., Heetkamp, M.J.W., Meijerhof, R. and Kemp, B. (2007). Effects of eggshell temperature and oxygen concentration on embryo growth and metabolism during incubation. *Poultry Science* 86 (10), 2194-2199.

Lourens, S. (2008). Embryo temperature during incubation: Practice and theory. Wageningen Universiteit, Leerstoelgroep Adaptatiefysiologie, 139 p.

Lu, R.F. (2004). Near-infrared multispectral scattering for assessing internal quality of apple fruit. In Monitoring food safety, agriculture, and plant health. Spie-Int Soc Optical Engineering, Bellingham. 313-320.

Maas, J.W.M., Le Noble, F.A.C., Dunselman, G.A.J., De Goeij, A., Boudier, H. and Evers, J.L.H. (1999). The chick embryo chorioallantoic membrane as a model to investigate the angiogenic properties of human endometrium. *Gynecologic and Obstetric Investigation* 48 (2), 108-112.

Mamin, H.J., Poggio, M., Degen, C.L. and Rugar, D. (2007). Nuclear magnetic resonance imaging with 90-nm resolution. *Nature Nanotechnology* 2 (5), 301-306.

Mancardi, D., Varetto, G., Bucci, E., Maniero, F. and Guiot, C. (2008). Fractal parameters and vascular networks: Facts & artifacts. *Theoretical Biology and Medical Modelling* 5 8.

Martelli, F., Del Bianco, S., Ismaelli, A. and Zaccanti, G. (2009). Light propagation through biological tissue. SPIE Press, Bellingham WA, USA,

Mcdonald, D.M. and Choyke, P.L. (2003). Imaging of angiogenesis: From microscope to clinic. *Nature Medicine* 9 (6), 713-725.

Mckay, T.L., Gedeon, D.J., Vickerman, M.B., Hylton, A.G., Ribita, D., Olar, H.H., Kaiser, P.K. and Parsons-Wingerter, P. (2008). Selective inhibition of angiogenesis in small blood vessels and decrease in vessel diameter throughout the vascular tree by triamcinolone acetonide. *Investigative Ophthalmology & Visual Science* 49 (3), 1184-1190.

Melkonian, G., Munoz, N., Chung, J., Tong, C., Marr, R. and Talbot, P. (2002). Capillary plexus development in the day five to day six chick chorioallantoic membrane is inhibited by cytochalasin d and suramin. *Journal of Experimental Zoology* 292 (3), 241-254.

Meyer, R.D., Mohammadi, M. and Rahimi, N. (2006). A single amino acid substitution in the activation loop defines the decoy characteristic of vegfr-1/flt-1. *Journal of Biological Chemistry* 281 (2), 867-875.

Miller, S.L., Green, L.R., Peebles, D.M., Hanson, M.A. and Blanco, C.E. (2002). Effects of chronic hypoxia and protein malnutrition on growth in the developing chick. *American Journal of Obstetrics and Gynecology* 186 (2), 261-267.

Molenaar, R., Meijerhof, R., Van Den Anker, I., Heetkamp, M.J.W., Van Den Borne, J., Kemp, B. and Van Den Brand, H. (2010). Effect of eggshell temperature and oxygen concentration on survival rate and nutrient utilization in chicken embryos. *Poultry Science* 89 (9), 2010-2021.

Moran, T. and Hale, H.P. (1935). Physics of the hen's egg: I. Membranes in the egg. http://jeb.biologists.org/cgi/reprint/13/1/35.pdf (05/09/2010).

Mortola, J.P. (2009). Gas exchange in avian embryos and hatchlings. *Comparative Biochemistry and Physiology a-Molecular & Integrative Physiology* 153 (4), 359-377.

Ni, M., Zhang, M., Ding, S.F., Chen, W.Q. and Zhang, Y. (2008). Micro-ultrasound imaging assessment of carotid plaque characteristics in apolipoprotein-e knockout mice. *Atherosclerosis* 197 (1), 64-71.

Niedorf, F., Jungmann, H. and Kietzmann, M. (2005). Noninvasive reflection spectra provide quantitative information about the spatial distribution of skin chromophores. *Medical Physics* 32 (5), 1297-1307.

Nikiforidis, G., Papazafiropoulos, D., Siablis, D., Karnabatidis, D., Hatjikondi, O. and Dimopoulos, J. (1999). Quantitative assessment of angiogenesis in the chick embryo and its chorioallantoic membrane by computerised analysis of angiographic images. *European Journal of Radiology* 29 (2), 168-179.

Nowak-Sliwinska, P., Ballini, J.P., Wagnieres, G. and Van Den Bergh, H. (2010). Processing of fluorescence angiograms for the quantification of vascular effects induced by anti-angiogenic agents in the cam model. *Microvascular Research* 79 (1), 21-28.

Numata, Y., Sakae, T., Nakada, H., Suwa, T., Legeros, R.Z., Okazaki, Y. and Kobayashi, K. (2007). Micro-ct analysis of rabbit cancellous bone around implants. *Journal of Hard Tissue Biology* 16 (2), 91-93.

Onagbesan, O., Bruggeman, V., De Smit, L., Debonne, M., Witters, A., Tona, K., Everaert, N. and Decuypere, E. (2007). Gas exchange during storage and incubation of avian eggs: Effects on embryogenesis, hatchability, chick quality and post-hatch growth. *Worlds Poultry Science Journal* 63 (4), 557-573.

Ooi, H., Cadogan, E., Sweeney, M., Howell, K., O'regan, R.G. and Mcloughlin, P. (2000). Chronic hypercapnia inhibits hypoxic pulmonary vascular remodeling. *American Journal of Physiology-Heart and Circulatory Physiology* 278 (2), H331-H338.

Otrock, Z.K., Mahfouz, R.A.R., Makarm, J.A. and Shamseddine, A.I. (2007). Understanding the biology of angiogenesis: Review of the most important molecular mechanisms. *Blood Cells Molecules and Diseases* 39 (2), 212-220.

Otsu, N. (1979). Threshold selection method from gray-level histograms. *Ieee Transactions on Systems Man and Cybernetics* 9 (1), 62-66.

Padhani, A.R. and Neeman, M. (2001). Challenges for imaging angiogenesis. *British Journal of Radiology* 74 (886), 886-890.

Park, S.J., Rogers, W.L. and Clinthorne, N.H. (2007). Design of a very high-resolution small animal pet scanner using a silicon scatter detector insert. *Physics in Medicine and Biology* 52 (15), 4653-4677.

Parsons-Wingerter, P., Lwai, B., Yang, M.C., Elliott, K.E., Milaninia, A., Redlitz, A., Clark, J.I. and Sage, E.H. (1998). A novel assay of angiogenesis in the quail chorioallantoic membrane: Stimulation by bfgf and inhibition by angiostatin according to fractal dimension and grid intersection. *Microvascular Research* 55 (3), 201-214.

Parsons-Wingerter, P., Elliott, K.E., Farr, A.G., Radhakrishnan, K., Clark, J.I. and Sage, E.H. (2000). Generational analysis reveals that tgf-beta 1 inhibits the rate of angiogenesis in vivo by selective decrease in the number of new vessels. *Microvascular Research* 59 (2), 221-232.

Parsons-Wingerter, P., Chandrasekharan, U.M., Mckay, T.L., Radhakrishnan, K., Dicorleto, P.E., Albarran, B. and Farr, A.G. (2006). A vegf(165)-induced phenotypic switch from increased vessel density to increased vessel diameter and increased endothelial nos activity. *Microvascular Research* 72 (3), 91-100.

Patan, S., Haenni, B. and Burri, P.H. (1993). Evidence for intussusceptive capillary growth in the chicken chorioallantoic membrane (cam). *Anatomy and Embryology* 187 (2), 121-130.

Patan, S., Haenni, B. and Burri, P.H. (1996). Implementation of intussusceptive microvascular growth in the chicken chorioallantoic membrane (cam) .1. Pillar formation by folding of the capillary wall. *Microvascular Research* 51 (1), 80-98.

Patan, S., Haenni, B. and Burri, P.H. (1997). Implementation of intussusceptive microvascular growth in the chicken chorioallantoic membrane (cam) .2. Pillar formation by capillary fusion. *Microvascular Research* 53 (1), 33-52.

Patterson, M.S., Chance, B. and Wilson, B.C. (1989). Time resolved reflectance and transmittance for the noninvasive measurement of tissue optical-properties. *Applied Optics* 28 (12), 2331-2336.

Patterson, M.S., Moulton, J.D., Wilson, B.C., Berndt, K.W. and Lakowicz, J.R. (1991). Frequency-domain reflectance for the determination of the scattering and absorption properties of tissue. *Applied Optics* 30 (31), 4474-4476.

Patterson, M.S., Anderssonengels, S., Wilson, B.C. and Osei, E.K. (1995). Absorption-spectroscopy in tissue-simulating materials - a theoretical and experimental-study of photon paths. *Applied Optics* 34 (1), 22-30.

Peebles, E.D. and Brake, J. (1987). Eggshell quality and hatchability in broiler breeder eggs. *Poultry Science* 66 (4), 596-604.

Peebles, E.D., Doyle, S.M., Zumwalt, C.D., Gerard, P.D., Latour, M.A., Boyle, C.R. and Smith, T.W. (2001). Breeder age influences embryogenesis in broiler hatching eggs. *Poultry Science* 80 (3), 272-277.

Pogue, B.W., Jiang, S.D., Dehghani, H., Kogel, C., Soho, S., Srinivasan, S., Song, X.M., Tosteson, T.D., Poplack, S.P. and Paulsen, K.D. (2004). Characterization of hemoglobin, water, and nir scattering in breast tissue: Analysis of intersubject variability and menstrual cycle changes. *Journal of Biomedical Optics* 9 (3), 541-552.

Prahl, S.A. (1988). Ligh transport in tissue. University of Texas at Austin, 210 p.

Qin, J.W. and Lu, R.F. (2006). Hyperspectral diffuse reflectance imaging for rapid, noncontact measurement of the optical properties of turbid materials. *Applied Optics* 45 (32), 8366-8373.

Qin, J.W. and Lu, R.F. (2007). Measurement of the absorption and scattering properties of turbid liquid foods using hyperspectral imaging. *Applied Spectroscopy* 61 (4), 388-396.

Rahn, H., Ar, A. and Paganelli, C.V. (1979). How bird eggs breathe. *Scientific American* 240 (2), 46-55.

Reizis, A., Hammel, I. and Ar, A. (2005). Regional and developmental variations of blood vessel morphometry in the chick embryo chorioallantoic membrane. *Journal of Experimental Biology* 208 (13), 2483-2488.

Renema, R.A. (2007). Creating the ideal hatching egg: Quality, efficiency, and fertility. http://en.engormix.com/MA-poultry-industry/articles/creating-ideal-hatching-egg-t624/p0.htm (27/01/2011).

Ribatti, D., Urbinati, C., Nico, B., Rusnati, M., Roncali, L. and Presta, M. (1995). Endogenous basic fibroblast growth-factor is implicated in the vascularization of the chick-embryo chorioallantoic membrane. *Developmental Biology* 170 (1), 39-49.

Ribatti, D., Vacca, A., Roncali, L. and Dammacco, F. (1996). The chick embryo chorioallantoic membrane as a model for in vivo research on angiogenesis. *International Journal of Developmental Biology* 40 (6), 1189-1197.

Ribatti, D., Vacca, A., Roncali, L. and Dammacco, F. (2000). The chick embryo chorioallantoic membrane as a model for in vivo research on anti-angiogenesis. *Current Pharmaceutical Biotechnology* 1 73-82.

Ribatti, D. and Presta, M. (2002). The role of fibroblast growth factor-2 in the vascularization of the chick embryo chorioallantoic membrane. *Journal of Cellular and Molecular Medicine* 6 (3), 439-446.

Richardson, M. and Singh, G. (2003). Observations on the use of the avian chorioallantoic membrane (cam) model in investigations into angiogenesis. *Current Drug Targets - Cardiovascular & Haematological Disorders* 3 155-185.

Rieder, M.J., Odrobinak, D.M. and Greene, A.S. (1995). A computerized method for determination of microvascular density. *Microvascular Research* 49 (2), 180-189.

Rokitka, M.A. and Rahn, H. (1987). Regional differences in shell conductance and pore density of avian eggs. *Respiration Physiology* 68 (3), 371-376.

Romanoff, A.L. (1960). The avian embryo: Structural and functional development. Macmillan, New York, 1305 p.

Ruijtenbeek, K., Le Noble, F.A.C., Janssen, G.M.J., Kessels, C.G.A., Fazzi, G.E., Blanco, C.E. and De Mey, J.G.R. (2000). Chronic hypoxia stimulates periarterial sympathetic nerve development in chicken embryo. *Circulation* 102 (23), 2892-2897.

Ruijtenbeek, K., De Mey, J.G.R. and Blanco, C.E. (2002). The chicken embryo in developmental physiology of the cardiovascular system: A traditional model with new possibilities. *American Journal of Physiology-Regulatory Integrative and Comparative Physiology* 283 (2), R549-R550.

Ruijtenbeek, K., Kessels, L., De Mey, J.G.R. and Blanco, C.E. (2003). Chronic moderate hypoxia and protein malnutrition both induce growth retardation, but have distinct effects on arterial endothelium-dependent reactivity in the chicken embryo. *Pediatric Research* 53 (4), 573-579.

Russ, J.C., Dehoff, R.T. (2001). Practical stereology. Plenum Press., New York, 312 p.

Sandau, K. and Kurz, H. (1997). Measuring fractal dimension and complexity - an alternative approach with an application. *Journal of Microscopy-Oxford* 186 164-176.

Schlatter, P., Konig, M.F., Karlsson, L.M. and Burri, P.H. (1997). Quantitative study of intussusceptive capillary growth in the chorioallantoic membrane (cam) of the chicken embryo. *Microvascular Research* 54 (1), 65-73.

Scott, G.F. (2003). Developmental biology. Sinauer Associates Inc., 838 p.

Seidlitz, E., Korbie, D., Marien, L., Richardson, M. and Singh, G. (2004). Quantification of anti-angiogenesis using the capillaries of the chick chorioallantoic membrane demonstrates that the effect of human angiostatin is age-dependent. *Microvascular Research* 67 (2), 105-116.

Smithies, D.J., Vangemert, M.J.C., Hansen, M.K., Milner, T.E. and Nelson, J.S. (1997). Three-dimensional reconstruction of port wine stain vascular anatomy from serial histological sections. *Physics in Medicine and Biology* 42 (9), 1843-1847.

Srinivasan, S., Pogue, B.W., Jiang, S.D., Dehghani, H., Kogel, C., Soho, S., Gibson, J.J., Tosteson, T.D., Poplack, S.P. and Paulsen, K.D. (2003). Interpreting hemoglobin and water concentration, oxygen saturation, and scattering measured in vivo by near-infrared breast tomography. *Proceedings of the National Academy of Sciences of the United States of America* 100 (21), 12349-12354.

Staton, C.A., Stribbling, S.M., Tazzyman, S., Hughes, R., Brown, N.J. and Lewis, C.E. (2004). Current methods for assaying angiogenesis in vitro and in vivo. *International Journal of Experimental Pathology* 85 (5), 233-248.

Strick, D.M., Waycaster, R.L., Montani, J.P., Gay, W.J. and Adair, T.H. (1991). Morphometric measurements of chorioallantoic membrane vascularity - effects of hypoxia and hyperoxia *American Journal of Physiology* 260 (4), H1385-H1389.

Summers, J. (1993). Ascites - a review and update. http://www.poultryindustrycouncil.ca/Factsheets/Factsheets/fact25.htm (28/07/2004).

Tazawa, H. and Mochizuki, M. (1976). Rates of oxygenation and bohr shift of capillary blood in chick-embryos. *Nature* 261 (5560), 509-511.

Tazawa, H. (1980). Oxygen and co2 exchange and acid-base regulation in the avian embryo. *American Zoologist* 20 (2), 395-404.

Tazawa, H. and Whittow, G.C. (2000). Incubation physiology. In Sturkie's avian physiology. Academic Press, San Diego. 617-634.

Telenkov, S.A., Vargas, G., Nelson, J.S. and Milner, T.E. (2002). Coherent thermal wave imaging of subsurface chromophores in biological materials. *Physics in Medicine and Biology* 47 (4), 657-671.

Tenbusch, M., Milakofsky, L., Hare, T., Nibbio, B. and Epple, A. (1997). Regulation of substances in allantoic and amniotic fluid of the chicken embryo. *Comparative Biochemistry and Physiology a-Physiology* 116 (2), 131-136.

Thueler, P. (2000). Optical spectral probing for epithelial tissue characterisation. École Polytechnique Fédérale de Lausanne (EPFL), Département de Microtechnique, 127 p.

Thueler, P., Charvet, I., Bevilacqua, F., St Ghislain, M., Ory, G., Marquet, P., Meda, P., Vermeulen, B. and Depeursinge, C. (2003). In vivo endoscopic tissue diagnostics based on spectroscopic absorption, scattering, and phase function properties. *Journal of Biomedical Optics* 8 (3), 495-503.

Tona, K., Onagbesan, O., Bruggeman, V., De Smit, L., Figueiredo, D. and Decuypere, E. (2007). Non-ventilation during early incubation in combination with dexamethasone administration during late incubation: 1. Effects on physiological hormone levels, incubation duration and hatching events. *Domestic Animal Endocrinology* 33 (1), 32-46.

Vangemert, M.J.C., Welch, A.J., Pickering, J.W., Tan, O.T. and Gijsbers, G.H.M. (1995). Wavelengths for laser treatment of port-wine stains and telangiectasia. *Lasers in Surgery and Medicine* 16 (2), 147-155.

Verhoelst, E., De Ketelaere, B., Bruggeman, V., Villamor, E., Decuypere, E. and De Baerdemaeker, J. (in press-a). Development of a fast, objective, quantitative methodology to monitor angiogenesis in the chicken chorioallantoic membrane during development. *International Journal of Developmental Biology*.

Verhoelst, E., De Ketelaere, B., Decuypere, E. and De Baerdemaeker, J. (in press-b). The effect of early prenatal hypercapnia on the vascular network in the chorioallantoic membrane of the chicken embryo. *Biotechnology Progress.*

Vickerman, M.B., Keith, P.A., Mckay, T.L., Gedeon, D.J., Watanabe, M., Montano, M., Karunamuni, G., Kaiser, P.K., Sears, J.E., Ebrahem, Q., Ribita, D., Hylton, A.G. and Parsons-Wingerter, P. (2009). Vesgen 2d: Automated, user-interactive software for quantification and mapping of angiogenic and lymphangiogenic trees and networks. *Anatomical Record-Advances in Integrative Anatomy and Evolutionary Biology* 292 (3), 320-332.

Villamor, E., Kessels, C.G.A., Ruijtenbeek, K., Van Suylen, R.J., Belik, J., De Mey, J.G.R. and Blanco, C.E. (2004). Chronic in ovo hypoxia decreases pulmonary arterial contractile reactivity and induces biventricular cardiac enlargement in the chicken embryo. *American Journal of Physiology-Regulatory Integrative and Comparative Physiology* 287 (3), R642-R651.

Wagner-Amos, K. and Seymour, R.S. (2003). Effect of local shell conductance on the vascularisation of the chicken chorioallantoic membrane. *Respiratory Physiology & Neurobiology* 134 (2), 155-167.

Walsberg, G.E. (1980). The gaseous microclimate of the avian nest during incubation. *American Zoologist* 20 (2), 363-372.

Weibel, E.R. (1979). Stereological methods. Academic Press Inc., London, 415 p.

West, D.C., Thompson, W.D., Sells, P.G. and Burbridge, M.F. (2001). Angiogenesis assays using chick chorioallantoic membrane. 107-129.

Willemsen, H., Everaert, N., Witters, A., De Smit, L., Debonne, M., Verschuere, F., Garain, P., Berckmans, D., Decuypere, E. and Bruggeman, V. (2008). Critical assessment of chick quality measurements as an indicator of posthatch performance. *Poultry Science* 87 (11), 2358-2366.

Wilson, B.C. and Jacques, S.L. (1990). Optical reflectance and transmittance of tissues - principles and applications. *Ieee Journal of Quantum Electronics* 26 (12), 2186-2199.

Wilting, J., Christ, B., Bokeloh, M. and Weich, H.A. (1993). In-vivo effects of vascular endothelial growth-factor on the chicken chorioallantoic membrane. *Cell and Tissue Research* 274 (1), 163-172.

Wilting, J. and Christ, B. (1996). Embryonic angiogenesis: A review. *Naturwissenschaften* 83 (4), 153-164.

Witters, A. (2009). Factors affecting the impact of hypercapnia during early egg incubation and its effects on pre- and postnatal physiological parameters of broilers. Katholieke Universiteit Leuven, Department of Biosystems, 184 p.

Xu, L., Fukumura, D. and Jain, R.K. (2002). Acidic extracellular ph induces vascular endothelial growth factor (vegf) in human glioblastoma cells via erk1/2 mapk signaling pathway. Mechanism of low ph-induced vegf (vol 277, pg 11368, 2002). *Journal of Biological Chemistry* 277 (21), 19242-19242.

Yahav, S. (2000). Domestic fowl - strategies to confront environmental conditions. *Avian and Poultry Biology Reviews* 11 (2), 81-95.

Yancopoulos, G.D., Davis, S., Gale, N.W., Rudge, J.S., Wiegand, S.J. and Holash, J. (2000). Vascular-specific growth factors and blood vessel formation. *Nature* 407 (6801), 242-248.

Zeng, L.M., Xing, D., Gu, H.M., Yang, D.W., Yang, S.H. and Xiang, L.Z. (2007). High antinoise photoacoustic tomography based on a modified filtered backprojection algorithm with combination wavelet. *Medical Physics* 34 (2), 556-563.

Zoer, B., Kessels, L., Vereijken, A., De Mey, J.G.R., Bruggeman, V., Decuypere, E., Blanco, C.E. and Villamor, E. (2009). Effects of prenatal hypoxia on pulmonary vascular reactivity in chickens prone to pulmonary hypertension. *Journal of Physiology and Pharmacology* 60 (1), 119-130.

LIST OF PUBLICATIONS

Publications in international peer-reviewed journals

Mertens, K., Bamelis, F., Kemps, B., Kamers, B., Verhoelst, E., De Ketelaere, B., Bain, M., Decuypere, E. and De Baerdemaeker, J. (2006). Monitoring of the eggshell breakage and eggshell strength in different production chains of consumption eggs. Poultry science 85 (9), 1670-1677.

Mertens, K., De Ketelaere, B., Kamers, B., Bamelis, F., Kemps, B., Verhoelst, E., De Baerdemaeker, J. and Decuypere, E. (2005). Dirt detection on brown eggs by means of color computer vision. Poultry science 84 (10), 1653-1659.

Verhoelst, E., De Ketelaere, B., Bruggeman, V., Villamor, E., Decuypere, E. and De Baerdemaeker, J. (in press). Development of a fast, objective, quantitative methodology to monitor angiogenesis in the chicken chorioallantoic membrane. International Journal of Developmental Biology.

Verhoelst, E., De Ketelaere, B., Decuypere, E. and De Baerdemaeker, J. (in press). The effect of early prenatal hypercapnia on the vascular network in the chorioallantoic membrane of the chicken embryo. Biotechnology Progress.

Verhoelst, E., Bamelis, F., De Ketelaere, B., Tsuta, M., Nguyen Do Trong, N., Decuypere, E., De Baerdemaeker and J., Saeys, W. (submitted). The potential of spatially resolved spectroscopy for monitoring angiogenesis in the chorioallantoic membrane. Biotechnology Progress.

Conference proceedings

Bamelis, F., Verhoelst, E., De Smit, L., Bruggeman, V., De Baerdemaeker, J. and Decuypere E. (2004). The effect of broiler eggshell conductance on hatchability and hatching time. Developmental Origins of Health and Disease Symposium, Maastricht, The Netherlands.

Bamelis, F., Kemps, B., Mertens, K., Verhoelst, E., De Ketelaere, B., Decuypere, E. and De Baerdemaeker, J. (2005). Time dependent changes in VIS-NIR transmission spectra

through white shelled eggs. European Symposium on the Quality of Eggs and Egg Products edition: XI, Doorwerth, The Netherlands.

Bamelis, F., Kemps, B., Mertens, K., Verhoelst, E., De Ketelaere, B., Decuypere, E. and De Baerdemaeker, J. (2005). VIS-NIR transmission for assessment of internal egg quality. European Symposium on the Quality of Eggs and Egg Products edition: XI, Doorwerth, The Netherlands.

Bruggeman, V., De Smit, L., Everaert, N., Witters, A., Debonne, M., Willemsen, H., Verhoelst, E., Kokou, T., Okanlawon, O., De Baerdemaeker, J., Arckens, L. and Decuypere E. (2007). The chicken embryo as a model for studying effects of differential CO2 concentrations during incubation. International Chick Meeting, Barcelona, Spain.

Bruggeman, V., Everaert, N., Witters, A., De Smit, L., Okanlawon, O., Debonne, M., Willemsen, H., Kamers, B., Kokou, T., Verhoelst, E., Arckens, L., De Baerdemaeker, J. and Decuypere, E. (2007). Tolerance of chick embryos to higher CO_2 concentrations during incubation: an overview. The 3rd Combined Workshop on Basic Physiology and Perinatal Development in Poultry edition: 3, Berlin, Germany.

De Baerdemaeker, J., De Ketelaere, B., Bamelis, F., Kemps, B., Mertens, K., Verhoelst, E. and Decuypere, E. (2005). New practical systems to measure eggshell quality. WPSA FR meeting, France.

De Ketelaere, B., Mertens, K., Kemps, B., Bamelis, F., Verhoelst, E., Decuypere, E. and De Baerdemaeker, J. (2005). Automated blood detection in eggs using combined optical reflection-transmission measurements. European Symposium on the Quality of Eggs and Egg Products edition: XI, Doorwerth, The Netherlands.

Decuypere, E., Okanlawon, O., De Smit, L., Kokou, T., Everaert, N., Witters, A., Debonne, M., Verhoelst, E., Buyse, J., Hassanzadeh, M., De Baerdemaeker, J., Arckens, L. and Bruggeman, V. (2006). Hypoxia and hypercapnia during incubation of chicken eggs on development and subsequent performance. European Poultry Conference edition: XII, Verona, Italy. Book of Abstracts, 62 (suppl), 486-487.

Decuypere, E., Verhoelst, E. and Bruggeman, V. (2008). New methods for quality and development measurements on consumption and incubation eggs. Inauguration lecture at the XXXVIII ESNA Annual Meeting, Krakow, Poland.

Mertens, K., Bamelis, F., Kemps, B., Kamers, B., Verhoelst, E., Decuypere, E. and De Baerdemaeker, J. (2005). Monitoring eggshell strength and eggshell breakage in different production chains of consumption egg. European Symposium on the Quality of Eggs and Egg Products edition: XI, Doorwerth, The Netherlands.

Mertens, K., De Ketelaere, B., Bamelis, F., Kemps, B., Kamers, B., Verhoelst, E., De Baerdemaeker, J. and Decuypere, E. (2004). Off-line dirt detection in brown eggs. Cost 923 – Multidisciplinary Hen Egg Research location, Barcelona, Spain.

Nguyen Do Trong, N., Erkinbaev, C., Watté, R., Verhoelst, E., Nicolaï, B.M. and Saeys, W. (2011). Non-destructive characterization of food microstructure and composition by spatially-resolved spectroscopy. 11th International Congress on Engineering and Food, Athens, Greece.

Nguyen Do Trong, N., Tsuta, M., Watté, R., Verhoelst, E., De Baerdemaeker, J., Nicolaï, B.M. and Saeys, W. (2011). Spatially-resolved spectroscopy for non-destructive quality inspection of foods. ASABE Annual International Meeting, Louisville, Kentucky, USA.

Verhoelst, E., Vandenheede, V., De Ketelaere, B., Bruggeman, V., Decuypere, E. and De Baerdemaeker, J. (2007). Structural analysis of the vascular network of the chorioallantoic membrane. 13th PhD Symposium on Applied Biological Sciences, Leuven, Belgium (poster price). Communications in agricultural and applied biological sciences 72 (1), 325-329.

Verhoelst, E., Vandenheede, V., De Ketelaere, B., Bruggeman, V., De Baerdemaeker, J. and Decuypere, E. (2009). Structural analysis of the vascular network in the chorioallantoic membrane. Proceeding of the 4th Workshop on Fundamental Physiology and Perinatal Development in Poultry, Bratislava, Slovak Republic.